Dependence of tropical cirrus clouds on sea surface temperature and consequences for the Archean climate

by

Roberto F. Rondanelli

Submitted to the Department of Earth Atmospheric and Planetary Sciences
in partial fulfillment of the requirements for the degree of

Doctor of Philosophy

at the

MASSACHUSETTS INSTITUTE OF TECHNOLOGY

Sept 2009

Author .....
Department of Earth Atmospheric and Planetary Sciences
August 17, 2009

Certified by .....
Richard S. Lindzen
Alfred P. Sloan Professor of Meteorology
Thesis Supervisor

Accepted by .....
Maria T. Zuber
E. A. Griswold Professor of Geophysics
Head, Department of Earth, Atmospheric, and Planetary Sciences

Dependence of tropical cirrus clouds on sea surface temperature and consequences for the Archean climate

by

Roberto F. Rondanelli

Submitted to the Department of Earth Atmospheric and Planetary Sciences
on August 17, 2009, in partial fulfillment of the
requirements for the degree of
Doctor of Philosophy

Abstract

In this thesis, we study observationally the variation of upper level cloud fraction with sea surface temperature in tropical oceanic regions. We also explore the consequences of a cloud feedback, arising from variations in the coverage of thin upper level clouds, in the climate of the Archean using a simple radiative-convective model that includes the effect of the variations in the area of thin cirrus clouds.

First, we look at the variation in area of upper level clouds using TRMM VIRS (Tropical Rainfall Measuring Mission, Visible Infrared Sounder) data. We quantify the effect of methodological choices on the magnitude of the observed correlations between upper level cloud cover and SST. We discuss several methodological choices that might contribute to the relatively small signals found by previous researchers ($\sim$ 0%/K to 2%/K) , namely, the classification of cloudy regions into convective updrafts and anvil, the use of cloud weighted SST, and the truncation and sampling error with respect to the evolution of mesoscale convective systems. All of these contribute to some extent to the weakness of signal. We show that the coarse sampling of orbital satellites can introduce biases in the estimation of the signal. Our observational evidence shows a negative correlation between the upper level cloud fraction normalized by convection and sea surface temperatures.

We also study the relation between local sea surface temperature (SST) and convective precipitation fraction and stratiform rainfall area from radar observations of precipitation, using data from the Kwajalein atoll ground-based radar as well as the precipitation radar on board of the Tropical Rainfall Measurement Mission (TRMM satellite). We find that the fraction of convective precipitation increases with SST at a rate of about 6 to 12%/K and the area of stratiform rainfall normalized by total precipitation decreases with SST at rates between -5 to -28%/K. These relations are observed to hold for different regions over the tropical oceans and also for different periods of time. Correlations are robust to outliers and to undersampled precipitation regions. Kwajalein results are relatively insensitive to the parameters in the stratiform-convective classification algorithm. Quantitative differences between the results obtained using the two different radars could be explained by the smooth-

ing in the reflectivity of convective regions due to the relatively large pixel size of the TRMM precipitation radar compared to the size of the convective clouds. We discuss how this observations can be interpreted as an increase in the efficiency of precipitation with temperature in mesoscale convective systems in the tropics.

Finally, we explore the consequences of a negative feedback mediated through tropical cirrus clouds in the climate of the Archean, and the possibility that this feedback could explain the so-called faint young sun paradox. We assume that rates of change in the area of detrainment cloud (from the observational estimates) are characteristic also for thin cirrus clouds that have a net positive cloud radiative forcing. We find that global mean surface temperatures above freezing can indeed be found for luminosities larger than about 0.8 (corresponding to $\sim$ 2.9 Ga and nearly complete tropical cirrus coverage). For luminosities smaller than 0.8, even though global mean surface temperatures are below freezing, tropical mean temperatures are still above freezing, indicating the possibility of a partially ice-free earth for the Early Archean. While it is feasible for tropical cirrus to completely eliminate the paradox, it is similarly possible for tropical cirrus to reduce the amounts of other greenhouse gases needed for solving the paradox and therefore easing the constraints on CO_2 and CH_4 that appear to be in disagreement with geological evidence.

Thesis Supervisor: Richard S. Lindzen
Title: Alfred P. Sloan Professor of Meteorology

Acknowledgments

¿Por qué di en agregar a la infinita
serie un símbolo más? ¿Por qué a la vana
madeja que en lo eterno se devana,
di otra causa, otro efecto y otra cuita?
El Golem, J. L. Borges

For a Latin American person this is a difficult piece to write in English (and in only two pages). I will not write it in Spanish, which would be the natural thing to do, and I will not thank every single member of my family so you Anglo-Saxons can keep reading. I warn you though, that this will necessarily be a bad translation from the language in which I think about gratitude.

First and foremost I would like to thank my advisor. In Professor Lindzen I have found not only a great advisor and scientist, but also a great human being. It appears as if his virtues are strengthened by his unsatiable curiosity about things, and therefore his wide and deep understanding of human nature (and of everything else). I thank him for his patience and sense of humor and also for his relentless desire for me to succeed in my studies. In these years working with him I hope I have learned a few things about science, although his influence in me has gone, undeliberately, way beyond that.

Many colleagues and friends helped me during my studies at MIT. I had the pleasure of sharing my office with great people, Masahiro, Yang and Daniela. I found in Masahiro a great person to be around either for science or for anything else. I miss him since the day he went back to Japan. I also miss Daniela and Yang since I went back to Chile. Only recently I had the good fortune of meeting Yong-Sang, sharing MIT with him for too little time. I also thank my friends at EAPS, Vikram, Bill, Jon, Fanny, Xue, Matt, Cegeon, Brian for company and great memories, I wish I had the chance to know each one of them better. I thank Miguel for advice, help, friendship and commiseration during good and though times. Everybody at EAPS was ready to make me and my wife feel welcome in the US, but specially two people went out the way to accomplish that, David Flagg and Mary Elliff. Thanks to them we are now also a bit American ourselves besides being the proud parents of an American girl. I also appreciate advice and help at different moments from Vicki, Carol, Joe Hankins and Roberta.

Our friends in Boston also made life easier and less of a shock during the first years, I thank every one of them. I will mention some names: I thank Lucho for his infinite patience in carrying a conversation, Patty and Marcos for being themselves, Marco and Monica for all the great moments and Gonzalo for being an artist.

The thesis work was mainly supported by DOE grant DE-FG02-01ER63257. I also acknowledge partial support for living expenses from the Chilean Presidential Fellowship program and from the University of Chile. I thank my colleagues from the University of Chile for their confidence and for moral support during all these years. Last but not least, the members of my thesis committee, Kerry Emanuel, Paul O'Gorman and Leon Golub for thoughtful comments on the thesis and specially for

their willingness to read my thesis with such short notice.

I thank all my family, specially my mother, for making me who I am and also for naively thinking that I am so smart that getting a PhD would be a piece of cake.

Finally, I dedicate this work to Maria Cristina. Not only has she been my companion for years, she has also given me the most precious gift. I give her all I have.

Contents

List of Figures

List of Tables

Chapter 1

Introduction

Cloud feedbacks are believed to be the major known uncertainty in evaluating the climate response to external forcings within global circulation models (e.g *Bony et al.*, 2006; *Schwartz*, 2008). Clouds are at the center of the interaction between complex physical processes such as the large-scale dynamics, radiative transfer, turbulent convection and microphysical effects. Uncertainties in any of these physical processes translate into uncertainties in the effect of clouds on climate. Observations are usually not sufficient to constraint modeling to a great detail; some of the parameters needed to parameterize clouds in the context of a model can be directly observed, others can only be tuned to find indirect agreement with observations. Therefore, climate models show a large disparity in the cloud responses to external forcing, about a factor of two larger than the disparity in the value of the rest of the feedbacks (*Soden and Held*, 2006). Of course, this alone does not imply that in reality the rest of the feedbacks are better constrained, neither does it imply that the real response of clouds is within the spread of current general circulation models.

For instance, the effect of microphysical processes in deep convective clouds remains a major source of uncertainty. Several studies have suggested on the basis of radiative convective equilibrium simulations (*Sun and Lindzen*, 1993b; *Renno et al.*, 1994; *Emanuel and Pierrehumbert*, 1996) and also on observational grounds (*Lindzen et al.*, 2001; *Lau and Wu*, 2003; *Del Genio and Kovari*, 2002; *Del Genio et al.*, 2005) that the temperature dependence of microphysical processes in deep convective clouds could result in climate feedbacks. *Renno et al.* (1994) for instance, presented radiative-convective simulations in which a low efficiency of precipitation resulted in warm climates due to the moistening of the environment by condensate detrained from the convective clouds and a strong greenhouse effect of water vapor. In a similar fashion, *Clement and Soden* (2005) studied the sensitivity of the tropical mean

radiative budget in a general circulation model (GCM) to changes in the circulation and microphysics. They found a relatively large sensitivity to changes in the fraction of cloud that is converted to precipitation in deep convection compared to changes in the strength of the Hadley circulation, emphasizing that changes in the microphysics can potentially provide a larger climate effect than cloud redistribution through dynamical processes. Also using a GCM, *Lau et al.* (2005) found that an increased auto-conversion rate in the parametrization of warm convective clouds leads to a stronger hydrological cycle, a reduction in upper level cloudiness and an increase in the overall fraction of convective precipitation.

Precipitation is the main process that competes with clouds for water condensate. There are theoretical reasons to suppose that a relation between local SST and the efficiency of the processes that form precipitation may exist. In particular, warmer sea surface temperatures (SST) will be accompanied by an increase in the saturation water vapor content (e_s) which scales according to the Clausius-Clapeyron relation,

$$\frac{1}{e_s}\frac{de_s}{dT} = \frac{L_v}{R_v T^2}, \tag{1.1}$$

where L_v is the latent heat of vaporization and R_v is the gas constant for water vapor. For temperatures closer to the current tropical sea surface temperatures, the relative rate of change of e_s is about 6%/K.

Clouds being rooted in this potentially moister air (assuming that relative humidity remains approximately constant) will also become moister. The effect of having a moister cloud has been studied in the context of the so-called cloud liquid water feedback (*Betts and Harshvardan*, 1987). As clouds form over warmer temperatures they have a larger cloud liquid water content, are optically thicker and therefore more reflective. The more striking feature of this cloud feedback is that it is purely thermodynamic, that is, arises independently of the circulation that gives rise to the cloud and therefore allow us to isolate a major confounding factor in evaluating feedbacks from observations. Also, for the time scale of formation and development of these clouds, one can confidently assume that sea surface temperature acts as a fixed boundary condition and therefore the thermodynamic response will be similar in a different climate[1]. In chapter 2 we will discuss the dependence of cloud liquid water with SST. Although we will be mostly concerned with upper level clouds, the cloud liquid

[1]For tropical clouds in particular we know that the thermodynamic effects might not be only a function of the local thermodynamic ascent path. To the extent that mixing with the environment plays a role, as it surely does, the cloud liquid water will also be determined by the environmental thermodynamic profile, which in the tropics is set by a global heat balance.

water dependence represents a logical first step to understand the thermodynamic variations of the cloud response in a different climate. Current climate variability, that is observations of clouds forming over different temperatures apparently confirm the theoretical expectation of the behavior of cloud liquid water at least for non-precipitating shallow clouds (*Betts and Harshvardan*, 1987, and references therein). Dynamics will still play a role insofar it will determine the distribution of the clouds.

The study by *Ramanathan and Collins* (1991) provides a classic example of the difficulties one finds when trying to deduce the behavior of a different climate using data from the present climate and controlling dynamical effects. The study by *Ramanathan and Collins* (1991) attempted to relate the sea surface temperature with the cloud radiative effects associated to those temperatures. The situation is shown in Fig. 1-1. The top panels of the figure show the sea surface temperature in the tropics for the months of April 1985 and 1987 (two different phases of the El Niño Southern Oscillation). In general longwave cloud forcing is associated with regions of relatively warm SST in the warm pool region and with the intertropical convergence zones where deep convection is prevalent. Shortwave cloud forcing is also prevalent in the deep convective regions and also in subtropical stratocumulus regions. Both shortwave and longwave forcing are anti-correlated in current climate and they closely balance each other to the extent that this cancelation has been proposed as a climate constraint (*Hartmann et al.*, 2001; *Chou and Lindzen*, 2002). *Ramanathan and Collins* (1991) proposed a simple model for the energy balance of the tropical troposphere in which the temperature dependence of the cloud radiative effects was directly derived from the dependence in observations such as the ones shown in Fig. 1-1. They deduced a strong thermostat in the tropical troposphere from the fact that a strong negative shortwave forcing appears associated with the warmer sea surface temperatures. The main difficulty with *Ramanathan and Collins* (1991) approach is the fact that variations observed have a large component simply due to the fact that warmer SST regions are also regions where convection tends to be concentrated (*Lindzen and Nigam*, 1987). However, a different climate, say a climate uniformly warmer by 5K, would concentrate convection in the same geographical regions and therefore similar cloud forcing-SST relations would be derived, displaced in 5 K from the original ones, making both sets of relations (the original and the one for a 5K warmer climate) inconsistent. In a similar fashion, the current climate threshold for deep convection appears to be about 27 C. Taken to an extreme, the argument of simply relating cloud forcing and SST would predict that no deep convection would form in climates whose maximum SST never approaches 27 C. As long as a given climate

has surface fluxes and radiative cooling destabilizing the tropical atmosphere, one still expects to have moist convection, no matter the surface temperature characteristic of such climate. That convection concentrates in regions of relatively high SST and therefore that the amount of convection will have a major effect in the magnitude of the cloud radiative forcing seems like an obvious point, but it has been a source of confusion in the literature. We will discuss our own approach to this problem in chapter 3 and we will connect it to the so-called dynamical-thermodynamical changes in cloud properties (*Bony et al.*, 2004).

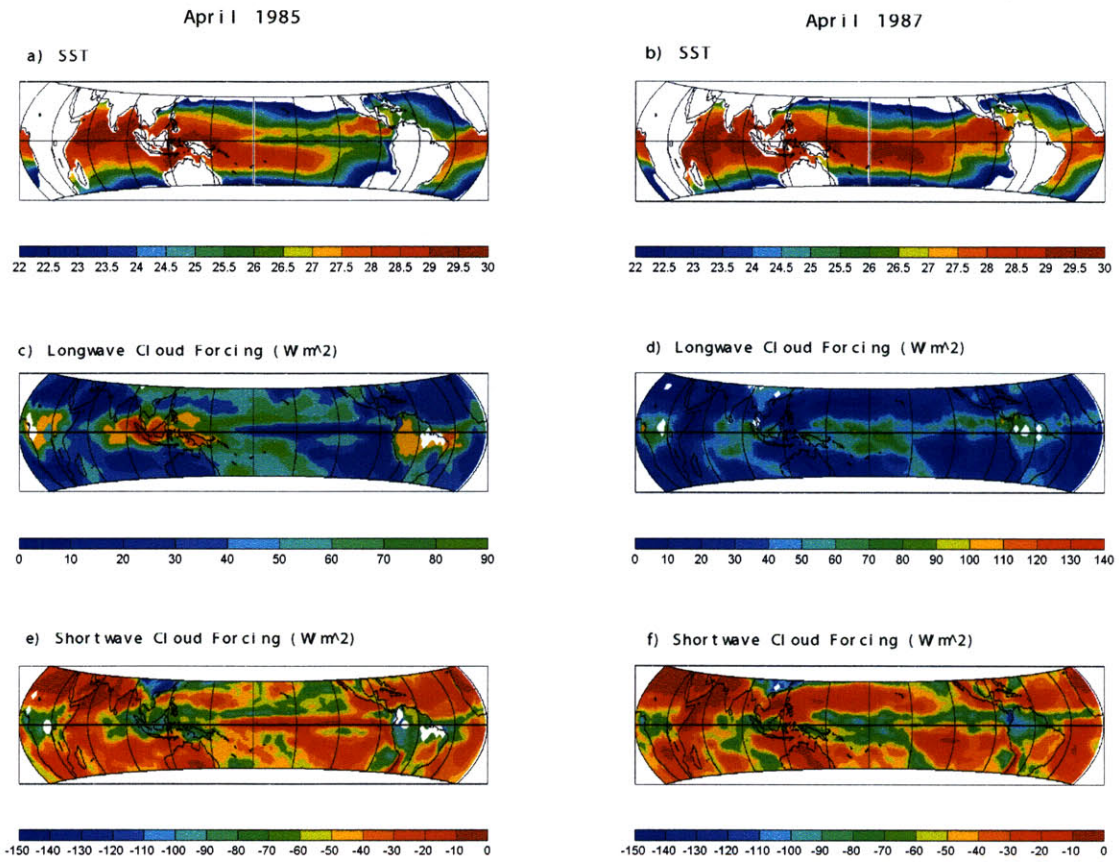

Figure 1-1: Sea surface temperature distribution in the tropics for the months of a) April 1985 and b) April 1987. c) and d) are the longwave cloud forcing and e) and f) are the shortwave cloud forcing. Data from Earth Radiation Budget Experiment

As can be deduced from Fig. 1-1, the cloud forcings have a seemingly bimodal distribution, with large areas of the tropics having very little water vapor and clouds, mostly controlling the radiative cooling of the tropics. These regions were called "radiator fins" by *Pierrehumbert* (1995) who emphasized the role of the relative coverage

of dry regions and regions moistened by convection in maintaining the heat balance in the tropics. In a similar fashion, *Lindzen et al.* (2001) proposed the possibility that, through the microphysical dependence of deep convective clouds, a negative feedback might operate increasing the relative area of the dry regions with respect to the moist cloudy regions in the tropics in a warmer climate. In chapter 3 we will review the mechanism proposed, and we will also examine critically some of the observational evidence for the variation of the upper level cloud area (defined according to infrared brightness temperature) with SST. We will discuss some of the attempts in the literature to quantify the rate of change in area of upper level cloud, in particular, how the sampling of orbital satellites can make the detection of a signal problematic. Our results confirm the variation in area of upper level cirrus clouds with local SST, originally found by *Lindzen et al.* (2001).

Infrared radiances provide only partial information about the cloud processes and only indirect information about the precipitation processes in convective clouds. Newly developed satellite missions starting with the Tropical Rainfall Measuring Mission satellite (TRMM) provide cloud and precipitation radar profiles from space, allowing for a more direct probe of the convective processes in the oceanic tropical regions. In chapter 4 we will study the dependence of the partition between stratiform and convective rain with SST for mesoscale convective systems in the tropics. We will discuss how this partition can be considered as a surrogate for the precipitation efficiency. We will show how convective rainfall (rainfall produced directly in the active deep convective cores) makes up a larger proportion of the total rainfall of the system for higher SSTs.

Tropical regions in current climate receive a much larger proportion of radiation than they are able to re-radiate back to space and therefore, the tropics are regions of net export of energy. Therefore, the heat balance in the tropics plays a major role in setting up the climate response to forcings. Also, having larger surface temperatures, feedback processes that depend on temperature or rainfall, for instance water vapor feedback, will be to a large extent controlled by the tropical temperature response. Challenging questions about past climates, can therefore, have their primary explanation in the behavior of the tropics. In particular, the climate during the first half of the earth's history was determined by a much reduced solar input. And yet, the geological record shows absence of evidence for glaciations and plenty of evidence for liquid water and stable oceans. A simple calculation assuming a constant atmospheric composition, would indicate temperatures below freezing and possibly a snowball earth, a situation that is at odds, for instance with the evolution of life.

This is the so-called faint young sun paradox (*Sagan and Mullen*, 1972; *Catling and Kasting*, 2007). A straightforward solution to the paradox is to imagine that a massive CO_2 atmosphere existed throughout most of the Archean. In fact, the proposed functioning of the carbon cycle can potentially act as negative feedback on climate in the geological scale, and predicts that, for a colder and therefore less rainy climate than present, concentrations of CO_2 in the atmosphere would necessarily increase in order to balance a slower removal of atmospheric carbon to the ocean (and eventually to the mantle) through weathering processes (*Walker et al.*, 1981). However, some geological evidence based on the formation of certain minerals in conserved Archean rocks (see *Rollinson*, 2007, and references therein) indicate much lower concentrations than those required for the CO_2 greenhouse effect to compensate the faintness of the early sun. This leaves open the possibility that the straightforward CO_2 solution needs to be replaced or supplemented.

In general, and given the relative ignorance about the precise boundary conditions for the climate of the Archean (e.g. distribution of the continents and oceans, earth rotation rate and obliquity, etc.), single column models in radiative-convective equilibrium have been the preferred tool to test ideas for the paradox resolution. Following this approach, we build a simple two-column radiative-convective model based on observed properties of thin cirrus clouds to explore the possibility that a negative of the sort of the one postulated in the iris hypothesis, could be operating in the Archean maintaining large regions of the earth above freezing (chapter 5). We will explore also the sensitivity of the solution to some of the assumptions in the processes included in the model.

Chapter 2

Preliminaries

As we briefly discussed in the introduction, a moister boundary layer seems to be an almost unavoidable consequence of the increase in sea surface temperature in a warmer climate. To the extent that the properties of the clouds are also dependent on the moisture content of the air that feeds convection, cloud feedbacks on climate will arise from this dependence. As an motivation for the observational results that will be presented in chapters 3 and 4 we will present some simple arguments applied to the continuous growth model of a single collector droplet that grows by collision-coalescence processes in a warm cloud. We will deduce the distribution of cloud liquid water and use the deduced vertical dependence of the cloud liquid water content to study the variations in the time that it takes for a droplet to growth to precipitation size. Also, we will present a simple model for the partition of condensate between precipitation and detrainment based in a similar model introduced by *Del Genio et al.* (2005). We acknowledge that this simplified treatment is hardly realistic. In fact most of the processes related to the growth of hydrometeors in the detrainment regions of convective clouds are related to the transport of water vapor which is muted in these simplified models. Therefore, the relation with the observational results is only indirect. However, these models help to illustrate and quantify the effects expected to arise from the dependence of the cloud liquid water on sea surface temperature.

2.1 Changes in the efficiency of precipitation in a continuous growth model

Based on the simple theory of continuous growth to simulate the collision-coalescence process in a cloud, we can expect that changes in the liquid water content of the cloud

and in the updraft velocity will result in changes in the size of precipitation droplets. In order to quantify this effect we will consider the simplest case in which a single collector droplet of radius R grows by interacting with a population of cloud droplets which have a size distribution $n(r)$. The growth rate of such a collector droplet can be written as (*Bowen*, 1950; *Rogers and Yau*, 1989),

$$\frac{dR}{dt} = \frac{\pi}{3}\int_0^\infty \left(\frac{R+r}{R}\right)^2 (u(R) - u(r))n(r)r^3E(R,r)dr \tag{2.1}$$

where $u(r)$ is the terminal velocity of droplets of radius r and $E(R,r)$ represents the efficiency of the collection (includes the collision efficiency and the coalescence efficiency) of the droplets r by droplets of size R, t is time.

In the most simple case in which a single collector droplet of radius R grows within a monodisperse cloud with droplets of size r, the change in size can be obtained from the integration of equation 2.1,

$$\frac{dR}{dt} = \frac{u(R)E(R)l}{4\rho_l} \tag{2.2}$$

where the efficiency $E(R)$ will now be only a function of the size of the collector droplet, l is the cloud liquid water content in units of mass per unit volume, ρ_l is the density of liquid water.

If we assume that the cloud droplets are subject to a constant updraft of magnitude w and we allow for vertical variations in the cloud liquid water content, the growth of the collector droplet with height can be written as,

$$\frac{dD}{dz} = \frac{u(D)E(D)l(z)}{2\rho_l}\frac{1}{w-u(D)} \tag{2.3}$$

where we have now written the results in terms of the collector droplet diameter D.

We use the settling velocities given by *Rogers and Yau* (1989) as a function of the droplet size,

$$u(r) = \begin{cases} k_1 r^2 & r < 35\mu m \\ k_3 r & 35\mu m \leq r < 0.6mm \\ k_2 r^{1/2} & 0.6mm \leq r < 2mm \end{cases} \tag{2.4}$$

with $k_1 = 1.19\times10^6 cm^{-1}s^{-1}1$, $k_3 = 8\times10^3 s^{-1}$ and $k_2 = 2.2\times10^3\left(\frac{\rho_0}{\rho}\right)^{1/2} cm^{1/2}s^{-1}$, where ρ_0 is the a reference value for the air density, $\rho_0 = 1.20\ kg/m^3$ and ρ is the

actual air density.

Using the fall velocities described above, the final size of a droplet leaving the cloud can be estimated as a function of the updraft velocity and cloud liquid water content.

We have used the continuous growth model to illustrate the behavior of the updraft velocity and cloud liquid water content on the size and trajectory of a growing collector droplet. As a starting point, we keep the usual assumption of a constant liquid water cloud throughout the cloud (*Bowen*, 1950; *Rogers and Yau*, 1989). Later we will allow the cloud to have an adiabatic vertical profile of cloud liquid water. The size of the cloud droplets is chosen as $r = 15\mu m$ and the initial collector droplet is chosen to have an initial size $R_o = 40\mu m$. The collector droplet is assumed to co-exist with the smaller cloud droplets at the base of the cloud (several theories account for the possibility of such a large droplets to exist near the base of the cloud.)

Fig. 2-1 shows the effect of the updraft velocity on the coalescence. We see a relatively large effect of the vertical velocity on the time that takes for a droplet to cycle through the cloud. The fact that precipitation occurs when the settling velocity equilibrates to the vertical updraft velocity, produces a size sorting of the droplets that fall out of the cloud. That is reflected in the relatively large variation of final sizes shown in Fig 2-1.c (The scaling is determined by the particular selection for the variation of settling velocity with size in 2.4). Since in this case the cloud liquid water is kept constant, the growth rate itself (Eq. 2.2) is constant. Size sorting based on differences in the updraft velocity of clouds is anticipated to have a significant effect on the rain droplet size distribution (RDSD).

Figure 2-2 shows the variation of the growth rate and size of the collector droplet as a function of the cloud liquid water content. We see that the effect on the time taken for the collector droplet to cycle through the cloud is relatively large. A few tenths of $[g/kg]$ in the cloud liquid water have an effect as large as the effect of a few m/s in the updraft velocity. In this particular case, relatively large cloud liquid water contents are related to relatively rapid growth and therefore the collector droplet falls out of the cloud faster (see Fig. 2-2.c). However, in this case the final size of the particles remains unchanged and are only controlled by the strength of the updraft. This situation differs from the one discussed by *Bowen* (1950). In his model, he finds a dependence (although small) of the final size of the droplet on the cloud liquid water. This dependence arises from Bowen's assumption that the collector droplet will first ascend without collecting droplets and only growing by condensation. This situation is equivalent to the situation in which the collector droplet starts growing at

a certain height over the base of the cloud in our simulations. For the case in which the collector droplet starts growing at a height of $h = 1000m$, the change in final radius of the collector droplet from $l = 0.5g/kg$ to $l = 1.5g/kg$ is only $0.20\mu m$. That is equivalent to a change in about $0.25\ m/s$ in the updraft velocity.

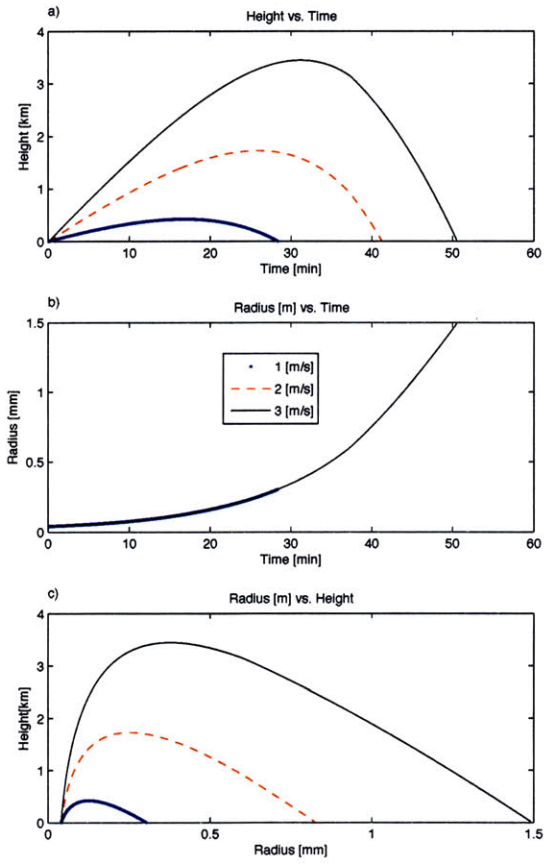

Figure 2-1: Continuous growth model (Bowen Model) for the growth of a rain droplet in a population of cloud droplets assumed to have a negligible fall speed and a collection efficiency of 0.7 respect to the collector drop ($r = 12.6\mu m$). For these cases cloud is assumed to have a base of 1 km and to have an homogeneous cloud liquid water content of 1g/kg.

2.2 Changes in the adiabatic cloud liquid water

A perhaps more accurate version of the continuous growth model can be constructed assuming the cloud liquid water content changes with height throughout the cloud. Since in a reversible ascent the total water mixing ratio r_T is conserved and is equal

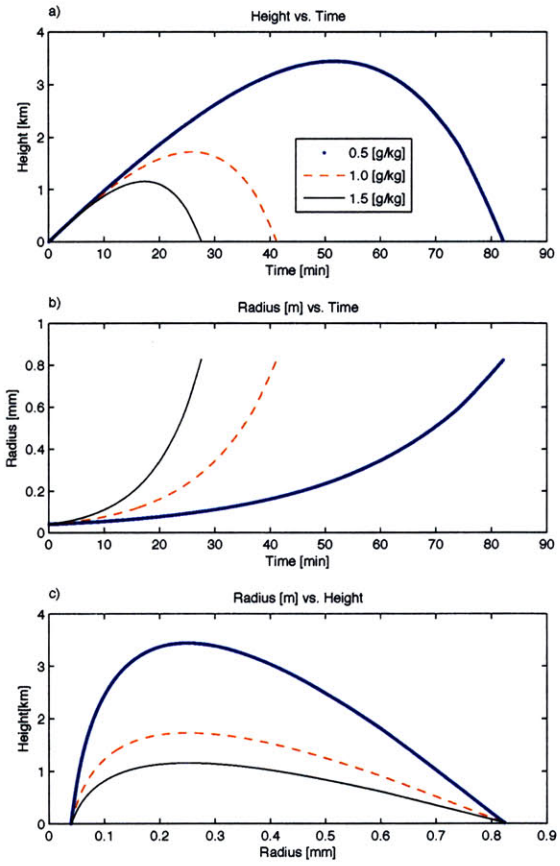

Figure 2-2: Same as figure 2-1 but for different values of cloud liquid water content.

to the mixing ratio of the original parcel $r(z_i)$, for each height above the lifting condensation level z,

$$r^*(z) + r_l(z) = r_T = constant \tag{2.5}$$

$$r_l(z) = r(z_i) - r^*(z) \tag{2.6}$$

As the temperature decreases with height, the saturation mixing ratio decreases and therefore this simple argument allows us to calculate the vertical variation of the cloud liquid water mixing ratio r_l under a reversible ascent. We will refer to this as the *adiabatic* cloud water mixing ratio. It is evident that coalescence (and further precipitation) and mixing of the cloudy air with environmental air, among other processes, will control the degree to which a real cloud will exhibit adiabatic

behavior. *Wallace and Hobbs* (2006) quote measurements in cumulus clouds in which the average cloud liquid water is about 20% of the value of the adiabatic liquid water, whereas the maximum observed cloud liquid water follows closely the adiabatic value with departures of about 10% to 20%. Figure 2-3 shows the theoretical calculations of the adiabatic values of the cloud liquid water content for parcels that ascend reversibly and adiabatically (that is moist entropy is conserved and no precipitation occurs during the ascent (see e.g *Emanuel*, 1994)).

The relative change of cloud liquid water with surface temperature is depicted in Fig.2-3.b and is small (about 2%/K near the base of the clouds at temperatures between 20 and 30 C) compared to the Clausius-Clapeyron rate of change (Fig.2-3.d).

One can easily derive an analytical expression for the relative change in cloud liquid water starting from the moist static energy conservation. When the heat capacity of liquid water is neglected and the hydrostatic approximation is made, one can write,

$$dr^* = -\frac{c_{pd}}{L_v} dT - \frac{g}{L_v} dz, \tag{2.7}$$

where dr^* represents the infinitesimal change in water vapor saturation mixing ratio along a moist-adiabat. Noting that $dr_l = -dr^*$, and rearranging the terms we can write,

$$\frac{dr_l}{dz} = \frac{c_{pd}}{L_v}\left(\frac{dT}{dz} + \frac{g}{c_{pd}}\right) = \frac{c_{pd}}{L_v}\left(\Gamma_d - \Gamma_m\right), \tag{2.8}$$

where the definitions of moist (Γ_m) and dry adiabatic lapse rate (Γ_d) have been used. When we are close to the base of the cloud, we can simply linearize 2.8 to find an approximation for r_l near the base of the cloud,

$$r_l \simeq \frac{c_{pd}}{L_v}\left(\Gamma_d - \Gamma_m\right) z, \tag{2.9}$$

and therefore the relative variation of r_l with surface temperature T_s defined as f can be written, near the cloud base, as,

$$f \equiv \frac{1}{r_l}\frac{\partial r_l}{\partial T_s} \simeq -\frac{1}{\left(\Gamma_d - \Gamma_m\right)}\frac{\partial \Gamma_m}{\partial T_s} \tag{2.10}$$

This result was first obtained by *Betts and Harshvardan* (1987) by simply linearizing the cloud liquid water content in terms of the potential temperature gradient along a moist-adiabat. This result was motivated as a correction of an earlier result by *Somerville and Remer* (1984) in which the value of f used to calculate an indirect cloud feedback through the increase of the optical depth with temperature

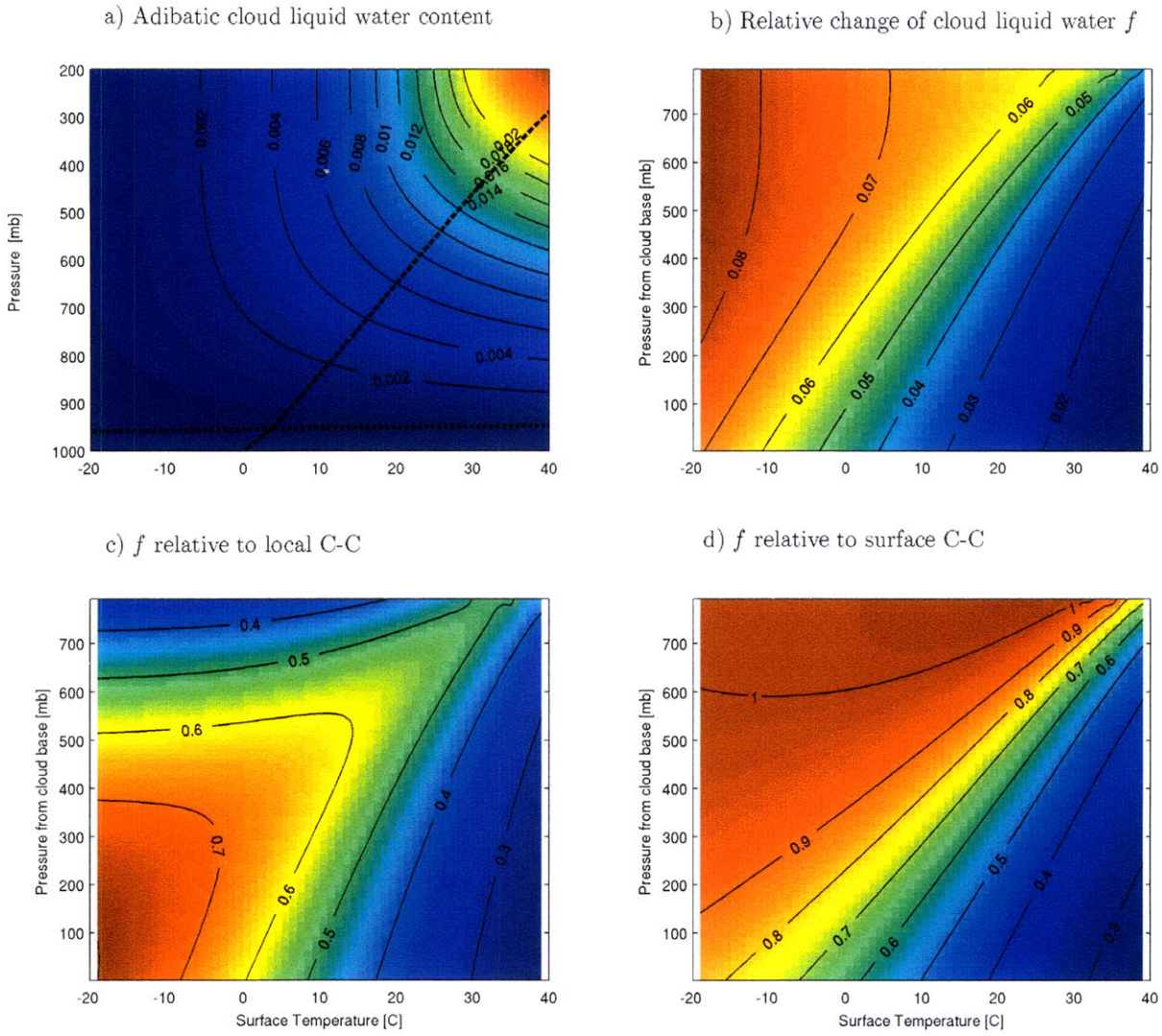

Figure 2-3: Cloud liquid water content for a reversible adiabatic ascent from the indicated surface temperatures, the air at the surface is assumed to have 80 % relative humidity. No ice thermodynamics is allowed. a) Cloud liquid water mixing ratio in [g/g]. The lower thick dashed line represents the cloud base and the upper thick dashed line represents the freezing level. b) Relative change of cloud liquid water, defined as $f = (1/r_l)(\partial r_l/\partial T)$. c) Ratio between f and the local rate of change of water vapor mixing ratio (given by the Clausius-Clapeyron relation). d) Ratio between f and the surface rate of change of water vapor mixing ratio.

was simply assumed to scale as Clausius-Clapeyron. On the other hand, for heights significantly above the cloud base, the local saturation mixing ratio $r^*(T)$ goes to zero and therefore the relative variation in cloud liquid water scales approximately as the relative variation in surface saturation mixing ratio, which is virtually identical

to Clausius-Clapeyron,

$$f \simeq \frac{1}{r^*(T_s)} \frac{\partial r^*(T_s)}{\partial T_s}. \tag{2.11}$$

Although the adiabatic behavior of r_l is an idealization, it gives us a theoretical framework for our expectations to find a significant change in the precipitation efficiency of convective clouds with temperature. As we will see later in this section, relative changes in some of the simple microphysical model parameters such as the time scale of precipitation formation and momenta of the rain droplet size distribution can all be related to the value of f. For deep convective oceanic clouds in which warm processes are observed to be the most important in determining rainfall formation, one could anticipate from this simple model that changes are within a half and third of the changes expected according to the Clausius-Clapeyron scaling (Fig. 2-3.d).

We will relax the assumption of a constant cloud liquid water in the context of the Bowen model and we will estimate some of the continuous growth model parameters using the more realistic vertically varying cloud liquid water profile. Fig. 2-4 shows the effect of the varying cloud liquid water content according to Fig. 2-3. The curves are labeled with reference to the surface temperature instead of cloud liquid water to emphasize that the calculation is now made assuming a reversible moist-adiabatic temperature profile that would be expected from surface parcels having 80% of relative humidity. For the more realistic cloud liquid water distribution, in particular, for the relatively small value of f near the base of the cloud, the model shows slow continuous growth rates (as shown in Fig. 2-4.b) at the beginning and end of the droplet trajectory (compare to Fig. 2-2.b). Not surprisingly, even when we have assumed the collector droplet to start growing at about 1000 m, the final size of the droplet remains virtually unchanged. More surprising perhaps is the fact that the residence time of the collector droplet in the cloud shows a relatively weak dependence on temperature.

The time that takes for a droplet to equilibrate to a particular updraft velocity in these models can be interpreted as a rough measure of precipitation efficiency. *Sun and Lindzen* (1993b) quote a value of $7\%/K$ for the relative change of this parameter in the Bowen model. This time scale will depend of course on the magnitude of the assumed constant updraft and also on the cloud liquid water content. Assuming a vertically varying adiabatic water content reduces the variation of this time scale to about only $1\%/K$. The first correction has to do with the magnitude of the relative variation of the cloud liquid water content with temperature. A second correction

comes from the vertical dependence of the cloud liquid water content. For the regions of the cloud in which approximation 2.9 holds, one can write $r_l \simeq C(T_s)z$ where $C(T_s) = \frac{c_{pd}}{L_v}(\Gamma_d - \Gamma_m)$. Integrating equation 2.2 and replacing l with the adiabatic approximation, one finds,

$$\tau_s = \left(\frac{8\rho_l \ln\left(\frac{w}{kR_o}\right)}{kEC(T_s)w} \right)^{1/2} . \tag{2.12}$$

From the previous equation we see that τ_s scales as $\frac{1}{C^{\frac{1}{2}}}$. Since all the temperature dependence of r_l is contained in C, the relative variation with temperature of C is simply f, and therefore the relative variation of τ_s is simply $-\frac{1}{2}f$ (to the extent that approximation 2.9 holds). This second correction explains the relative insensitivity of the precipitation efficiency time scale to the value of surface temperature over which the adiabatic calculations are made. This insensitivity is a consequence of the relatively steep variation of cloud liquid water content with height near the base of the cloud in this idealized situation. Again, as we go higher up in the troposphere, as seen in Fig. 2-3, clouds can be considered closer to having constant cloud liquid water, and the relative variation in the time scale will also approach f. For colder temperatures, for instance, below zero in Fig.2-3.d, lapse rates are steeper and therefore small values of saturation occur at a relatively low height from the cloud base, and f approaches the Clausius-Clapeyron scaling.

The detection of a surface temperature dependence of the cloud liquid water content in warm clouds that occur in the tropics under the current climate conditions seems to imply that we require to be able to test for a signal that is about a third of the original 6-7 % implied by a Clausius-Clapeyron dependence (Fig. 2-3). Moreover, the detection of a temperature dependence in the time scale of precipitation formation as given by τ_s would require to distinguish an even more modest signal of about $1\%/K$ under current climate conditions. Similarly as seen in Fig. 2-4 the relative change of diameter with surface temperature as predicted by the continuous growth model is also about $1\%/K$, and therefore a relatively small correction to the use of a fixed $Z - R$ (radar reflectivity-rainfall) relationship seems to be suggested from this calculation. Although the results from this simple model seem to be discouraging in the sense that microphysical variations appear to be small with respect to Clausius-Clapeyron, we provide the model as an illustration on how the variations in the boundary layer air forming convection could potentially explain variations in precipitation efficiency of warm clouds. We are not attempting to claim any realism for

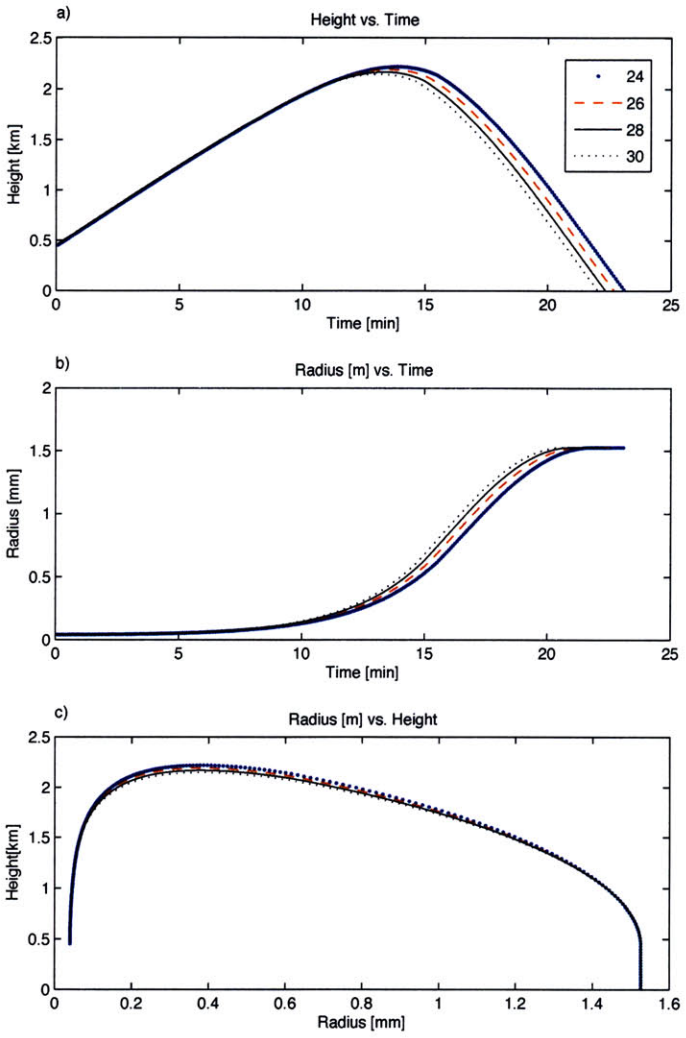

Figure 2-4: Same as figure 2-1 but for an adiabatic cloud liquid water content. The curves are labeled according to the surface temperature of the moist adiabat used in the calculation of the cloud liquid water content. The collector droplet is assumed to start growing 1 km above the base of the cloud. The constant updraft velocity is 2 m/s.

the behavior of the model, rather we present the results as a motivation. It remains to be seen what relevance if any, have these results for the precipitation efficiency of a mesoscale convective system where ice physics plays a major role.

2.3 *Del Genio et al.* (2005)'s conceptual model for the convective detrainment with temperature

In the same kinematic fashion as in the Bowen formulation, *Del Genio et al.* (2005) describe a conceptual two-box model to study the relative partition of condensate between precipitation and detrainment when a fixed constant updraft and a bulk microphysical parameterization are used. This two box model can be considered a very primitive version of a full bulk microphysical parameterization. The interest in looking at this model is twofold. First, it allows us the simplest possible representation of bulk microphysics that predicts the relative amount of detrainment with temperature and second, it provides us with a stepping stone towards more complex microphysical parameterizations such as the ones used in mesoscale convective models.

2.3.1 Description of the model

The model cloud is divided into two regions by the freezing level. The cloud liquid water content in each of the two regions in *Del Genio et al.* (2005)'s formulation is given by,

$$l_l = rh \cdot r^*(T_s, p_s) - r^*(T_f, p_f) \tag{2.13}$$

$$l_i = r^*(T_f, p_f) - r^{\#}(T_{top}, p_{top}) + l_{Dl}\frac{\Delta p_l}{\Delta p_i}, \tag{2.14}$$

where T_f is the freezing temperature, $r^{\#}$ represents the saturation mixing ratio with respect to ice and T_{top} is the temperature of the top of the clouds, and Δp is the thickness of each of the layers, p is the pressure. l_{Dl} is the mixing ratio of liquid water that does not precipitate in the first box. In each of the boxes, it is assumed that the cloud liquid water is completely and instantaneously converted into precipitation-sized particles so that all liquid water follows an exponential (rain droplet size distribution) RDSD, $N(D) = N_0 \exp(-\lambda D)$, that is, conversion from vapor to cloud and from cloud to precipitation occur instantaneously with a efficiency of one. Given the selection of the RDSD, the parameter λ in the distribution is related to the total liquid (or ice) water through,

$$\lambda_{i,l} = \left(\frac{\rho_{i,l}\pi N_0}{\rho_d l_{i,l}}\right)^{\frac{1}{4}}, \tag{2.15}$$

where ρ_d is the density of dry air. Three different hydrometeors are allowed in the model, liquid water, ice-snow and graupel. For simplicity the parameter N_0 is kept as a constant. The relative partition into ice-snow and graupel in the ice layer is, in this formulation, a weak function of T_f in degrees C, $f_i = 0.25(1 - \exp(T_f/10))$. The critical settling velocities are a function of the particle size and therefore, the critical diameter associated to the settling velocity that equilibrates to the constant updraft will determine what fraction of the droplets will precipitate out of each of the layers.

We first note that in equation 2.13, the value of the liquid water content is actually the one at the freezing level under adiabatic and reversible conditions. That is, the value assigned for the cloud liquid water of the warm box is the value at the very top of the box. We have seen in the case of the Bowen model that the variation of r_l for a given temperature scales as α, although in the lower part of the cloud the appropriate scaling is f. A first correction of the model is to introduce a more realistic variation for l_l, for instance, the mass-average cloud water in the liquid region. The cloud water in the ice region is such that the air crossing to the ice part of the cloud is being depleted in the amount l_l of water in the first layer. The cloud water in the warm layer will be partitioned into precipitation and detrainment to the ice layer according to the critical diameter so that $l_l = l_{Pl} + l_{Dl}$, where l_{Pl} and l_{Dl} represent the precipitation and detrainment out of the liquid layer respectively. The cold box will be supplemented by this l_{Dl} amount as well as the condensation that is produced within the layer as given by equation 2.14. We notice again that the quantity $r^*(T_f, p_f) - r^{\#}(T_{top}, p_{top})$ is the value of l_i at the top of the box, and a value representative of the whole box should be used.

2.3.2 Results

Figures 2-5.a and b show the results of the model for the case in which the temperature of the top of the clouds is specified according to the observed variation in the current climate. The cloud top temperature decreases with surface temperature, as the surface buoyancy increases for a relatively constant free tropospheric temperature profile. This will be the situation for variations of temperature within a given climate rather than variations between different climates. Although we are using average cloud liquid water content for each layer, and we are considering variations in density and thickness of each of the layers according to a moist adiabatic temperature profile, our results are qualitatively similar to those of *Del Genio et al.* (2005). For this particular case in which the updraft velocity is relatively small, we observe that most

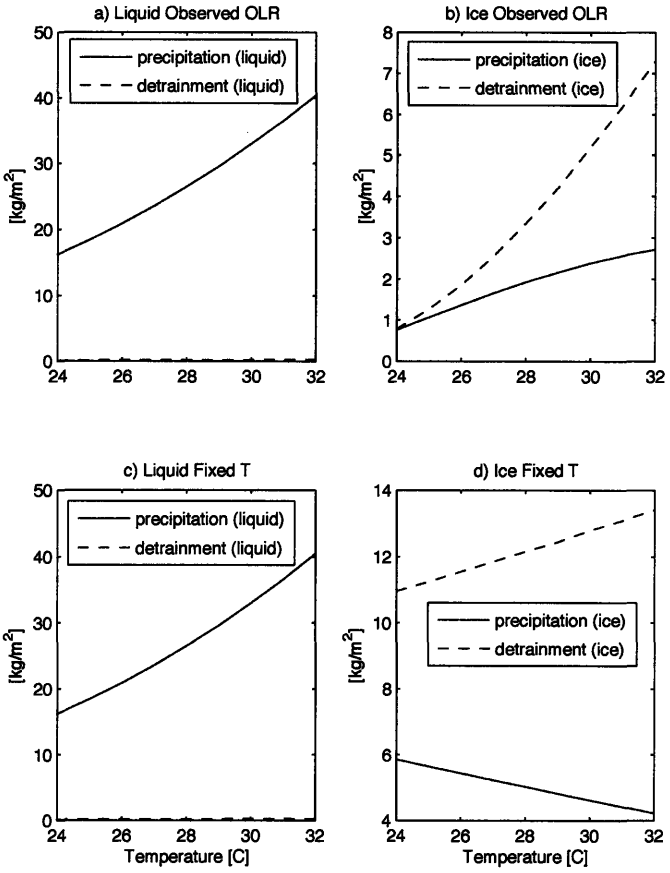

Figure 2-5: Precipitation and detrainment for each of the two model boxes with the two different assumptions about the temperature at the top of the model. The results are for a constant updraft of 2 [m/s]. The top temperature for the fixed case (c,d) is 220 K.

of the condensate that is formed in the lower box is precipitated out of the column and relatively little condensed water is transported upwards (Fig. 6a). In the ice layer the situation is different, the detrainment of ice increases rapidly with temperature so that the relative increase of the detrainment in the ice box is stronger than the increase in precipitation in any of the boxes.

As proposed by Hartmann and colleagues (e.g *Hartmann and Michelsen*, 2002; *Kuang and Hartmann*, 2007) the variation of the temperature of the detrainment of deep convection can be strongly damped by the requirement of the divergence in the vertical to be determined by the vertical gradient of radiative cooling. Since the radiative cooling is strongly dependent on the water vapor content (and therefore on water vapor saturation), radiative cooling is also a strongly dependent on tempera-

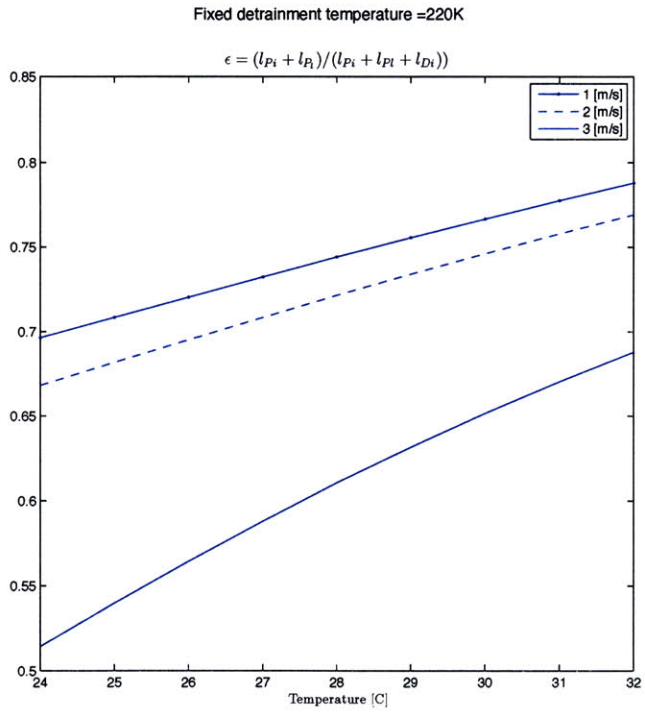

Figure 2-6: Precipitation out of the column for the modified *Del Genio et al.* (2005)'s model. The precipitation is normalized by the total condensate in the column. In this case the temperature of detrainment is fixed at 220 K for all surface temperatures. The curves are plotted for 1, 2 and 3 [m/s] of constant updraft.

ture. Hartmann argues therefore that the temperature at which detrainment occur can not change significantly from one climate to another. In Figs. 2-5.c and d are shown the results when the top box of the model is determined by a fixed temperature of 220 K. The liquid box partition between precipitation and detrainment remains the same since nothing has changed from the previous case. The ice model shows now a different behavior, although detrainment still increases with temperature in absolute terms, the increase in detrainment is no longer faster than the total increase in precipitation.

Figs. 2-6 and 2-7 show the relative change of total precipitation normalized by the total condensate for three different values of the updraft. The detrainment is here normalized by the total amount of condensate in the model, and this is the coarse equivalent to the relative partition of precipitation into convective and stratiform in our observational results (and we will use the same symbol ϵ to refer to it, see chapter 4). We see that the magnitude of the updraft has a strong effect on the magnitude of ϵ and it is larger than the magnitude of the liquid water content, at least for the typical

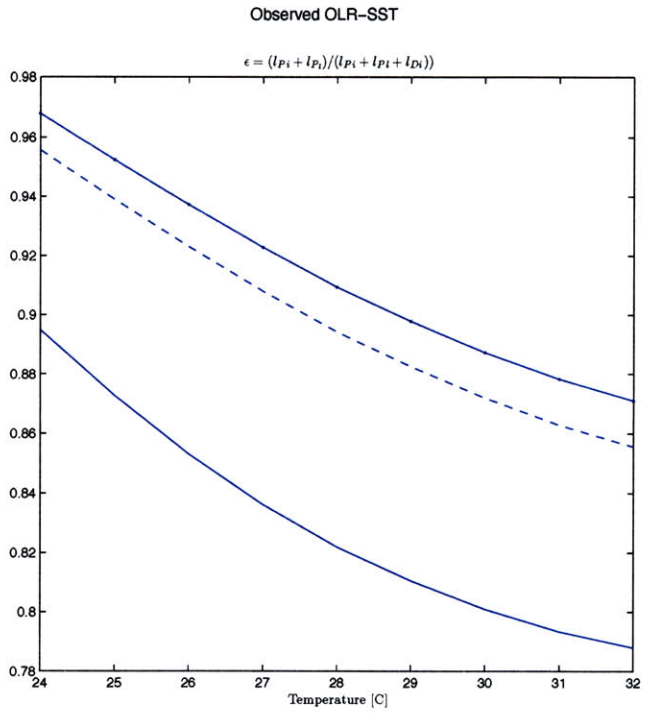

Figure 2-7: Same as Fig. 2-6 but in this case the detrainment temperatures are given by an observed OLR-SST relationship.

variations of a few meters per second considered. According to *Emanuel* (2007) cloud resolving simulations of tropical equilibrium atmospheres show that even though the total convective mass flux can change, the typical velocity of a single updraft does not change significantly for different cooling rate profiles. Recently, *Parodi and Emanuel* (2009) have provided a theory that identifies the terminal velocity of rain droplets as an important parameter in setting the updraft scaling. Therefore, even though the effect of updraft velocity is stronger than the temperature variations, this effect seems to be confined mostly to variations within a given climate. More interesting is the fact that the assumption on how to treat the top of the cloud in the model determines the sign of the change in ϵ.

2.3.3 Discussion

Although extremely simplified, this model allows us to understand some of the consequences of the bulk microphysical parameterizations in the distribution of cloud liquid water and in the fraction of detrainment in convective systems. In this particular model, the partition between precipitation and detrainment and the variation

with cloud water can be simply understood by looking at the mass weighted diameter D_m. If the rain droplet size distribution is exponential with parameters N_0 and λ, such that

$$N(D) = N_0 \exp(-\lambda D), \tag{2.16}$$

then the mass weighted rain droplet diameter is given by $D_m = 4/\lambda$. Therefore, the scaling of D_m with respect to water content is, according to 2.15,

$$D_m \sim l^{1/4}. \tag{2.17}$$

Given this scaling, the relative change in mass weighted diameter is therefore $\frac{1}{4}f$. Since an increase in D_m implies that the relative partition between precipitation and detrainment will increase, an increase in cloud water in this bulk formulation has the same qualitative behavior as the in the Bowen model, and almost the same quantitative behavior. In the fixed temperature case the water content in the ice box decreases with temperature since the decrease in the ice produced *locally* in the ice box can not be compensated by the increase in the cloud water that is imported from the liquid box. Therefore, according to 2.17 a reduction in D_m in the ice box implies an increase in the relative proportion between ice and water in the ice box as implied by Fig.2-6. Again, we do not claim any realism for these models outside the very simple warm cloud physics presented. We use these models to illustrate how variations in the relative fraction of detrainment and precipitation can be controlled by the local surface temperature. In particular, in chapter 4 we will return to this problem from a purely observational approach.

Chapter 3

SST dependence of the tropical cirrus area

3.1 The Iris Hypothesis

Significant open questions remain attached to the poor understanding of cloud processes and in particular to the expected behavior of the area and properties of the tropical clouds under climate change conditions. *Lindzen et al.* (2001) postulated the Iris hypothesis as a possible negative climate feedback acting through tropical cirrus clouds. The hypothesis can be summarized as follows (with numbers referred to the schematic in Fig.3-1.b): (1) Over warm SST regions (as shown in the schematic in Fig. 3-1) mesoscale convective systems are fed by relatively moister air. (2) As we discussed in the previous chapter, a moister boundary layer leads to moister convective clouds and presumably more efficient warm rain processes. (3) The higher precipitation efficiency in a warmer climate was argued to imply a reduction in the amount of condensate detraining at the top of the cloud. (4) This would further imply a reduction in the area of clouds detrained from the updraft in a warmer climate. *Lindzen et al.* (2001) further argued that the area of thin cirrus (which are formed as a consequence of this detrainment) would also decrease. (5) To the extent that thin cirrus clouds have a net positive cloud radiative forcing (due to being mostly transparent to shortwave radiation and mostly opaque to infrared), a decrease in the total area of these clouds in a warmer climate would produce a significant negative climate feedback.

The original observational evidence in favor of the hypothesis was presented in the form of correlations between the sea surface temperature and the area of upper

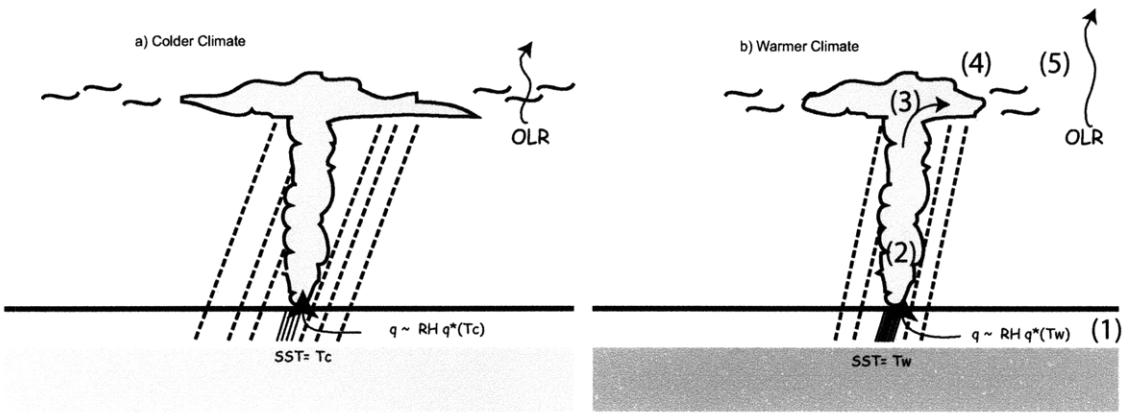

Figure 3-1: Cartoon of the Iris Hypothesis. In a) convection develops over a relatively colder ocean. b) In a warmer climate precipitation in the convective region is more efficient, the detrainment area is reduced and also the area of thin cirrus clouds.

level clouds. The area of upper clouds was obtained from geostationary infrared radiances and defined according to brightness temperature in the 11μm infrared channel. Furthermore, based on the rate of change of the area of high clouds a simple energy balance model was used to estimate the climate feedbacks.

A large number of papers criticizing several aspects of the hypothesis has continued to appear in the literature. The criticism ranges from issues related to the empirical evidence presented in support of the hypothesis to issues about the radiative effect and the possibility to carry the changes observed in current regional variability to the climate problem. These has lead to a number of smaller controversies within the larger issue of the negative feedback mediated by thin cirrus clouds, namely:

- The relation between the area of the upper level clouds and the sea surface temperature was due to the variation of clouds in the subtropical region, unrelated to deep convection (*Hartmann and Michelsen*, 2002). However, correlations between normalized upper level cloud and SST appear to be strong even for regions well within the tropics (*Lindzen et al.*, 2002, and results in this chapter).

- The relation between the area of upper level clouds and the sea surface temperature was not nearly as strong as proposed originally (*Rapp et al.*, 2005; *Su et al.*, 2008). However, these authors use polar satellite data and, as we will

see in this chapter, the correlations can be made too small if sampling is not properly accounted for.

- A decrease in the area of upper level clouds with temperature does not necessarily imply a (strong) negative feedback given differences in the estimation of the radiative properties of the clouds and regions defined in the energy balance model. (*Fu et al.*, 2002; *Lin et al.*, 2004). Some of the issues raised by these papers have been refuted (*Chou and Lindzen*, 2002, 2005), however this criticism has some merit to the extent that, so far, there has been no attempt to test for the iris effect looking directly at the variations of the thin cirrus clouds that have the net positive cloud radiative effect.

- The decrease in area of normalized upper level clouds with temperature is not the relevant measure for calculating the effect in a different climate. Rather the absolute (or global) properties of these clouds are of importance to quantify the climate effect. (*Del Genio and Kovari*, 2002; *Del Genio et al.*, 2005). This issue was already explained in the original iris paper: in order for the magnitude of the feedback to be meaningful for the climate problem, the upper level cloud variation needs to be normalized by a measure of convective activity. In the next section we will discuss the issue of normalization in more detail, in particular the observational and theoretical limitations for the use of precipitation as a normalization measure.

3.2 Normalizing the area changes by a measure of convection

In the absence of SST gradients, one expects convection to be distributed homogeneously over the tropical oceans and the amount of convection to be determined by the free troposphere energy balance. In reality, SST is not homogeneous and SST gradients can pattern convection by providing low level convergence (*Lindzen and Nigam*, 1987). In studying variations in the amount of detrained clouds with respect to SST (regardless of the gradients), one must first remove the dependence of the convergence (and therefore the dependence of the amount of convective activity) on the underlying SST gradients. *Lindzen et al.* (2001) illustrated this point by focusing on cloud variations in only one hemisphere, where the relation between cloud area and SST is overwhelmingly controlled by the migration of the ITCZ. After applying

a normalization, the tropical and hemispheric results showed a very similar variation with SST.

In order to see that local SST does not form a useful surrogate for variations in SST associated with global temperature change, we will focus on the tropics and consider a particularly simple idealization. We will consider two climate states for the tropics, each characterized by a constant SST: one cool and the other warm (Fig. 3-2.a and b). In steady state, the balance of water vapor below the trade inversion includes a source from surface evaporation and a sink from convection (*Sarachik*, 1978; *Held and Soden*, 2006) [1]. When average values are taken and the tropics are considered in isolation, convergence of water vapor cancels out and the balance between the surface evaporation and the vertical convective transport implies,

$$\overline{M_c} = \frac{\overline{E}}{q_m} \tag{3.1}$$

where $\overline{E}$ is the average evaporation and q_m is the specific humidity in the well mixed region below the trade wind inversion (*Schneider*, 1977; *Sarachik*, 1978).

If we take evaporation E to be approximated by a bulk aerodynamic formula (with a constant drag coefficient C which buries the effect of the mean wind and gustiness), one can write

$$\overline{E} = C(q_s^* - q_m) \tag{3.2}$$

where q_s^* is the saturation value of specific humidity near the surface. If one neglects the temperature difference between the surface and the mixed layer, then $q_m = q_s RH$, where RH is the relative humidity of the mixed layer. Then, equation 3.1 can be rewritten as,

$$\overline{M_c} = \frac{C(1 - RH)}{RH} \tag{3.3}$$

[1] We will consider this idealization for the sake of argument. In reality, subsidence of air entraining at the top of the boundary layer can also modify the water vapor balance. Including this effect will make $M_c = \frac{C(1-RH)}{RH}\frac{q_m}{\Delta q}$, where Δq is the difference between the mixed layer specific humidity and the humidity just above the mixed layer. For instance, in the quasi-equilibrium model of *Betts and Ridgway* (1989), Δq increases at a steeper rate than evaporation, and therefore a decrease in M_c is implied from this model. Global circulation models (*Held and Soden*, 2006) as well as observations (*Vecchi and Soden*, 2007) seem to agree on a decrease in M_c for a warmer climate. The main argument of this section, that is, the need for normalization when cloud effects are considered for a partial region of the tropics, does not depend on the correctness of this model, and we will indeed argue later in this section that precipitation is perhaps closer to invariant than the mass convective flux.

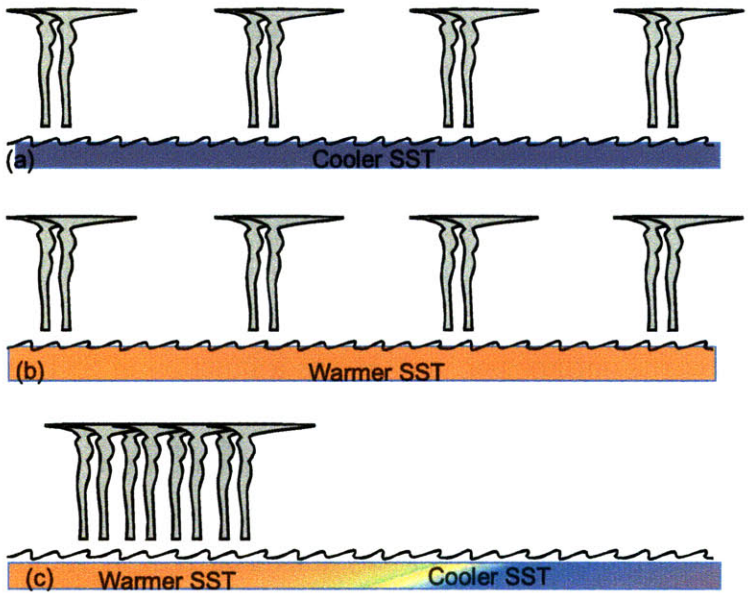

Figure 3-2: Schematic of three different idealized climates.

Thus, under the (strict) assumption of a constant relative humidity in the mixed boundary layer and neglecting the subsidence contribution to the water vapor balance in the boundary layer, M_c will be the same for both idealized climate with homogeneous SST distributions. Now let us consider a more realistic climate characterized by warmer and cooler regions. Such a situation is illustrated schematically in panel c of Figure 3-2. Convection is concentrated in the warmer region which has a greater M_c than the cooler region (for which M_c is essentially zero). The reason for this is that when there are horizontal inhomogeneities in surface temperature, then the left hand side of eq. 3.1 must also include the horizontal convergence of moisture in air that is potentially convective. As noted in *Lindzen* (1988) this consists primarily in moisture convergence below the trade inversion. *Lindzen and Nigam* (1987) showed that the motion induced by gradients of SST could produce such convergence, but as noted by *Lindzen* (2003), even when this convergence is insufficient to fully concentrate convection, such convergence can be supplemented by convergence induced by the convection itself. However, it should be noted, in view of eq. 3.1 that even though the value of M_c increases locally due to the additional contribution of the convergence, the possibility of creating or suppressing overall convection (that is changing the value of $\overline{M_c}$ averaged over the whole domain) is very limited even in the case of the non-homogenous SST distribution depicted in Fig. 3-2.c, since $\overline{M_c}$ is bound to satisfy a global balance. However, the main point is not the invariance of M_c which is a feature of this simple idealization, but rather that M_c in the lo-

cally warmer region in Figure 3-2.c will be larger than the locally M_c in a warmer climate depicted in Fig. 3-2.b. This is true not only for this particular model, but for every model and also for nature. Overall, we expect more cirrus to be associated with regions of locally larger values of M_c. Under the circumstances, it would also be inappropriate to associate the cirrus outflow in the warmer region in Fig. 3-2.c with that which might occur in a warmer climate. A potentially correct alternative would be to determine the cirrus outflow per unit M_c (that is to normalize by M_c). The resulting cirrus outflow per unit M_c, as a function of SST, might be associated with climate change. The appropriateness of this procedure depends on three further issues. The first is practical: namely, how does one measure M_c? The second is more theoretical: namely any relation between normalized outflow and climate requires that the observed relation be essentially universal (i.e. it should be quantitatively the same regardless of the situation being measured). The third issue involves the quantification of a climate effect given that we know the normalized effect with SST. The assumption that relative humidity does not change with changing climate under the present model seemingly eliminates this difficulty. However, equation 3.3 suggests significant sensitivity to this assumption, pointing to the relatively important role of the dynamics of the boundary layer and its interaction with convection leaving open the possibility that $\overline{M_c}$ might not be a climate-invariant quantity. In fact, as we have pointed out at the beginning of this section, boundary layer quasi-equilibrium theory predicts a decrease in the mass convective flux with increasing temperatures (*Betts and Ridgway*, 1989; *Betts*, 1998).

3.2.1 Sensitivity to boundary layer relative humidity

In the context of the simple idealization of the tropical climate presented in the previous section, M_c is a climate invariant as long as RH is constant. However, the assumption of constant RH cannot be easily relaxed in this simple model. If we write the percentage change of M_c as $\delta M_c/M_c$ differentiating equation 3.3 we find,

$$\frac{\delta M_c}{M_c} = -\frac{\delta RH}{RH(1-RH)}. \tag{3.4}$$

For values of humidity near saturation we see that M_c is sensitive even to small changes in RH. So for instance for $\delta RH = 0.01$ at $RH = 0.8$, Mc decreases by 6.25%. This amplification of the change in M_c comes directly from the sensitivity of evaporation to relative humidity which can be similarly written as $\left(\frac{\delta E}{E}\right)_{T=constant} = -\frac{\delta RH}{(1-RH)}$. The high sensitivity of the evaporation to the relative humidity of the mixed layer,

as long as the the aerodynamic formula is appropriate, was already recognized as a critical factor in the heat budget of the tropics by *Hartmann and Michelsen* (1993). This high sensitivity is in fact at the heart of the reasoning invoked to justify the relative invariance of the relative humidity in the mixed layer (e.g *Held and Soden*, 2000; *Schneider and O'Gorman*, 2007). One can not change the relative humidity by a large amount without disrupting the surface heat balance through a large change in evaporation. For instance, in order to balance an increase of 1% in relative humidity, for a typical value of the latent heat of 100 W/m^2, a net reduction of 5 W/m^2 would be required. The decrease in the latent heat flux produced by a mere 1% increase in relative humidity is equivalent to the decrease in the latent heat flux of a surface cooling of about 0.8 K. This illustrates the significance of the relative humidity of the mixed layer at least in the context of the simple model.

3.2.2 Relation to dynamic-thermodynamic component of cloud changes

From the previous discussion we see that in this particular simplified model of the tropical circulation, under the assumption of constant relative humidity and neglecting the effect of the subsidence on the water vapor budget of the boundary layer, M_c is a nearly invariant quantity to homogeneous changes in the surface temperature. Therefore, the role of large scale temperature distribution in equilibrium would appear to be limited to pattern or concentrate convection that is constrained by the large scale balance to occur. We can see how this picture plays into the dynamic-thermodynamic separation of cloud effects that has been proposed by *Bony et al.* (2004) as a method to disentangle the covariation of local and spatial distribution of temperature in the cloud properties.

Bony et al. (2004) considered the the change in cloud properties from one climate to another can be written as the sum of 3 terms, where ω is a proxy for the vertical velocity and C is some cloud property as,

$$\delta C = \int P_\omega \delta C_\omega d\omega + \int \delta P_\omega C_\omega d\omega + \int \delta P_\omega \delta C_\omega d\omega \tag{3.5}$$

C_ω and P_ω are the value of the cloud property and the particular probability distribution of finding a certain vertical velocity ω. The first two terms are the thermodynamic and dynamic component of the cloud changes as they named them. We see that the dynamical component contains the changes associated to the variations in the distribution of the vertical velocity proxy.

We can argue on the basis of the idealized model that the first term is generally small when C is a cloud property that is *extensive* on the amount of convection, that is if we can suitable regard C as approximately proportional to the amount of convection in a particular region. This is the case, for instance, with variables such as the cloud fraction and presumably the cloud radiative forcing as well. If we compare the situation between the warm and the cold case in Fig.3-2, neither the area of the tropics nor the total amount of convection changes, the term δP_ω is zero and all observed changes would be by definition thermodynamic. On the other hand, when comparing the situation between an homogeneous case and the case in which a partial fraction A of the area of the tropics has a warmer temperature, we see again that the increase in mass convective flux relative to the homogeneous case will be M_c/A^2, so that δC_ω will be in direct proportion to the area increase, whereas P_ω will be in inverse proportion to the area A, canceling each other out. Although the realism of the simple model presented can be questioned, more sophisticated models give compelling evidence about the limited role of changes in circulation. In particular, *Clement and Soden* (2005) studied four different GCMs concluding that only very large changes in the intensity of the Hadley circulation could explain observed decadal changes in OLR (*Wielicki et al.*, 2002, although further corrected by *Wong et al.* (2006)), therefore showing evidence of the relatively minor role that changes in circulation play in the average radiative effect of clouds. A similar point was raised by *Chou and Lindzen* (2005) in response to *Lin et al.* (2004). From the previous arguments and the body of results that have accumulated, one can anticipate that the source of uncertainty in cloud radiative feedbacks in current models lies in the dependence of clouds in the local thermodynamic effects, rather than in the differences in the global dynamics.

3.2.3 Global Relation between M_c and precipitation

One can relate the tropical mass convective flux and the total precipitation through the heat balance in the tropical free troposphere,

$$\int M_c \frac{\partial s}{\partial z} dz = LP \tag{3.6}$$

If we regard M_c as constant with height and also noting that the integral of is simply Lq_m (e.g *Sun and Lindzen*, 1993a) we recover the balance of equation 3.1

[2]Strictly speaking there will be a change in M_c related to the fact that the evaporation is the total evaporation over the tropics whereas the humidity that is transported upwards is the humidity that participates in convection and therefore one could write $M_c \sim C \frac{Aq_s(SST1)+(1-A)q_s(SST2)}{q_s(SST1)} \frac{(1-rh)}{rh}$

except that now instead of evaporation we have precipitation. This is essentially the simple model used by *Held and Soden* (2006) to study the robust responses of the hydrological cycle to climate change. They claim on the basis of coupled climate model results that the total precipitation increases at a smaller rate (2%/K) than the Clausius-Clapeyron scaling. Given the simple balance $P = M_c q_m$, one can write the fractional change of precipitation as,

$$\frac{\delta P}{P} = \frac{\delta M_c}{M_c} + \frac{\delta RH}{RH} + \frac{\delta q_s}{q_s} \tag{3.7}$$

We see that under a strict assumption of constant relative humidity (and neglecting changes in gustiness (circulation) buried in the constant C in the bulk aerodynamic formula 3.2) the fractional change in precipitation scales as Clausius-Clapeyron. One can obtain a value of $\delta P/P$ of 0.02 similar to the behavior of the climate models in Held and Soden (2006), if an increase in the surface temperature of 1 K is accompanied by an increase in the relative humidity of a mere 0.8 %. In fact, in the context of global climate models, P is closer to invariant than M_c. M_c decreases with warming at rate needed to almost compensate the C-C increase in the third term of equation 3.7. Perhaps, a more fundamental argument for the small change in the relative rate of change in precipitation has been recently offered by *Stephens and Ellis* (2008). The balance in 3.6 can be also written as the balance between the latent heat released in the free troposphere and the cooling rate in the clear regions of the tropics (e.g. *Emanuel et al.*, 1994). Since the cooling in these regions will be mostly controlled by the behavior of water vapor, and water vapor emission does not scale linearly with water vapor content but rather with a power law with a exponent close to 0.5 (*Stephens and Ellis*, 2008), even if column water vapor follows C-C in a warmer climate the increase in radiative cooling will be much smaller. This analysis does not include the role of possible cloud feedbacks. As discussed in *Stephens and Ellis* (2008) as we will also see later in chapter 5, clouds can potentially change both the surface energy budget and the radiative cooling rate so that changes in precipitation much larger than 2%/K to 3%/K are also possible. Therefore, when attempting to quantify a cloud feedback, even when the results are normalized they would need a further correction due to the lack of invariance of convective activity (either M_c or P). Given that precipitation is a variable that can be measured and estimated from space much more easily than mass convective flux, we simply take the practical approach of choosing precipitation as the normalization measure for the observational results that follow.

3.3 Using TRMM orbital data to test for the Iris Hypothesis

In the remainder of this chapter, we perform an independent analysis of variation of cloud cover with SST using TRMM infrared radiances. We focus on attempting to replicate the results by *Su et al.* (2008) and *Rapp et al.* (2005) (whose methodologies are based in *Lindzen et al.* (2001) but differ from it in some important aspects). Here, we address some of the methodological issues expected to play a role in identifying a correlation between SST and cloud cover.

Su et al. (2008) study the variations with SST of upper tropospheric cloud fraction, ice water path, and ice water contents using data from the Atmospheric Infrared Sounder (AIRS) on the Aqua satellite and find that the normalized cloud area decreases at a rate of $\sim$ -2%/K with SST, therefore showing only a weak dependence of the normalized upper tropospheric cloud area with SST.

Previously, *Rapp et al.* (2005) studied the behavior of "individual storms" by classifying storm area using infrared brightness and precipitation from the TRMM-PR, also finding a relatively weak relation between the normalized area and SST.

3.3.1 Data

We use infrared data from the visible and infrared scanner (VIRS) on board the Tropical Rainfall Measuring Mission Satellite (TRMM) (*Kummerow et al.*, 1998). The data is brightness temperature (BT) measured from the channel 4 of the VIRS instrument at a wavelength of about 11 μm (1B01 product, version 6). The VIRS instrument has a horizontal resolution of $\sim$ 2 km. We use data from January to March 2001. We also make use of TRMM Microwave Imager (TMI) SST and precipitation data, to match *Su et al.* (2008) methodology that requires precipitation instead of brightness for normalization of the cloud fractions. Both instruments, AIRS and TRMM, have similar coverage over the tropics, although since TRMM is in a non-sun-synchronous orbit, it allows sampling of the diurnal cycle (*Imaoka and Spencer*, 2000) as opposed to the sun-synchronous orbit of AIRS that samples only around 01:30 and 13:30 LST. In *Su et al.* (2008) upper level cloud fraction is defined as the fraction of clouds below 300 hPa in pressure. Here we will use BT thresholds to define the anvil clouds as in *Lindzen et al.* (2001).

τ [days]	1	2	5	10	15	30
Gridded [%/K]	-6.7	-7.4	-11	-14	-15	-19
Binned [%/K]	-21	-22	-26	-26	-27	-27

Table 3.1: Slope of the correlations between the normalized upper level cloud area as a function of the integration time τ, for the gridded and binned data. The regressions are robust non-linear least-square fit of an exponential as shown in Fig. 3-3.

3.3.2 Results using VIRS and TMI data

The sampling of the orbital satellites (with revisit times of about 1 to 3 days for the relevant scales) does not allow one to capture the evolution of any individual mesoscale convective system. Therefore, there is a need for integrating the results of many convective systems either in time, in space or both. The main assumption here is that by adding sufficient samples for a particular area or for a particular SST bin one is increasingly compensating for the sampling error (we will return to this point in section 3.4).

Before attempting to replicate *Su et al.* (2008) methodology, we will use two different approaches to find the variation of the upper level cloud cover with SST. First, for each 1°×1° grid in the region between 15°S-15°N, the values of A(220<BT<260) (that is, the area of pixels having brightness temperatures between 220 and 260 K) are added over a period of time that ranges from 1 to 30 days (we call this time the integration time) and then cloud cover is normalized by the sum of the area of brightness temperature below 220 K, A(BT<220). We call this the gridded data. Figure 3-3 presents the results for an integration time of 30 days. The variation of the gridded data with SST shows a large scatter. In fact about 10% of the data are outside the upper bound of the plot, corresponding to grids with very few deep convective clouds over that particular sampling region/interval). Second, we construct the binned data by adding all values of A(220<BT<260) with temperatures within 0.5 C of the observed SSTs and normalizing by the sum of A(BT<220) over each bin. The slopes of the regressions are calculated by fitting decaying exponentials using robust non-linear least-squares (since the regressions are exponential, the reported rates of change are constant over the SST range). Both the gridded and the binned regressions show a significant decrease in the area of anvil per unit area of convection (-19 %/K and -27 %/K respectively). The 95% confidence interval for the slope of the binned data regression is -22%/K to -32 %/K. These numbers are consistent and independent from the original area effect documented in *Lindzen et al.* (2001) using geostationary data. The magnitude of the slope of the regression increases signifi-

cantly with the integration time for the gridded data (see Table 3.1). For the binned data, *the slope of the regression is only weakly sensitive either to the integration time or to the size of the grid*, and therefore the quantitative results using the binned data appear free from spatial truncation artifacts described by *Del Genio et al.* (2005).

The previous procedure has allowed us to recover a signal that is quantitatively similar to the one found in *Lindzen et al.* (2001). We now apply *Su et al.* (2008) methodology to the same dataset, that is, we calculate the fraction of anvil and convective cloud as defined by the brightness temperature thresholds, then we calculate a cloud weighted SST for each day over the 15°× 15° region. Next, we use TMI precipitation data that is coincident with TRMM-VIRS brightness temperature to calculate mean precipitation over the tropical oceans and we normalize the mean cloud fractions by the mean precipitation. In Figure 3-4.a we show the result of this procedure for both the total anvil area (blue dots) and for the anvil area excluding deep convective regions (black dots). We find a negative slope of about -6%/K that should be compared with *Su et al.* (2008)'s result of -2%/K. The resulting values for the slopes are similar so as to suggest that we have replicated the results of *Su et al.* (2008) analysis. Nevertheless, we will discuss in the next section several issues that might favor a larger effect than the one found by using *Su et al.* (2008) methodology.

3.4 Sampling and the lifecycle of mesoscale convective systems

Besides a physical reason behind the apparent disconnect between precipitation and cloud there is also a sampling issue. At the scale of each 1°× 1° grid, the twice-daily observation provided by the Aqua satellite is inadequate to capture the evolution of a mesoscale convective system.

A mesoscale convective system over the oceanic Kwajalein region will serve to illustrate this point (Fig. 3-5). The Kwajalein radar covers a mostly oceanic region which is about the same size as a 2.5°× 2.5° grid. The reflectivity measured by the Kwajalein radar is converted to rainfall rate and each rainy pixel is classified into convective and stratiform (*Steiner et al.*, 1995; *Yuter and Houze*, 1997; *Houze et al.*, 2004). The sequence in Fig. 3-5 depicts a period of 48 hours, and each panel corresponds to a snapshot taken from the radar data every 3 hours (the actual time resolution of the radar is about 10 min and all data was used to produce the curve in Fig. 3-5.a). Three different stages similar to the ones described by *Houze* (1993) can

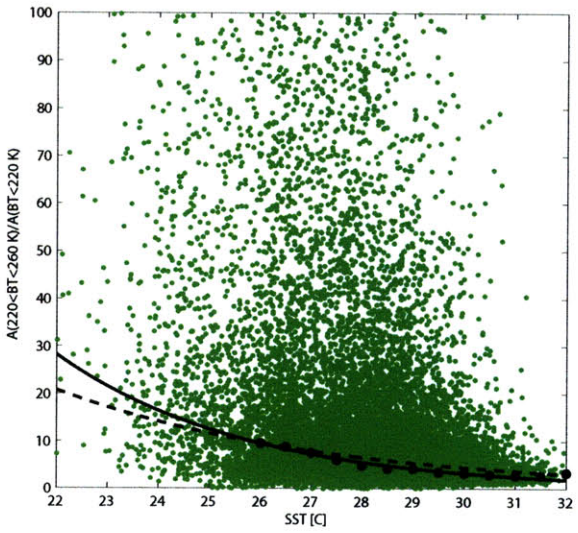

Figure 3-3: Scatter plot of the fraction of anvil clouds A(220K<BT <260K) normalized by A(BT<220 K). The data is for January to March 2001 for oceanic regions between 15° S and 15° N. Green dots represent the value of A(220K<BT<260K)/A(BT<220K) for individual 1 °× 1° grid over the course of a whole month. These results are referred as to gridded. The black dots are the result of adding the areas for all data within 0.5 C SST bins, (the sum carried over the whole 3-month period for all 1 ° × 1° grids within the monthly average SST for each bin). The black curves are non-linear least-squares fit for the gridded data (dashed line) and for the binned data (solid line).

be distinguished from the figure. In the formative stage from 0 to about 12 hours, strong radar echoes (corresponding to individual convective updrafts) are scattered around the radar area and have little structure; most of the precipitation falls from these convective updrafts. As enough condensate is detrained from the top of the convective updrafts, a common stratiform region can be sustained and the system develops a structure with an identifiable line of storms and a trailing stratiform region (12-24 hours). Finally after 24 hours, both the weakening of the convective activity and the propagation of the active line of storms outside the region covered by the radar are evident. Most of the precipitation at this stage is stratiform.

Although we show the evolution of the system in terms of area of stratiform and convective precipitation rather than detrainment and convective cloud, the following arguments can be equally applied to the relation between the convective clouds and the non-precipitating parts of the anvil cloud. For a given instant in time, the fraction of convective precipitation to the total precipitation can vary widely (as it is the case with the variation of any measure of detrainment area normalized by convective

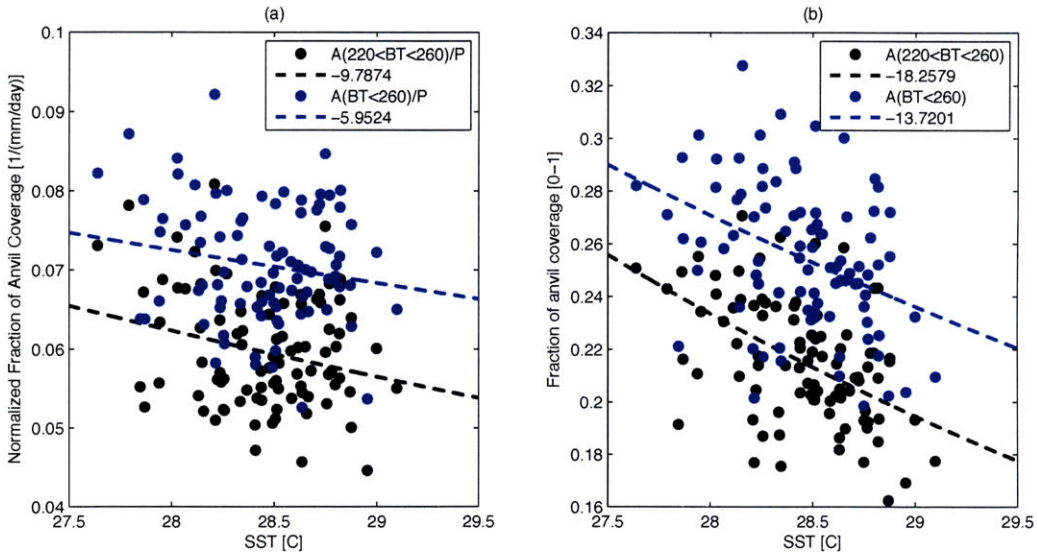

Figure 3-4: Scatterplot of mean cloud fraction and cloud weighted SST, using TRMM VIRS brightness temperature and TMI precipitation data. The curves are non-linear least-square fits of a decreasing exponential for each of the corresponding variables (a simple linear regression gives quantitatively similar results in all cases). For the blue dots, cloud fraction is defined using all pixels colder than 260 K. For the black dots the area is defined as the pixels between 220 K and 260K. Panels a) and b) show the normalized and the non-normalized cloud fractions, respectively. The figure is for the 15°S- 15°N region in the tropics.

activity, see Fig. 3-5.c). Therefore the snapshot values are of little interest for quantifying an SST-dependence, as it is almost guaranteed that any possible value will be observed at some instant over the lifecycle of the storm.

Nevertheless, individual snapshot observations were used by *Rapp et al.* (2005) to study the normalized area variations with SST. *Su et al.* (2008) cite this study as consistent with their own results. The interpretation of the lack of signal in the study of *Rapp et al.* (2005) is problematic due to the large scatter that arises from correlating the snapshot values with local SST. We must note however, that the increase in scatter does not automatically prevent one from finding a signal. Our own approach to these difficulties is not free from limitations either; the binning of all samples at the same SST regardless of the spatial location, and the integration over a period encompassing enough samples, both require us to combine the properties of different mesoscale convective systems to compensate for the sampling error. Moreover, choosing the right integration period in the gridded analysis is a compromise between reducing the sampling error and keeping a dynamical connection between convection and average SST at the convective scale.

By adjusting the integration time of the gridded data analysis we can indirectly quantify the impact of the sampling error in the correlations (at least in our own analysis). We find that the signal is about -7%/K for integration times of 2 days (which for TRMM contains only about 2 snapshots of the size of Kwajalein) and increases in strength close to -14%/K after an integration period of about 10 days (see Table 3.1). One could still entertain the possibility that the decrease in slope is a real dynamical effect rather than the effect of the sampling (for instance a cloud shading effect on SST, as suggested by one anonymous reviewer). Two pieces of evidence argue against a dynamical effect. First, when the data are binned, even the 1-day gridded data exhibit a relatively large slope. In other words, when the sampling error is increasingly canceled, one recovers the original magnitude of the signal. Second, when using the relatively high temporal sampling of the Kwajalein radar dataset, the slope of the cloud cover variation with temperature is only weakly dependent on the integration time (see section 4.3).

Nevertheless, we further investigated the effect of sampling by analyzing a year of geostationary data over the tropical western pacific (see appendix A). We find that the results suggest the possibility of a bias probably due to the combined effect of coarse sampling and a diurnal cycle in convection (although other causes for the bias could also be envisioned). The bias can either overestimate or underestimate the value of the slope depending on time of the day of the images selected for the calculation. However, the bias is largely reduced in our analysis when the normalization measure is calculated using nearly full sampling as done by *Su et al.* (2008).

Many of the difficulties associated with spatial and temporal sampling in our present analysis as well as in *Su et al.* (2008) have been controlled in a recent study conducted by *Horváth and Soden* (2008). They diagnosed the relation between anvil cloud normalized by the area of deep convection using a Lagrangian framework, benefiting from the sampling of geostationary satellites and using brightness temperature thresholds to define the cloud categories. From their plots (in particular their Fig. 11.a) one can estimate a decrease in the relative area of cirrus (defined using temperature thresholds) of about -17%/K between what they define as the cold and medium categories, and of about -5%/K between the medium and warm categories. These estimates are roughly consistent with the results shown here and also with *Lindzen et al.* (2001) and indicate a significant reduction of the anvil area normalized by convection with SST. Nevertheless, the lower bound estimate of the slope from the *Horváth and Soden* (2008) data is not very different from the *Su et al.* (2008) tropical-wide estimate. These two results might be reconciled by a simple change in

the definition of the area of the cirrus anvil, as we will see in the next subsection.

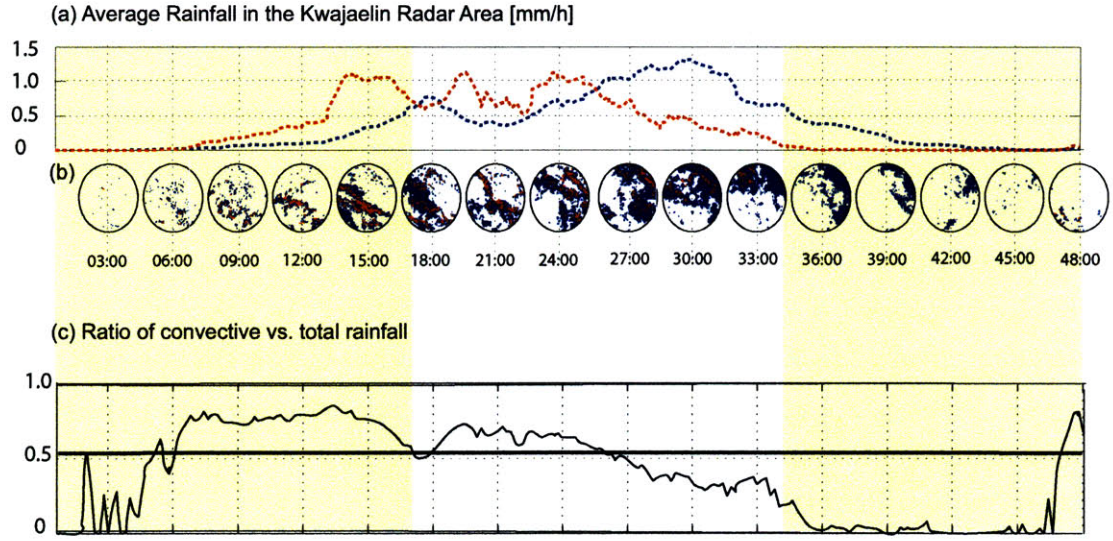

Figure 3-5: a) Evolution of the convective and stratiform rainfall over the Kwajalein radar region for the period between April 9 2003 00:00 Z to April 11 2003, 00:00 Z. b) Panels showing the rainfall area over the Kwajalein area classified into convective (red) and stratiform (blue) regions. Panels are separated from each other by 3 hours and time is labeled in hours from April 9 2003 00:00 Z. c) Instantaneous fraction of convective rainfall over total rainfall. The thick black line is the integrated value of the variable over the period.

3.5 Defining the area of the anvil cloud

Since the area of active convective cores is small compared to the area of the anvil, correlations are expected to be largely insensitive to whether or not convective cores are separated from the anvil when considering the area variations. For instance, for the linear correlations between the stratiform area in Kwajalein reported in chapter 4, the magnitude of the slopes decreases from -26%/K to about -22%/K when convective cores are included in the anvil region (and a similar small effect is shown in *Lindzen et al.* (2001)). We see in Fig 2.b that both the area of anvil and the area of anvil including convective cores decrease with cloud weighted SST for the whole tropics but the area of anvil decreases more rapidly with temperature. Consistent with this behavior, the normalized value of the area in Fig.3-4.b decreases at a larger rate of -10%/K.

3.6 Tropical-wide quantification of a local convective scale effect

An additional difficulty arises when one uses the whole tropics (or a region much larger than the scale of a single mesoscale convective system) as a testbed for the variations in the high cloud cover that occur at the local convective scale. The cloud-weighted SST (or any other averaging procedure) acts to filter the local signal. To be sure, this effect is not substantial, but reduces the magnitude of the signal, and we have estimated it quantitatively using synthetic data. We first draw independent values of SST from a normal distribution with a mean of 27° C and standard deviation 1.6° C (similar to current climate values for the region between 15°S-15°N. SST values are independent from each other so we assume no spatial correlation). We then assume an exponential dependence between the normalized cloud fraction and the local SST with a specified rate of change, so that each synthetic SST value corresponds to a normalized cloud fraction. (Notice that for the purpose of estimating the effect of the averaging alone, we are assuming that this exponential relation is satisfied perfectly at the local scale and therefore we are neglecting the sampling error that we discussed in section 3.4). Then we calculate the cloud weighted SST to find the relation between the tropical cloud coverage and the tropical cloud weighted SST. For the case of an exponential dependence with a rate of change of -28%/K such as the one shown in Fig.1 for the binned data, one recovers a relation between cloud weighted SST and averaged normalized cloud fraction that has a rate of change of about -22.5%/K. For a local -22%/K rate of change, as deduced now from the gridded data, one obtains a global rate of change of -19.5%/K. (These particular numbers are not sensitive to the size of the sample.) The effect of the averaging in the strength of the tropical-wide signal is proportional to the magnitude of the local signal.

3.7 Results using snapshots of individual storms

Rapp et al. (2005) studied the relationship between SST and the normalized area of individual storms in an attempt to test for the Iris hypothesis. They defined single core storms as those having at least one pixel with rainfall higher than 10 mm h^{-1} and measured the upper level cloud area defined by brightness temperature thresholds. They found no evidence for a negative correlation between upper level area and SST. The rationale behind studying single core systems is that by isolating the behavior of a single convective cloud one can confidently attribute the upper level cloud region

to the identified convective core. After the discussion in section 3.4 the difficulties with this approach should be evident. The situation in which a single convective core is observed represents only a fraction of the life cycle of the system. Moreover, by selecting a threshold precipitation for convection one is truncating both the initial and the final stage of development of the system.

Using TRMM PR and VIRS data, we replicated the analysis by *Rapp et al.* (2005). As in their study, we find very low correlation coefficients for the regressions, although a slope can still be discerned from the correlations. A bias is evident from the plots in Fig. 3-6. As one increases the value of the threshold to classify convective cores, the slope increases from 5%/K for a threshold of 10 mm h^{-1} to about 20%/K for threshold of 30 mm h^{-1}. However, when no truncation by precipitation rate is performed, that is when the threshold is 0, the slope of the correlation becomes negative with a magnitude of about -20%/K. Again, when the results are binned according to SST, the scatter is significantly reduced. In particular the two set of large dots in the panels in Fig. 3-6 show two different ways of binning the results. The gray large dots represent taking the average of the individual storms as in the study by *Rapp et al.* (2005) and the black dots are the sum of the area and precipitation for each bin.

3.8 Concluding Remarks

In this chapter we have used TRMM orbital infrared radiances as well as GMS-5 geostationary infrared radiances to study the discrepancy between the estimates of *Rapp et al.* (2005); *Su et al.* (2008) and *Lindzen et al.* (2001) for the variation of the normalized upper level cloud area with SST. We have replicated the results of *Rapp et al.* (2005) and *Su et al.* (2008). Contributions from the separation of deep convective clouds and anvil, and the effect of the cloud weighted SST seem to explain only a few percent of the discrepancy. On the other hand, we find that the slope of the regressions is sensitive to the integration time in the gridded analysis. If this sensitivity is due to the cancellation of the sampling error, it would suggest that the small negative dependence between upper level cloud area and SST found by *Su et al.* (2008) could be reconciled with larger values by simply increasing the sampling size at the grid scale, and therefore reducing possible biases associated to the coarse sampling. We quantify the magnitude of the diurnal cycle bias using geostationary satellite data. Also, we find a large bias due to the use of a precipitation threshold in the analysis by *Rapp et al.* (2005). Besides showing that results by *Rapp et al.* (2005) and *Su et al.* (2008) are not robust to changes in the methodology, we provide additional

confirmation for the decrease with SST of the upper level cloud area normalized by convection, as documented originally by *Lindzen et al.* (2001).

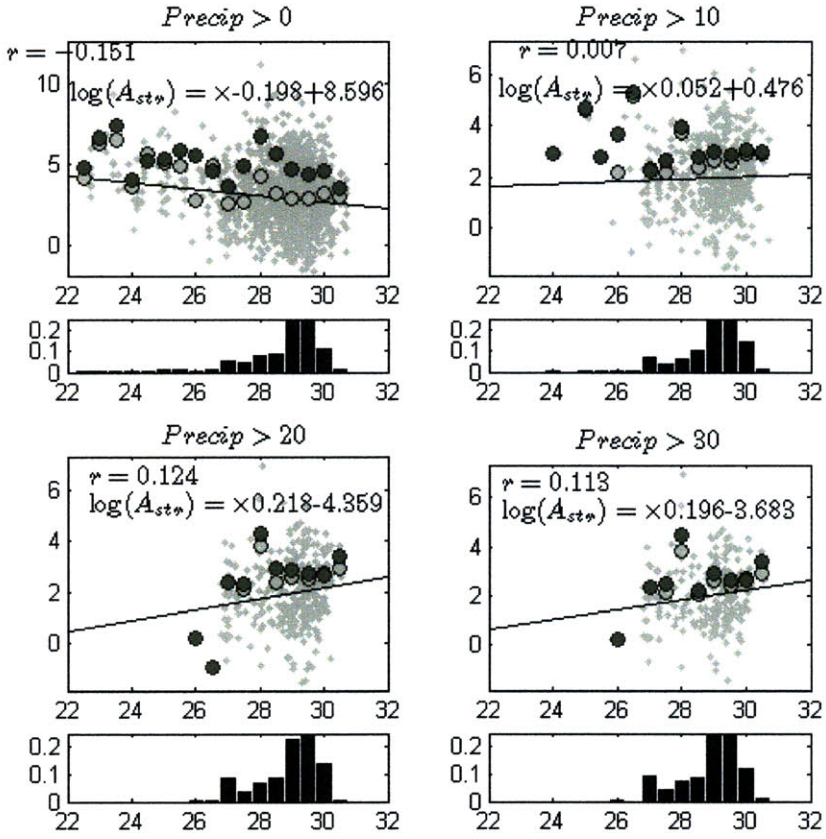

Figure 3-6: Analysis of the sensitivity of correlations between SST and normalized cloud area (see the text) to a threshold in the precipitation intensity of individual "storms" as in *Rapp et al.* (2005). The small light dots and the corresponding linear regressions are for the individual storms within a PR-TRMM swath over a period of 1 month and for oceanic regions within 20°S and 20°N. The large dark dots correspond to the mean of the individual storms for bins of SST. The large light dots are the binned values for the storms. The histograms below each panel show the frequency of the individual storms with SST. The panels are for the precipitation threshold indicated in units of mm h^{-1}

Chapter 4

Observed variations of convective rainfall area and precipitation with SST

4.1 Introduction

In this chapter, we deal, and only indirectly, with one aspect of the Iris hypothesis, namely the possibility that an increase in precipitation efficiency with SST manifests itself as modifying the partition between the condensate that is rained out of the convective regions and the condensate that is transported to the stratiform anvil. In this regard, several observational studies using a combination of satellite data, have recently provided evidence for an increase in the efficiency of precipitation with temperature over the tropical oceans (*Del Genio and Kovari*, 2002; *Lau and Wu*, 2003; *Del Genio et al.*, 2005; *Lin et al.*, 2006).

Here we use radar observations to study the relation between SST and the fraction of convective precipitation as well as the stratiform area normalized by precipitation in convective systems that develop over tropical oceans. Although our motivation for this study arises from the expectation that precipitation efficiency can control the water budget in convective systems thus ultimately acting as a climate feedback, we focus exclusively on the observational relation between convective fractions and stratiform area and SST, as opposed to the speculative attribution of a mechanism or the climate implications. We use data from the Kwajalein atoll ground-based radar (hereafter KR) and the precipitation radar of the TRMM instrument (hereafter PR), and we rely heavily on the algorithms that classify rainfall pixels into convective

and stratiform. We realize that, besides SST, other properties of the environment in which convection is growing will have an effect on the water budget of the convective systems, namely large scale wind shear, relative humidity of the free troposphere, magnitude of the convective updrafts, etc (see e.g. *Ferrier et al.*, 1996; *Schumacher and Houze*, 2006). All these processes could provide plausible mechanisms for the relations between SST and detrainment properties documented in the literature. Not only can the local variation of SST be confounded by other processes that might bias the results but also, as we discussed in the previous chapter, some methodological provisions have to be made to account for the normalization of the results by a measure of convection. These provisions have been frequently overlooked when analyzing the climate implications of changes in the area of detrainment of convective systems.

We focus here on the relation between convective precipitation fraction and stratiform area with SST over the tropical oceans using two different instrumental datasets. We argue in section 4.2 that to the extent that the stratiform precipitation region is primarily controlled by the detrainment of water from the convective regions, the partition between convective and stratiform precipitation can be regarded as a useful, although admittedly rough, observable of the water budget in these systems. Section 4.3 presents results using the Kwajalein radar dataset. In Section 4.4 we attempt to extend the analysis to the rest of the tropical oceans and we discuss the origin of some of the differences found between the two different datasets, in particular differences in the pixel size, in the stratiform-convective separation algorithm and in sampling. Finally in Section 4.5 we offer some discussion and conclusions. Two appendices deal with the sensitivity of the Kwajalein results to the parameters of the stratiform and convective separation and with the statistical significance of the Kwajalein results.

4.2 Data and Methods

4.2.1 Stratiform Convective Separation

There are physical as well as observational reasons for separating the precipitation produced by tropical mesoscale convective systems into stratiform and convective. Here we give a very brief account of these two precipitation types and the reader is referred to *Houze* (1993, 1997) for an extensive treatment of the terminology, physics and observational aspects of the classification. The convective precipitation refers to the regions of the convective system in which vertical motion is strong ($w > 1$ ms^{-1}) and the formation of precipitation occurs mainly through the collection of

cloud particles (coalescence or riming). On the other hand, stratiform precipitation regions are characterized by a slow ascent (less than about 1 ms^{-1}) and the growth of the precipitation size particles occurs mainly by vapor diffusion (*Rutledge and Houze*, 1987; *Houze*, 1997) on the surface of ice particles that were detrained from the convective region.

From an observational perspective, the weak horizontal gradients of reflectivity in the stratiform regions can be distinguished from the peakedness of the reflectivity in the most vigorous convective regions, giving the basis for the algorithms to distinguish between convective and stratiform regions (*Steiner et al.*, 1995). The two types of precipitation are not independent of each other since the balance of water in each of the two regions of the system is coupled by the transport of condensate and water vapor from the convective region to the stratiform region (*Houze*, 1993). However, besides detrainment of condensate from the convective regions significant in-situ condensation can also occur provided that there is a source of water vapor in the stratiform region. Observations of mesoscale convective systems in the tropics show the existence of a slantwise layer of ascent originating as a gravity wave response to the convective heating (*Houze*, 2004). This mean ascent in the mid-troposphere, with magnitudes of about 0.1 to 1.0 ms^{-1} (*Cotton et al.*, 1995) provides a supplementary source of water vapor to the stratiform region. The relative importance of each of these two sources of condensate, that is the in-situ condensate production and the detrainment from active convective regions in observed mesoscale systems, is largely unknown. However, *Gamache and Houze* (1983) estimated that the transport from the convective updrafts is the most important source of condensate in the stratiform region (about 1.5 to 3 times larger than in-situ condensation in the stratiform region). Even if a significant fraction of the condensate is produced in-situ, detrainment from the active convective towers seems to be a pre-requisite for the existence of stratiform rainfall.

As a consequence of this causal relation between the condensate produced in the convective elements and the stratiform precipitation, in the early stages of the lifecycle of a mesoscale convective system, the precipitation will be mostly convective, whereas in the dissipating stages of the system, when detrainment has been efficient in producing a cloud anvil and active convective elements have decayed, the precipitation will be mostly stratiform. From these considerations we can expect that the partition between stratiform and convective precipitation can change widely if periods of time much smaller than the lifetime of the system are considered (see Fig. 3-5). Therefore, in order to assess a possible change in the partition of the precipitation between these

two categories and SST, there is an essential need for an integral measure over the lifecycle of the system. We define ϵ_c as,

$$\epsilon_c = \frac{\int^\tau c(t)dt}{\int^\tau (c(t) + s(t))dt}, \tag{4.1}$$

where c and s are the total convective and stratiform precipitation in the mesoscale convective system and τ is a timescale sufficiently long to encompass the entire evolution of the system. We also define a measure of the area of stratiform rainfall to the total precipitation of the system as a proxy for the spatial extent of the detrainment normalized by a measure of convection,

$$\mathcal{A}_s = \frac{\int^\tau a_s(t)dt}{\int^\tau (c(t) + s(t))dt}, \tag{4.2}$$

where $a_s(t)$ is the area of stratiform rainfall at each time over the lifecycle of the system. In estimating the dependence of the distributions of ϵ_c and $\mathcal{A}_s$ on SST, we ideally would like to follow a large number of mesoscale convective systems over their complete lifecycle. This would require a high temporal sampling over an area of a size at least comparable to the size of the largest mesoscale convective systems (a few hundred kilometers).

4.2.2 Kwajalein Radar

The observational setting described in the previous section is most nearly found at the Kwajalein ground-based radar (KR). The KR is located on the Kwajalein atoll in the Republic of the Marshall Islands (8.7 ° N, 167.7 ° E). The instrument covers an annular region of 17 km of internal radius and 150 km of external radius, which is enough to completely observe most of the mesoscale convective systems (about 1% of the systems can have cloud shields larger than the area covered by the radar (*Houze*, 1993)). The area covered by the radar is almost completely oceanic. The radar operates in the S-band at a frequency of 2.8 GHz. In this work we make use of the University of Washington Kwajalein dataset, in particular the 2A53UW and 2A54UW products of the TRMM database, which correspond to the surface precipitation and the rain type classification, respectively. The temporal resolution of the data is about 10 minutes. We have used the full dataset available to date; it comprises 49 months between the years 1999 and 2003.

The main uncertainties in the estimation of the average monthly area rainfall measured by the Kwajalein radar have been identified and quantified by *Houze et al.*

(2004). All of these uncertainties are also relevant to the stratiform convective separation.The most important uncertainty which accounts for fluctuations of ±30% of the monthly mean value of rainfall is the calibration uncertainty. A calibration of the Kwajalein radar is performed by matching the areas of radar echo with reflectivity larger than 17 dBZ at the 6-km level with similar observations performed by the precipitation radar on board of the Tropical Rainfall Measuring Mission (TRMM) satellite. Other uncertainties include the extrapolation of surface reflectivity values made from the reflectivity at a higher level and the assumed $Z - R$ relationship based on observed distributions of rain droplet sizes.

The classification of echoes into stratiform and convective is made from reflectivity measurements at the lowest level measured by the radar, following the procedure developed by *Churchill and Houze* (1984) and further refined by *Steiner et al.* (1995) and *Yuter and Houze* (1997).

4.2.3 SST

We use the Pathfinder Version 5.0 SST dataset, which is retrieved using the five channels of the Advanced Very High Resolution Radiometer (AVHRR). The daily maps of SST are averaged into 8-day and monthly periods. We use the 8-day period data to construct three time series of average SST, one over the region covered by the Kwajalein radar and the other two in square regions of $5° \times 5°$ and $10° \times 10°$ centered at Kwajalein. Since SST is not estimated over pixels covered by clouds, significant gaps can occur over cloudy periods or regions. We use these two regions that are larger than the region that is sampled by the radar, in order to increase the accuracy of the average SST and also to account for the possibility that some detraining clouds could have originated from convection occurring outside the Kwajalein region.

4.2.4 Radiosonde Data

Here we use 12-hourly operational soundings at Kwajalein (taken at 00Z and 12Z) of temperature and dew point from all reported pressure levels for the period 1999-2003. The data were obtained from the NOAA Radiosonde Database access web site (http://raob.fsl.noaa.gov/). The soundings were linearly interpolated from the reported pressure levels to 100 mb intervals from 1000 mb to 300 mb and checked for obvious errors (missing data, unphysical values).

4.3 Kwajalein Radar

4.3.1 Results

		τ [days]					
		8	16	30	8	16	30
			ϵ_c			$\mathcal{A}_s$	
$\%/°K$	KR	10.1	8.37	9.37	-24.4	-23.3	-22.5
	5°×5°	11.4	9.3	10.13	-27.0	-25.6	-24.1
	10°×10°	11.8	10.0	10.21	-27.5	-26.0	-24.4
	Surface q	9.2	9.0	9.5	-26.3	-25.7	-26.0
r	KR	0.39	0.38	0.46	-0.44	-0.48	-0.49
	5°×5°	0.41	0.40	0.47	-0.48	-0.52	-0.53
	10°×10°	0.42	0.42	0.48	-0.49	-0.53	-0.53
	Surface q	0.46	0.49	0.58	-0.53	-0.59	-0.64

Table 4.1: Percentage change ($\%/°K$) and correlation coefficient (r) for the linear regression between the variables ϵ_c and $\mathcal{A}_s$ with respect to SST. The correlations are for the total of 5 years of ground-based radar data and for different periods of integration τ of 8, 16 and 30 days (the number of observations for the correlations is 162, 76 and 41 respectively for each of the periods). Only periods in which valid data are available more than 70% of the time are considered. KR (Kwajalein radar), 5° × 5° and 10° × 10° refer to the areas over which SST data is averaged, centered at Kwajalein. The row Surface q shows the results for the linear regression using the surface q averaged over the corresponding period instead of SST.

The variables ϵ_c and $\mathcal{A}_s$ are calculated for varying periods of 8, 16 and 30 days, within the five years of available radar data. Periods in which less than 70% of valid data are available are discarded from further analysis. Least squares linear regressions are performed and the slope of the regression (expressed as percentage increase per degree Kelvin) as well as the correlation coefficient r are shown in table 4.3.1. The scatter diagram for the period of 8 days using the average SST over the 10° × 10° is shown in Fig. 4-1.

Correlations between ϵ_c and SST are positive over the three different time scales considered and over the different regions over which the SST is averaged. The values for the slope of the linear regression are between 8%/K to 12 %/K. Correlation coefficients are low and explain a relatively small fraction of the variance of the data (15 to 25%). However the scatter is reduced as larger areas and longer periods of time are considered for the averages. As seen in Fig. 4-1a the variance of the data

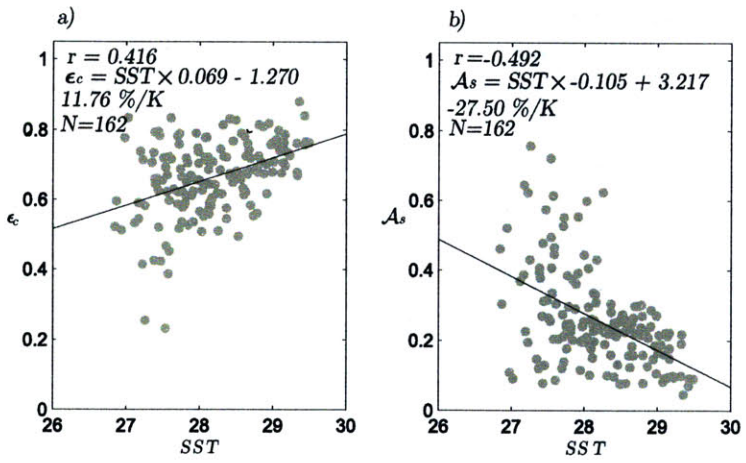

Figure 4-1: Linear regression between (a) convective fraction ϵ_c and (b) stratiform area per unit precipitation $\mathcal{A}_s$ with respect to the average SST of a region of $10° \times 10°$ around Kwajalein. The period of integration is $\tau = 8$ days. The units of $\mathcal{A}_s$ are $KR/[mmh^{-1}]$, where KR is the area covered by the Kwajalein radar.

seems to decrease with SST. The behavior of the variance might be expected given the low frequency of rainfall associated with colder SSTs, and hence the temperature dependence of the sampling. We expect a larger scatter at relatively lower rainfall rates, and a reduction of the difference in variance over the range of SST as we average over longer periods. This reduction of the variance is indeed observed when longer integration times are considered.

The normalized stratiform area $\mathcal{A}_s$ has a negative correlation with SST and the value of the slope ranges between -22 to -28 %/K. The correlation coefficients are slightly larger than in the case of the correlations between ϵ_c and SST. We also notice, the relatively large scatter particularly between 27°C and 28°C. When the distribution of the residuals is calculated some outliers in the correlations are evident (the points that have $\epsilon_c < 0.3$ in Fig. 4-1a). Removing these outliers produces an insignificant change in the slopes (from -27.5 %/K to -27%/K for $\mathcal{A}_s$)

In order to evaluate the conjecture that the mechanism for the increase in the fraction of convective precipitation acts through the specific humidity of the air participating in convection, we have looked at how correlations differ when instead of using SST we use the average specific humidity at the surface as measured by the operational soundings at Kwajalein. The rows *Surface q* in table 4.3.1 show the results for the linear regression of specific humidity q and ϵ_c and $\mathcal{A}_s$. We see that the values of r are slightly larger than for SST (r is 0.58 for τ=30 days so they explain up to 35% (r^2) of the variance). This is a surprising result given the local nature of

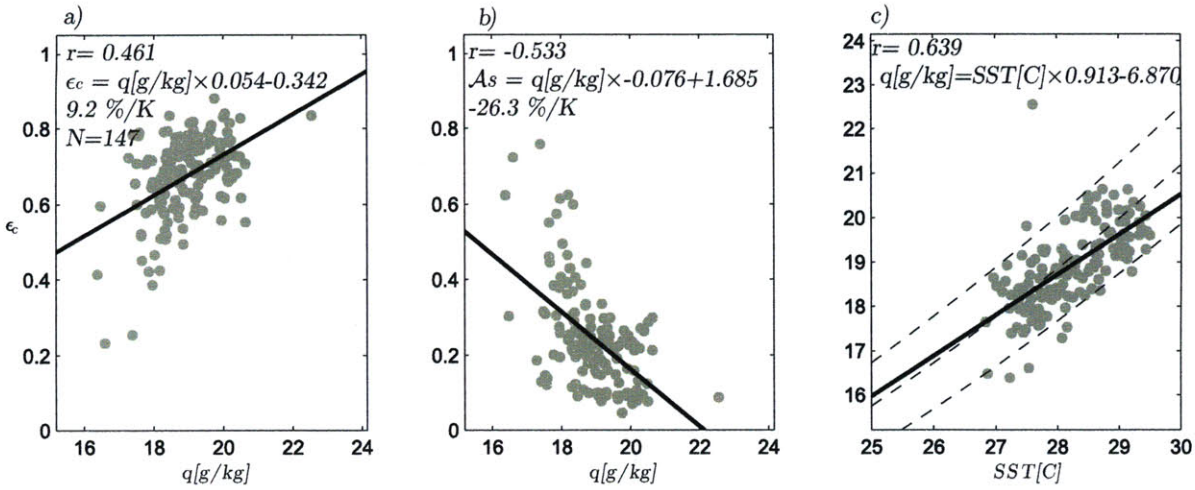

Figure 4-2: Linear regression of (a) ϵ_c, (b) $\mathcal{A}_s$ and (c) SST averaged over the Kwajalein region on the average specific humidity at the surface as measured by the operational soundings at Kwajalein. The period of integration is $\tau = 8$ days. In panel (c) dashed lines show the 0.75, 0.80 and 0.85 relative humidity curves as calculated from the Clausius-Clapeyron relation for the corresponding SST

the radiosonde observations compared to the broader spatial extent of the remotely sensed SST. Figs. 4-2a and 4-2b show the regression of ϵ_c and $\mathcal{A}_s$ against the average q at the surface for a period of integration of 8 days. In Fig. 4-2c we show a regression between the mean SST over the Kwajalein region and the specific humidity q at the surface. At least two effects contribute to the scatter, the first is that the measurements are not completely comparable since the SST is averaged in space over the entire radar region whereas q is a local value. The second effect and probably the most important is that the relative humidity is not constant from one period to another and therefore different values of specific humidity are associated with a single SST. Besides the linear regression, we also plot in Fig. 4-2c the curves corresponding to 0.75, 0.80 and 0.85 relative humidity according to the Clausius-Clapeyron relationship. We see that most of the data is contained within the 0.75 and 0.85 curves and that over the time scale of 8 days only about 40% of the variance in q (r= 0.64) is explained purely by changes in SST.

In Fig. 4-3 we show the result of the regression between ϵ_c and specific humidity in the vertical from the radiosonde measurements at Kwajalein. We see that correlations ($r \sim 0.4 - 0.5$) and slopes are positive and relatively constant up to about 850 mb. The scatter increases above 800 mb for all the time scales considered. We see that mid-tropospheric humidity is also positively correlated with ϵ_c; however, slopes and scatter are consistently smaller above the 800 mb level. This is the behavior than one

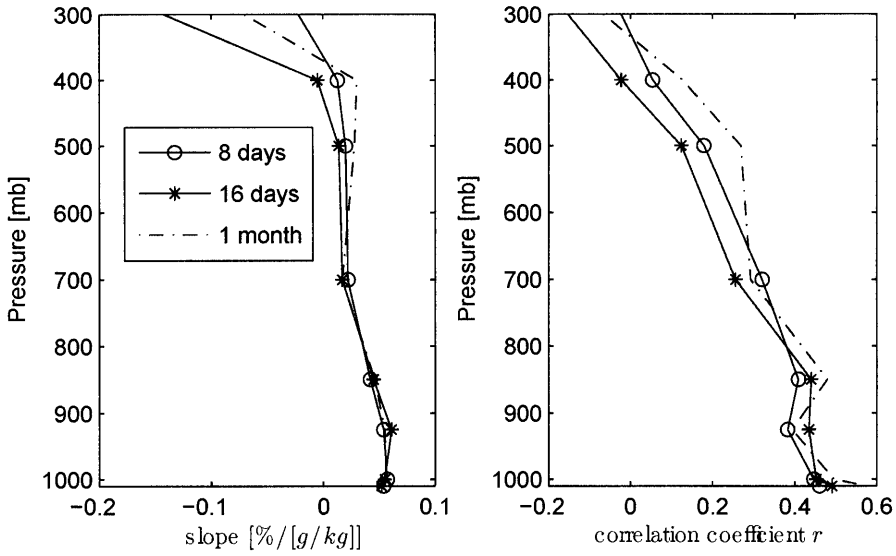

Figure 4-3: (a) Slope of the regression and (b) correlation coefficient between the convective fraction ϵ_c and the specific humidity as measured at different pressure levels by the radiosondes at Kwajalein. Correlations are shown for the three different integration periods

would expect if the main control of ϵ_c would reside in the boundary layer. However, it is also possible that a single sounding site is less adequate to make inferences in the mid-troposphere than in the boundary layer since the variability of specific humidity may be larger (due to episodic evaporative downdrafts and horizontal advection) than in the boundary layer where the specific humidity is relatively close to 80% of the saturation value at SST.

We finally present the regressions using the results for the period of 8 days in which the sample has been divided into three similar subsamples according to the total rainfall observed during the period (Fig. 4-4). The correlation coefficients in each of these regression are smaller ($r \sim 0.2 - 0.3$) than the ones in which the original sample is used, so inferences have to be made with even greater caution. To the extent that inferences can be made with these reduced samples, the results suggest that the regressions are somewhat dependent on the rainfall amount. The largest slopes are found for the lower rainfall category that contain some outliers from the original regression. This might indicate that some of the original numbers for the slopes of the regression might be overestimated. It might also indicate that the linear regression is not adequate in this case. For the medium and the higher rainfall categories the slopes appear to be similar, between $4\%/K$ and $6\%/K$ for the increase of ϵ_c and around -10%/K, for $\mathcal{A}_s$ (significantly smaller than the number estimated using the

totality of the data). The fact that at least the two larger rainfall categories show similar regressions might be interpreted as evidence that mid-tropospheric humidity variations, that are expected to be related to the total rainfall over the region, are not a dominant factor in the correlations.

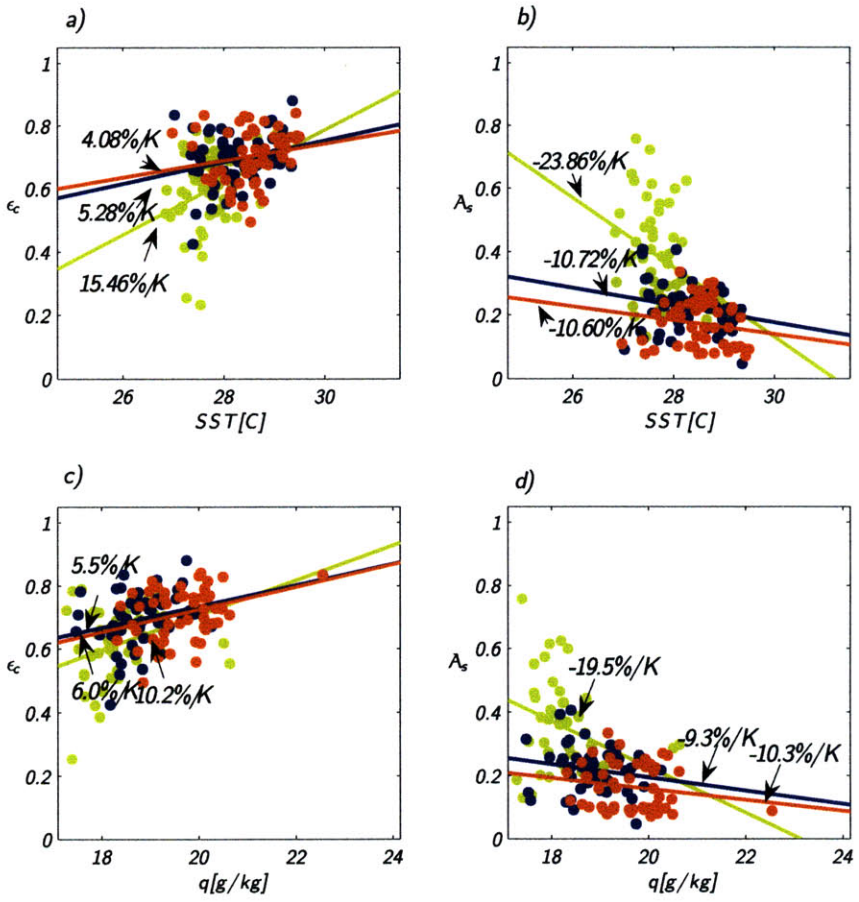

Figure 4-4: Linear regression between (a) ϵ_c and (b) $\mathcal{A}_s$ with respect to SST and (c) ϵ_c and (d) $\mathcal{A}_s$ with respect to q at the surface. The colors represent the lower (cyan), medium (magenta) and upper (green) tercile of the distribution of rainfall over the period.

4.4 TRMM Precipitation Radar

Although the KR provides a high temporal and spatial resolution dataset of stratiform and convective rainfall, the dataset only represents a very small area of the tropical ocean. The obvious choice to extend the analysis to the rest of the tropical oceans is to use data from the precipitation radar on the TRMM satellite (PR). The PR

instrument provides estimations for the rainfall and classification for each rainfall pixel (products 2A23 and 2A25A version 6 *Awaka et al.*, 1997; *Iguchi et al.*, 2000; *TRMM Precipitation Radar Team*, 2005)). The TRMM satellite orbits the earth at a height of about 350 km and with an inclination of about 35°. The precipitation radar (PR) on board of TRMM measures at a frequency of 13.8 GHz. Significant attenuation occurs at this frequency primarily by rainfall and has to be corrected before producing the precipitation product *Iguchi et al.* (2000). The data is gathered over a swath width of 215 km with a horizontal resolution of 4.3 km at nadir (for data before August 2001) and a vertical resolution of 250 m. The instrument is sensitive to echoes with reflectivity higher than about 18 dBZ (for more details see e.g. *Kummerow et al.*, 1998).

The immediate extension of the Kwajalein analysis using the PR data is not free of limitations. Perhaps the most important limitation is the inability to resolve mesoscale convective systems due to the low temporal resolution of the PR orbits. A region of the size of the area covered by the KR will be, on average, completely covered by the footprint of the PR once in about 3 days compared to the 10 min time resolution provided by the KR. A strategy to use the PR data has to balance the need to use a sufficiently long period of time to minimize the sampling error and a sufficiently short period of time so that the SST measured over that period is not significantly different from the SST relevant to the convective time scale.

4.4.1 Estimating TRMM sampling error using the Kwajalein dataset

In this section we will estimate the sampling error made by the PR in monthly accumulations of orbital data by using resampling over the more frequent KR data. We can form synthetic months by taking a piece of the original five year series long enough so that it is larger than the decorrelation time for the the particular variable observed. In the case of average rainfall, and for this particular grid size, the decorrelation time is about 5 days, so we arbitrarily choose the length to be 10 days. We create 1000 synthetic months out of the Kwajalein data and at the same time we preserve the statistical characteristics of the time series for the shorter scales. A similar methodology was suggested by *Bell and Kundu* (2000).

Fig. 4-5 shows the dependence of the relative root mean squared error with rainfall for the three variables, ϵ_c, $\mathcal{A}_s$ and R. The curves are least squares fitting of power laws for each of the variables. We see that the relative error for rainfall is between

20% to 50% for the revisit time of the TRMM instrument, whereas the sampling error for $\mathcal{A}_s$ is between 20% and 30% and the error for ϵ_c is only about 10%. This behavior seems consistent with the idea of a relatively longer decorrelation time scale for ϵ_c and $\mathcal{A}_s$ than for R itself as the relative sampling error is inversely proportional to the decorrelation time. The dependence of the sampling error on rainfall is similar to other observational estimates and also to the theoretical model presented by *Bell and Kundu* (2000) that predicts a $R^{-\frac{1}{2}}$ dependence of the relative error of rainfall and a sampling error of magnitude inversely proportional to the decorrelation time scale. The power law dependence for the relative sampling error of rainfall in our case seems to be closer to $R^{-\frac{1}{5}}$. However a $R^{-\frac{1}{2}}$ curve that fits the data is within the standard deviation of the average of the errors depicted in Fig.3.4.

The existence of the sampling error does not a priori precludes the possibility of observing a signal in the TRMM data. The sampling error, if uniform over the range of temperatures, will only decrease the confidence of the estimation of the parameters of the regression to the extent of the magnitude of the error. Since the scatter of the regression not only depends on the error but also on the proportion of the variance of the error to the variance of the dependent variable, the detection of the signal is made difficult both by the sampling and also by the relatively small range of temperatures over which deep convection occurs.

4.4.2 PR convective-stratiform classification

The classification of echoes among two broad categories is done using both the vertical and horizontal variability of the reflectivity in TRMM (*Awaka et al.*, 1997; *TRMM Precipitation Radar Team*, 2005). Given the relatively high vertical resolution of TRMM of 250 m, a bright band (that is, a region of a few hundred meters in the vertical of enhanced reflectivity due to melting of ice hydrometeors (*Doviak and Zrnic*, 1993)) can be determined providing a complementary method to the horizontal texture classification algorithms (e.g. *Steiner et al.*, 1995). Using the height of the storm top (the maximum height at which significant echo is observed) a shallow and non-shallow classification is performed. Also all rainy pixels are classified as isolated or non-isolated, depending on whether they are surrounded by other rainy pixels.

We show in Fig.4-6 the geographical distribution of rainfall separated in four broad categories constructed by merging some of the original categories in the 2A23 product as indicated in Figure 4-7 for the month of April 2001. We see that convective and stratiform rainfall pixels are constrained to the ITCZ regions in the Atlantic

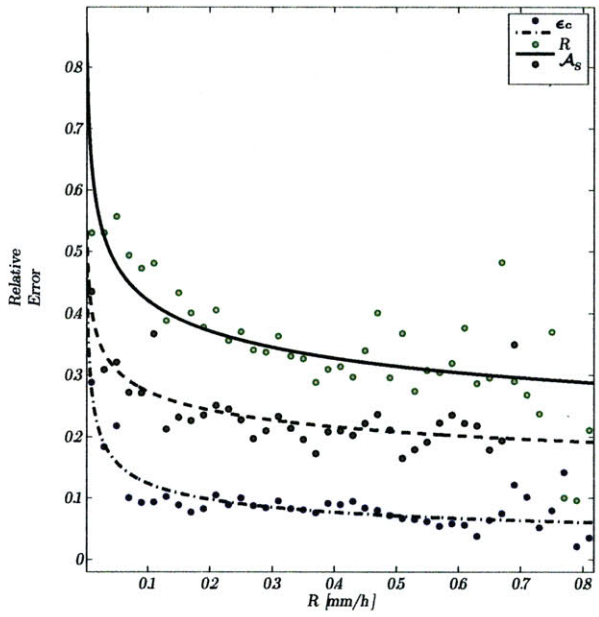

Figure 4-5: Relative sampling error estimated for TRMM revisit times using resampling of the Kwajalein Radar data. The curves are the least square fitting of a power law for the three variables, ϵ_c (dash-dotted line), $\mathcal{A}_s$ (dotted line) and total rainfall R (solid line). The fitting is done for the average value of the relative sampling error binned according to rainfall in $[mmh^{-1}]$

and Eastern Pacific (where there is a hint of a double ITCZ) and they are more widespread in the Indian Ocean and in the Western Pacific. Fig. 4-6.d shows the distribution of shallow isolated pixels, these are usually called cumulus congestus and they are precipitating clouds capped by an inversion layer near the freezing level as described by *Johnson et al.* (1999). Although these clouds are convective in nature as argued by *Schumacher and Houze* (2003), they are not necessarily associated with detraining mesoscale convective systems. Shallow isolated rainfall is more prevalent in subtropical (the Eastern coasts of South America and Australia close to 20°S in this particular month), in which no corresponding stratiform or deep convective precipitation is observed. Although shallow isolated pixels are also also observed over regions of deep convection we have decided to leave these pixels out of the convective category in our analysis (including these pixels makes only a minor quantitative difference in the results). We realize that this might not be necessarily consistent with the Kwajalein analysis, however including these pixels in the convective category in

regions in which deep convection is frequently observed does not have a large impact, as can be deduced from Fig. 4-7 which indicates that shallow isolated rainfall makes up about 5% of the total rainfall for these particular orbits over Kwajalein. (A caveat to this argument is that the prevalence of shallow isolated rainfall can be seriously underestimated by TRMM, as we will discuss in Section 4.4.4). On the other hand, there are also shallow non-isolated pixels and their distribution is shown in Fig.4-6.e. By definition these pixels are located closer to the deep convective systems in the tropics and not surprisingly their distribution resembles the distribution of deep convective and stratiform rainfall, therefore we have included these pixels under the convective category.

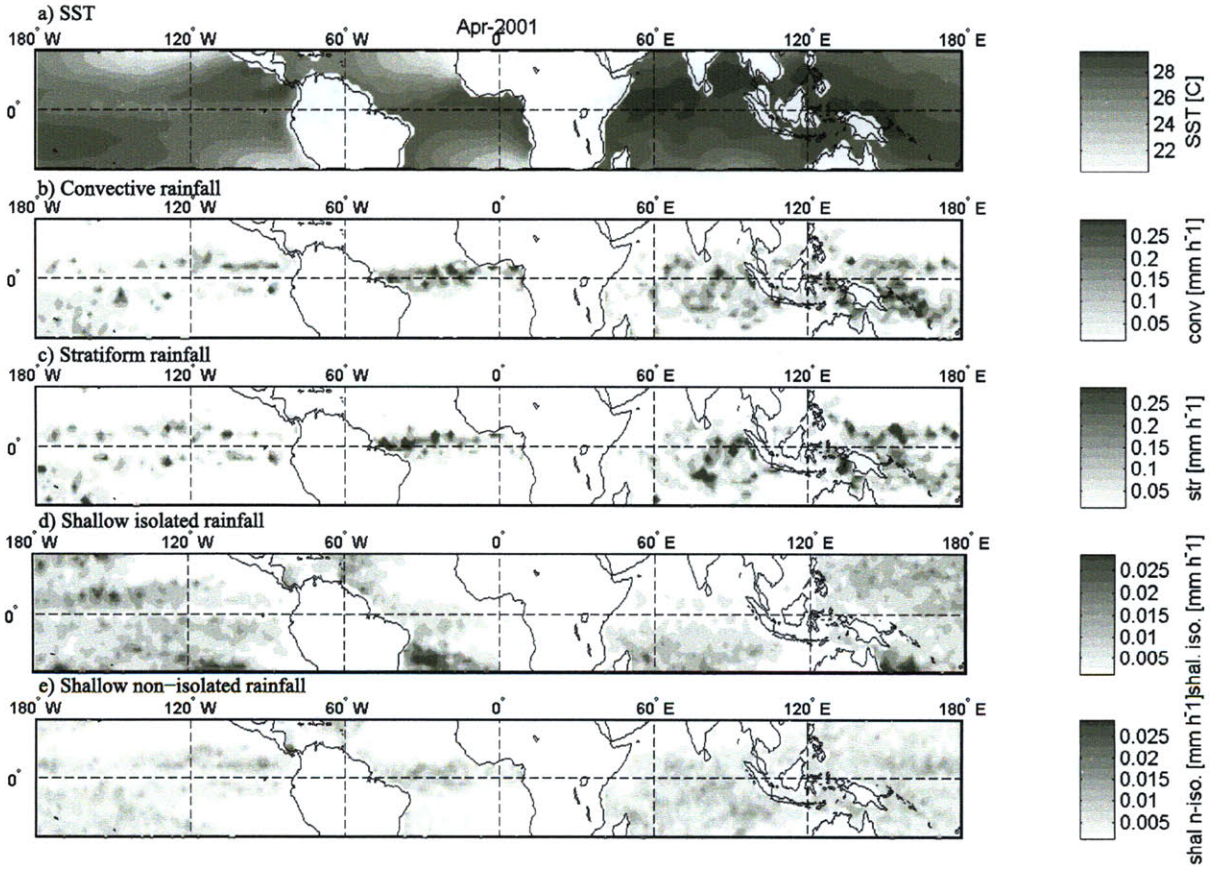

Figure 4-6: Rainfall intensity for different categories according to TRMM-PR for April 2001. a) Sea surface temperature. b) Convective rainfall (200-240). c) Stratiform rainfall(100-170) d) Shallow Isolated rainfall (251, 261, 271, 281, 291) e) Shallow Non-Isolated rainfall (252, 262, 272, 282)

Fig. 4-7 shows the histogram of the different sub-categories of precipitation derived

from the classification algorithm of PR. The figure was made using a small set of TRMM orbits coincident with the Kwajalein region.The labels on the top of the figure are based on the TRMM categories provided, in which *probably convective* and *probably stratiform* are used to denote pixels in which only one of either the vertical or the horizontal method classified the pixel in the corresponding category. Hereafter and for the purpose of the analysis, stratiform will include those pixels classified as *stratiform certain*, *probably stratiform* as well as the *other* category. Convective will include pixels classified as *convective certain*, *probably convective* and *shallow non-isolated* as argued above.

4.4.3 Results

Correlations between ϵ_c, $\mathcal{A}_s$ and SST are shown in Fig.4-8. The correlations are calculated for monthly data over strictly oceanic grids of 2° × 2° size for the year 2001 between $20°S - 20°N$. Each of the small dots represents a single grid in which the monthly values of the variables have been estimated from the available orbits. We notice that the classification algorithm detects "deep convection" even in regions in which the monthly average SST appears too cold to sustain tropical convective systems. It is possible that these convective systems are simply cumulus congestus that grow above the freezing level and are classified alternatively as either convective or stratiform. To avoid biases due to this or other possible artifacts we also bin all data according to SST regardless to their spatial location (large dots in Fig. 4-8). We will refer to these two related datasets as *gridded* and *binned.* Table 4.2 summarizes the relative change with temperature deduced from the regressions for different size of the griding of the orbital data, as well as for two different subdomains within the 20°N 20 °S tropical belt. The regressions for ϵ_c are linear and for $\mathcal{A}_s$ are exponential. In the case of the binned data, we have used a robust regression weighted according to the number of samples in each bin. In this way the correlations are representative of the regions in which deep convective pixels are more prevalent.

The gridded data shows a relatively large scatter (r^2 is about 0.25 for both variables). When the regression is taken on the binned data, the scatter and the magnitude of the slope of the regression are reduced. As shown in the previous section the sampling error has a rainfall dependence, on the other hand rainfall has a positive dependence on temperature over the tropical oceans. Therefore, it is expected only on the basis of the nature of the sampling error that the variance of the gridded data will also show a SST dependence. Consistent with the sampling error being larger

for relatively cold SSTs, the difference between the gridded and binned regression is largest in the colder regions specially for $\mathcal{A}_s$ as shown in Fig.4-8.

Table 4.2 also shows the results for two subdomains; the Western Pacific (WP) is defined as the region between 140°E and 150°W, whereas the EP is the region between 150°W and 80 °W. Correlations in the EP region have a smaller scatter (for instance

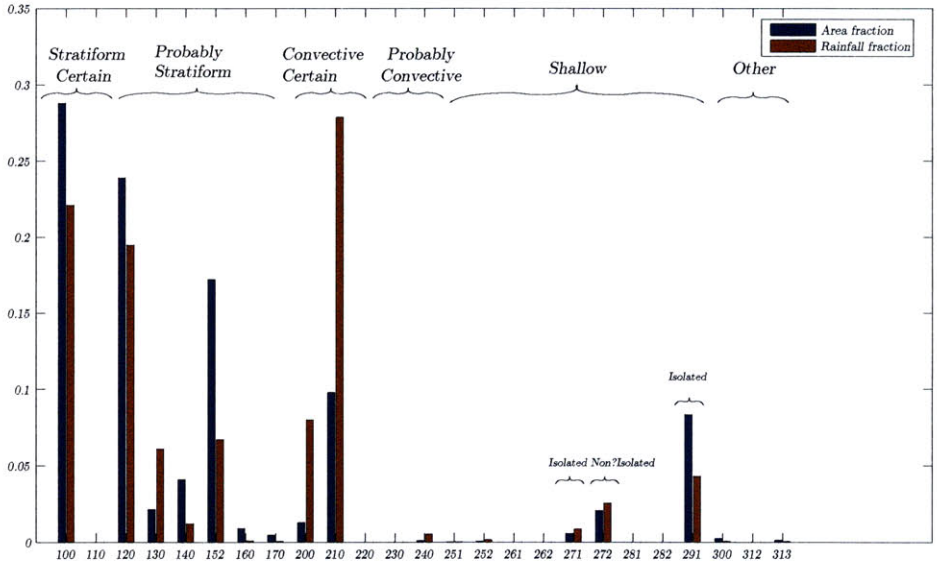

Figure 4-7: Distribution of rainfall and area according to the TRMM classification for the orbits that are coincident to Kwajalein over 5 years of data. Abscissa is numbered according to the different sub-categories, and we have also labeled some of the categories

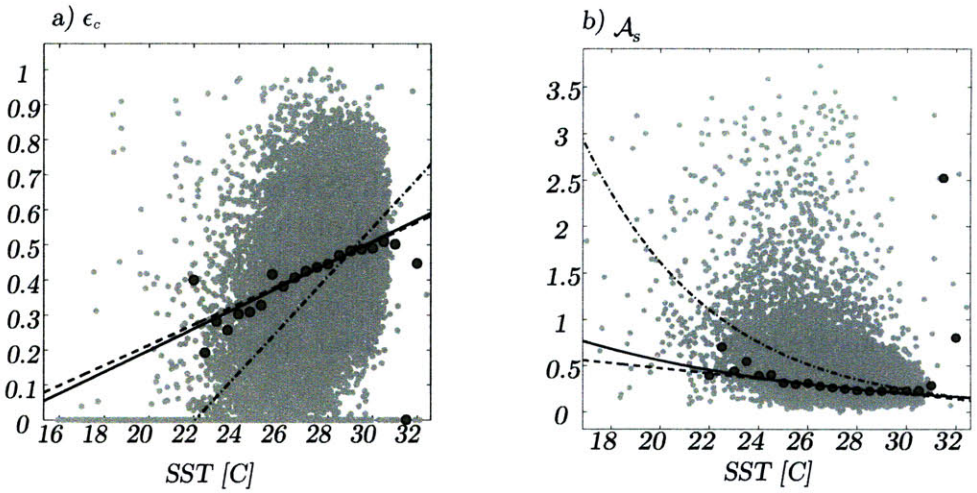

Figure 4-8: Regression of the variables a) ϵ_c and b) $\mathcal{A}_s$ with respect to SST obtained from the TRMM data set for the year 2001, when the pixel data were aggregated monthly in time and in grids of size 2°× 2°in space. Light gray dots are monthly-2°×2°observations whereas dark gray circles are obtained after adding all data for a given SST range (binned data). The curves in the two panels are different versions of the least squares fitting (LS) of the data, in a) linear LS of all the data (dash-dotted line), the linear LS of all binned data (dashed line) and robust linear LS of the binned data (solid line). In panel b) the curves are the exponential LS of all data (dash-dotted line), the exponential LS of the binned data (dashed line) and the robust exponential LS of the binned data (solid line)

for ϵ_c, $r^2 = 0.16$ in the WP compared to $r^2 = 0.28$ in the EP), and also a larger slope for the correlation. Correlations are positive for each region separately suggesting that the correlation is universal. Fig.4-9 shows the regressions for the EP and WP regions. The regression in both figures are the robust regressions for the binned datasets in each of the regions. In general it seems that for the same SST the EP shows a higher value of ϵ_c and a smaller value of $\mathcal{A}_s$. This seems in apparent contradiction with observations that indicate a higher proportion of stratiform rainfall in the EP than in the WP (e.g *Berg et al.*, 2002; *Schumacher and Houze*, 2003). However, given the larger proportion of relatively colder SSTs over the EP, at least for the year 2001 the overall fraction of convective precipitation is smaller in the EP than in the WP region.

We notice that ϵ_c is smaller for Kwajalein than what is observed with the PR. However in terms of the relative change with temperature, PR results seem to agree quantitatively with the range between 8 to 12 %/K increase for ϵ_c obtained from the

	data type	2°× 2°			10°× 10°
		All	WP	EP	All
ϵ_c (%/K)	gridded	13.9	13.1	17.8	12.4
	binned	6.47	6.7	10.7	6.98
$\mathcal{A}_s(\%/K)$	gridded	-21.8	-15.9	-17.7	-18.9
	binned	-15.6	-5.5	-12.6	-10.2

Table 4.2: Relative increase in ϵ_c and $\mathcal{A}_{str}$ with SST estimated from the regression of the data from the precipitation radar on board of the TRMM satellite. The results are given in (%/°C) at 27 °C. *All* refers to the calculations including all oceanic regions. WP and EP stand for Western Pacific and Eastern Pacific respectively. All calculations are between 20°S and 20°N, except for the column indicated as 10°S and 10°N.

Kwajalein observations. In the case of $\mathcal{A}_s$, PR correlations are smaller than those obtained for KR, specially over the Western Pacific where the relative change in $\mathcal{A}_s$ can be about -5.5 $\%/K$, compared to -22 $\%/K$ for Kwajalein. We also notice that the rate of change of $\mathcal{A}_s$ with temperature seems closer to zero for temperatures higher than about 28.5 C (Fig. 4-8.b), so even an exponential decrease does not seem to be an appropriate fit for this part of the curve. This flattening towards higher temperatures might be a consequence of the instrument resolution as we will discuss in the next section. However, we can anticipate that to the extent that PR errors can be reduced by binning the data with SST, and considering some of the differences in the instruments as well as in the classification methods, PR and KR seem to agree in the magnitude and sign of the variation with SST of ϵ_c and $\mathcal{A}_s$.

4.4.4 Kwajalein and PR radar comparison

In order to discuss the differences between the Kwajalein and TRMM results, it is useful to compare the classification and rainfall of pixels when both instruments are measuring the same region at the same time. We used all simultaneous TRMM orbits within 10 minutes of a radar scan made by the ground-based radar at Kwajalein and close enough in space to have a significant coverage ($\sim$ 60% in average) of the Kwajalein area by the swath of the PR. We identified 176 orbits fulfilling these conditions over the period of 5 years of the Kwajalein radar record. Previous work by (*Schumacher and Houze*, 2000) focused on the differences in reflectivity between these two instruments. Since the KR is calibrated based on matching the reflectivity areas, we have done our comparison using rainfall rather than reflectivity to emphasize differences without regard to their origin (different Z-R (radar reflectivity-rainfall) re-

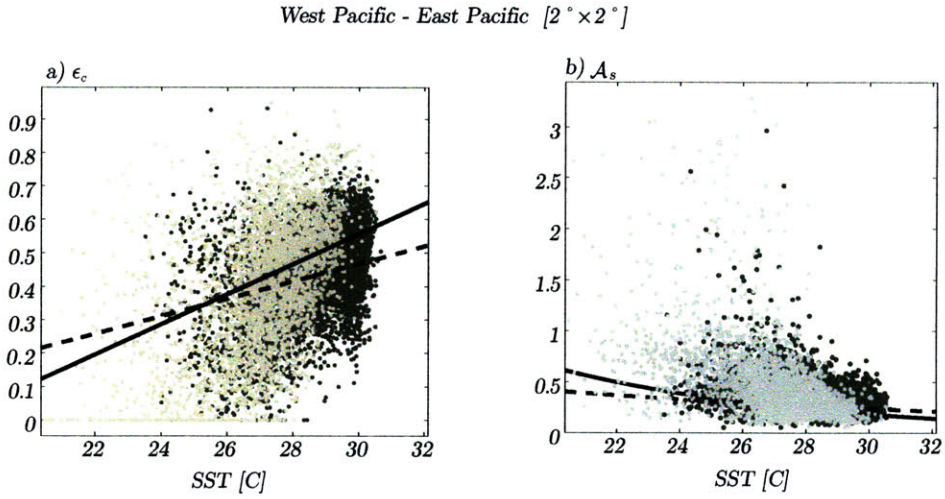

Figure 4-9: Same as Fig.4-8 but the data have been divided into West Pacific grids (dark gray) and East Pacific grids (light gray). The regression curves are the robust LS estimates of the binned data for each region. EP (solid curve) and WP (dashed curve). The regressions are robust, and linear for ϵ_c and exponential for $\mathcal{A}_s$

lations, instrument sensitivity) Fig. 4-10 shows the distribution of rainfall according to the two broad categories of stratiform and convective rainfall, for the coincident orbits. One of the most noticeable differences is the higher sensitivity of the KR to lower rainfall rates which appears in the histogram as a KR stratiform distribution extending towards values smaller than 0.1 mmh^{-1} (notice logarithmic scale in Fig. 4-10). For the same region in the histogram the PR distribution begins abruptly at about 0.2 mmh^{-1} coincident with the lower threshold in reflectivity of the TRMM-PR instrument of about 17 dBZ. Also, the mode of the convective precipitation distribution is located at a lower rainfall rate for TRMM probably a consequence of the larger pixel size in the PR (4.3 km compared to 2 km for KR). For the same reason the KR has a higher frequency of high rainfall rates than TRMM.

The convective stratiform algorithm is applied to the reflectivity data before it has been corrected for attenuation, this might result in a misclassification of some convective echoes into stratiform. *Heymsfield et al.* (2000) show calculations for a bell shaped reflectivity distribution intended to mimic a single convective cloud. For instance if we consider a cloud of 1.2 km in diameter (which is the median diameter of convective updrafts reported over the Kwajalein region between 5 and 9 km height (*Anderson et al.*, 2005)) that is centered along the PR beam, the maximum reflectivity is reduced from 50 dBZ to 45 dBZ. For the extreme case in which the convective cloud

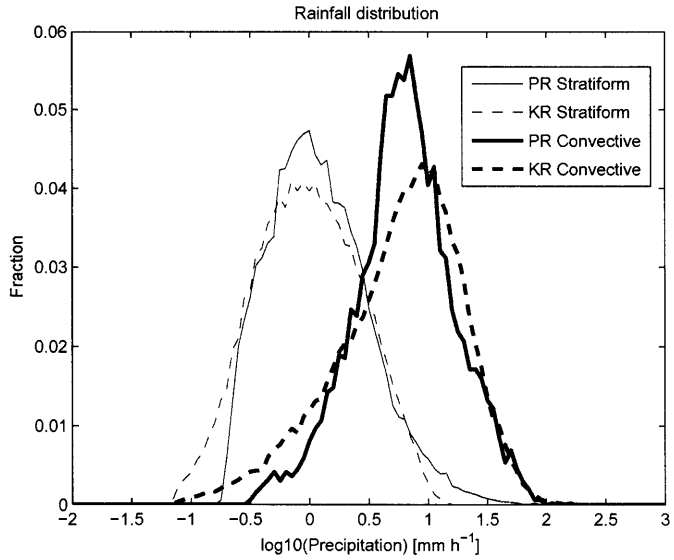

Figure 4-10: Distribution of the intensity of rainfall for TRMM-PR orbits over Kwajalein. The solid lines are for the TRMM-PR instrument and the dashed lines for the Kwajalein instrument

is located in a corner of the PR footprint, reflectivity is further reduced to less than 10 dBZ, so in this case not only the cloud would be misclassified but it would be undetected by the PR. Both the misclassification and the no detection of convective clouds due to beam filtering point in the same direction, towards a negative bias in the value of ϵ_c and a positive bias of $\mathcal{A}_s$ towards higher convective fractions. Since we have documented a convective fraction dependence on SST, this very dependence implies a bias with temperature; as a higher proportion of convective cores are present in the sample there will be a larger amount of those cores misclassified or missed by the instrument. Rough estimates using a 20% of misclassified convective cores and 10% missing cores can explain a 10%/K difference in the value of the relative change of $\mathcal{A}_s$. A more precise estimation of this effect could be made observationally by comparing TRMM data before and after the satellite's boost maneuver when pixel size increased from 4.3 to 5.0 km (For the small set of coincident orbits over Kwajalein, the previous numbers for the percentage of missing and misclassified cores seems reasonable). From cloud physics considerations, and assuming that correlations are primarily controlled by the specific humidity of the boundary layer, one could alternatively argue that the flattening of the correlations towards higher temperatures is due to a saturation effect on the change of the cloud liquid water with temperature rather than an instrumental effect. However, the change over the observed range of temperatures would be too small to explain the flattening. Additionally an instrumental effect is favored by the

fact that in the higher resolution data of Kwajalein the flattening is less evident.

4.4.5 Comparison between radar and infrared cloud areas

The stratiform rainfall area is one of several observables connected to the detrainment from convective clouds. *Lindzen et al.* (2001) for instance, used the area of clouds between 220 and 260 K as a proxy for the area of detrainment in deep convective regions. Since the area of precipitation in a convective system is smaller than the area covered by clouds, the use of the stratiform rainfall area minimizes the possibility of an error in which size of the grid over which the statistics are being taken influences the correlations (through the higher rainfall frequency and coverage of the grids at higher SSTs as discussed by *Del Genio and Kovari* (2002)). In fact our results do not show a strong dependence on the size of the grids (Table 4.2). Related to this advantage is the fact that precipitation detrained from the convective region is short-lived with respect to the clouds and therefore, the error which one incurs by truncating the life cycle of the system either in time or in space is minimized (in other words, the convective towers in which detrainment originates are "closer" in time and space to the stratiform rainfall area than to the thin cirrus area). Figure 4-11 shows the lagged correlation coefficient between the area of stratiform precipitation and the area of the cloud shield over the radar region as measured by the 11 μm infrared satellite brightness temperature. In this particular figure the infrared area excludes regions colder than 220K and includes regions colder than a certain temperature BT, so we denote this area by A(BT-220). Lag-correlations are maximized along the solid line in Fig. 4-11 with a lag of about 3 hours for A(235-220) and a lag of about 10 hours for A(275-220). The relatively large values of the correlation coefficient (~ 0.6) indicate good correspondence between the rainfall area and the cloud area as measured by the infrared satellite. Moreover, the increase in the time lag in which correlations are maximized for warmer temperatures suggest that even instantaneous measurements as those made by the PR instrument stratiform area capture some information on the time evolution of the detrainment (possibly because the sample includes clouds at various times in their evolution).

4.5 Discussion

We have presented an observational analysis of the dependence of the convective fraction and stratiform area (normalized by total precipitation) on SST. Our motivation

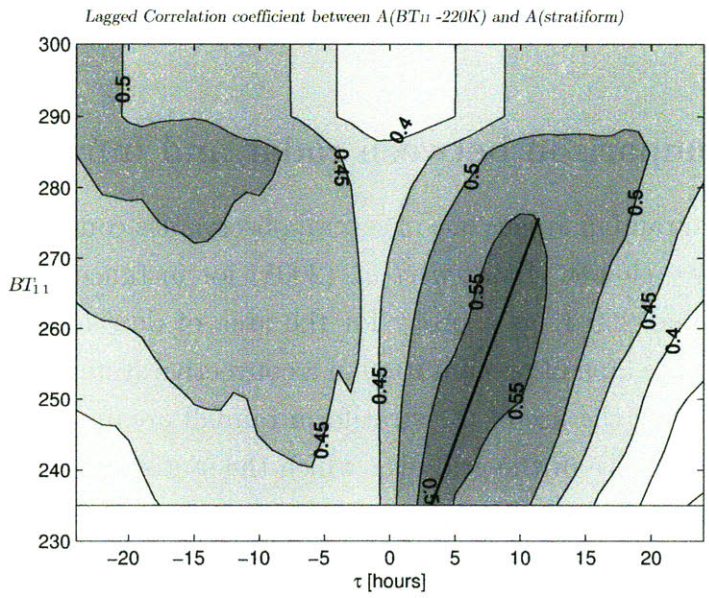

Figure 4-11: Lagged correlation coefficient between the time series of area of cloud warmer than 220 K from geostationary brightness temperature data and the area of stratiform precipitation as measured by the Kwajalein radar over a period of three months. Solid line indicates the region for which correlations are maximized.

for this analysis, as in other previous work, is to explore whether we can obtain constraints on observables that are related to the water budget of deep convective systems in the tropics. The declared or undeclared purpose of such studies (including ours) is not limited to the characterization of the natural variability of convective system in the current climate, but usually there is the expectation that the current variability provided by SST variation in the tropics can serve as a proxy for the changes that can be brought about by climate variability on various scales.

In this chapter we focused on the variation with SST of two observables derived from radar data over the tropical oceans: ϵ_c, the fraction of convective precipitation, and $\mathcal{A}_s$ the area of stratiform precipitation normalized by total precipitation. The normalization is a necessary condition to obtain a meaningful result since to the first order the SST distribution organizes the spatial variation of convection in the tropics. Cloud properties such as the area of detrainment, total rainfall and cloud radiative effects can be considered *extensive* with respect to the amount of convection. The normalization simply takes into account the fact that the amount of convection in a region of a given temperature is not indicative of the amount of convection in a climate with the same temperature, since the global amount of convection is determined by global energy balance considerations. It remains an open question whether total precipitation, mass convective flux or some other measure of convection is the most

adequate normalization factor with regard to climate effects.

Our results show an increase in the fraction of convective precipitation with SST together with a decrease of the area of stratiform precipitation per unit of total rainfall. Results for both instruments indicate an increase in the fraction of convective precipitation of about 6-12 %K, and an decrease in the normalized stratiform area of about 5-28 %/K. Furthermore, the observations seem to be independent of the particular geographical area chosen for the analysis, as long as the range of temperatures is sufficiently large.

Although observations are presented here without regard to a specific mechanism, they are in agreement with an increase in precipitation efficiency with temperature required in the functioning of the Iris mechanism (*Lindzen et al.*, 2001). SST explain a small percentage of the variance for both ϵ_c and $\mathcal{A}_s$, but this does not invalidate the existence of a signal. For instance, established correlations such as the correlation between SST and q shown in Fig. 4-2.c show substantial scatter, in part due to the reduced range of temperatures in which a signal can be measured. If physical relations between ϵ_c, $\mathcal{A}_s$ and SST exist, and especially if these relations are related mechanistically to variations in the boundary layer relative humidity, the scatter between SST and boundary layer specific humidity represents a lower estimate (However, we notice that our observational estimate for this scatter in Fig 2.c must be at least in part explained by sampling). Confidence in the physical reality of the signals (i.e. as opposed to noise or instrumental artifacts) is also based upon the generalization of the Kwajalein results to the rest of the tropical oceans using the PR instrument. Additionally, we have tested the sensitivity of the relation to the stratiform-convective separation algorithm (see Appendix B) and the significance of the correlations using a Monte Carlo method (see Appendix C). Furthermore, we emphasize that small values of the regression coefficients as the ones we observe do not imply a small effect but rather the presence of noise. The magnitude of the effect is the relevant quantity for estimating possible climate feedbacks.

We notice that the improved linear linear fit (a slight increase in the correlation coefficient and less structure in the residuals of the linear regressions) when specific humidity at the surface is used instead of SST as the independent variable for the Kwajalein data, would seem to point in the direction of boundary layer humidity control of the relation. It has been suggested to us, that our observations as well as some other observations that indicate an increase in the efficiency of precipitation with temperature (Sherwood, personal communication) can be explained by the different mid-tropospheric relative humidity to which convective updrafts are subject. Since re-

gions of relatively warm SST also concentrate most of the precipitation in the tropics, these regions are frequently moister than their colder counterparts. Convection growing in a moister environment has a higher chance of reaching the upper troposphere, and suffers less entrainment of dry air that will reduce cloud liquid water content and therefore decrease efficiency of precipitation. Based on the Kwajalein data, we observe a weaker dependence of ϵ_c and $\mathcal{A}_s$ on the specific humidity above the boundary layer as suggested by the smaller r's and slopes when regressions are calculated using q above 800 mb. Also, given the fact that our analysis for TRMM includes only deep convective systems we are already filtering out convective clouds in regions that were too dry to sustain convection. However, the attribution of an specific mechanism (or several) that explain the observations remains an open question.

Several other processes besides SST should have a bearing in the amount of condensate that is detrained from the convective regions and a bias, resulting from the possibility that some of these alternative processes can be controlled by SST as well, cannot be ruled out. Of course such biases would have implications on the question of whether this effect can be extrapolated to a different climate. In tropical climates where temperature gradients in the free troposphere are small, the buoyancy of the convective parcels can be expected to be controlled by the surface density, which in turn is a function of SST. The magnitude of the convective updrafts can have a large effect in the amount of condensate that is detrained from the convective clouds, although a simple relation between the magnitude of the updrafts and buoyancy would seem to indicate the opposite relation as found here (stronger updrafts would produce more detrainment). Several other not so obvious processes that determine the growth and dissipation of precipitation-size particles (e.g. evaporation in the sub-saturated environment below the stratiform cloud) could also be controlled by SST. In this respect, it is unclear whether the transport of water vapor to the stratiform region by the mid-tropospheric ascent can also have an SST dependence, either by changes in the strength of the circulation of the system or by changes in the amount of water vapor that is available to be transported. Some of these questions could begin to be explored by making use of coincident cloud liquid water and precipitation vertical profiles from TRMM and CloudSat instruments.

Recent observational papers have explored the relation between SST and variables related to the efficiency of precipitation in tropical convective systems. *Del Genio and Kovari* (2002), for instance, studied 6 days of TRMM orbits and found that an index of precipitation efficiency (defined as the ratio between the rain rate and a measure of the specific humidity in the subcloud layer) increases with SST over the regions

of deep convective clouds in the tropics. Similarly, *Lau and Wu* (2003) found an increase in the ratio between the cloud liquid water in light warm precipitating clouds, as estimated from passive microwave data from TRMM. Recently *Lin et al.* (2006) using ECWMF reanalysis and TRMM data, estimated that the ratio between rainfall rate and the moisture supply to the convective clouds increases by about 2%/K in the tropics. These observational studies seem to be consistent with the findings in this chapter and give support to the possibility of an SST control on the efficiency of precipitation. However, a more definitive claim of consistency would require one to sort out methodological as well as conceptual differences in the definition of precipitation efficiency (this could presumably be done in a cloud resolving model framework). We also notice that some of the previous observational studies emphasize the total change of detrainment area as opposed to the normalized quantity as the relevant measure to evaluate climate feedbacks (e.g. *Del Genio et al.*, 2005). If model expectations (e.g. *Held and Soden*, 2006) regarding the relative change of rainfall with temperature are realized, we could expect that any decrease in the normalized area of detrainment at a rate larger than 2%/K would imply a global decrease in the area detrainment, and to the extent that tropical cirrus clouds have a net warming effect on climate, this decrease would imply a negative cloud feedback.

Chapter 5

Thin cirrus as a solution to the Faint Young Sun Paradox

5.1 Introduction

5.1.1 The paradox

Models for the evolution of the sun during the main sequence call for a reduced solar luminosity and therefore a reduced solar constant of about $S = 0.75S_0$ at around 3.8 Gyr ago (Ga) (S_0 is the present solar constant $\sim 1353\ W/m^2$). The increase in solar luminosity is a relatively well understood feature of main sequence stars. A star like the Sun, initially composed mostly of Hydrogen, must increase its density, internal pressure and temperature as Hydrogen is converted to Helium. The implied increase in temperature outweighs the composition effects in determining the nuclear reaction rates in the Sun (*Gough*, 1981), and therefore luminosity increases with time.

On the other hand, multiple pieces of evidence shows the presence of a stable ocean and liquid water in the planet at least after 3.9 Ga (*Pinti*, 2005) and possibly even at around 4.4 Ga, in a geologically short time after the origin of the planet (e.g. *Wilde et al.*, 2001). Besides the positive evidence for liquid water, there is lack of evidence of widespread glaciations up to 2.4 Ga (*Young*, 1991), although it is likely that a mid-latitude glaciation occurred around 2.9 Ga (*Young et al.*, 1998).

Despite of the warm Archean earth implied by the geological record, the solar luminosity implied by the standard model together with the assumption of constant atmospheric composition (or more precisely a constant atmospheric greenhouse effect and a constant atmospheric solar reflectivity) strongly suggest temperatures below freezing for about half of the earth's existence. The simplest way to illustrate this is

to write zero-dimensional energy balance for the atmosphere to calculate the mean global surface temperature (T_s) as a function of the solar insolation S (e.g. *Catling and Kasting*, 2007),

$$T_s = T_g + \left(\frac{(1-A)S}{4\sigma}\right)^{\frac{1}{4}}, \tag{5.1}$$

where A is the planetary albedo and T_g is a temperature that encapsulates the greenhouse effect of the atmosphere and clouds. For current climate with $A = 0.3$ and $T_g = 34$, the mean global surface temperature is $T_s = 288K$. According to the standard solar model , the luminosity, and therefore the variation of the solar constant can be approximated by (*Gough*, 1981) ,

$$S = \frac{S_0}{1 + 0.4t/4.6} \tag{5.2}$$

where t is the time in Ga.

The solar constant at 3.9 Ga was $S \sim 0.75S_0$ (see Fig. 5.1.1), and the simple zero dimensional model gives $T_s = 269K$. Under the assumption of a constant greenhouse effect, T_s rises above freezing for $S \sim 0.78S_0$, which corresponds to ~ 3.2 Ga. A first correction to this simple model would be the inclusion of a water vapor feedback by assuming a constant relative humidity (instead of the implicit assumption of constant specific humidity which would provide a constant value for T_g). By including this positive water vapor feedback in a 1-D radiative convective model one increases the time range of the paradox. *Kasting et al.* (1988) found that T_s remains below freezing up until ~ 2 Ga or $S \sim 0.85S_0$. *Pierrehumbert* (2009) shows that including an ice-albedo feedback the paradox is even more dramatic and the solution for $S = 0.75S_0$ is a snowball earth with $T_s = 228K$. These simple models predict exactly the opposite as what the evidence (or lack of it) suggest, that is, glaciations should have been widespread for the first 2 billion years of earth's history if atmospheric composition were to remain the same.

The resolutions to the paradox fall mostly either on questioning the standard model for the solar evolution or on questioning the assumption of constant atmospheric composition. The original solution proposed by *Sagan and Mullen* (1972) was an early atmosphere containing at least 10 ppbv of NH_3, however, such solution has been contested given the relatively short lifetime of NH_3 to photolysis (*Kuhn and Atreya*, 1979). Most of the solutions have relied on changes in T_g produced by either CO_2 or CH_4 (e.g *Owen et al.*, 1979; *Kasting*, 1987; *Kasting et al.*, 1988; *Pavlov et al.*, 2000). Solutions that involve high CO_2 atmospheric concentrations are particularly

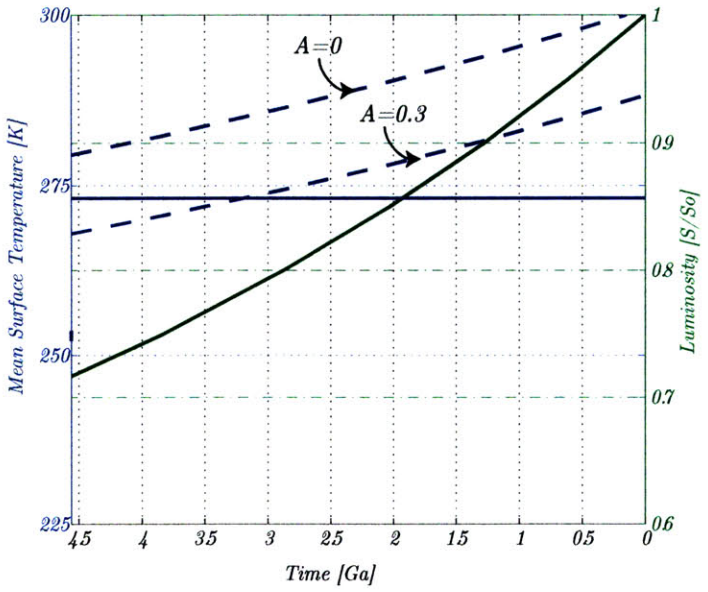

Figure 5-1: Variation of the solar insolation with respect to the present value (green) and temperature according to the zero-th dimensional model in equation 5.1 for two different values of the planetary albedo (dashed lines). The solid horizontal line indicates the 273 K.

appealing given the existence of large reservoirs of carbon in the earth's mantle and continents (and the relative smallness of the atmospheric and oceanic reservoirs). The temperature dependence of the silicate weathering rate (mainly through the temperature dependence of the precipitation) can act as a negative feedback on climate acting through the CO_2 geological cycle (*Walker et al.*, 1981). According to this mechanism, climates colder than present are expected to have a slower weathering rate and therefore a slower cycling of CO_2. Higher CO_2 concentrations expected for colder climates would compensate to some extent for the reduced solar luminosity.

However, some geological evidence from paleosols and other proxies indicates that CO_2 concentrations must be at least ten times smaller than those required to produce mean surface temperatures above freezing in 1-D radiative-convective models (*Rye et al.*, 1995; *Rollinson*, 2007)). *Zahnle and Sleep* (2002) also argue on the basis of theoretical calculations of the carbon geological cycle, that high CO_2 concentrations are implausible. If the geological evidence is taken at face value, the paradox seems to be unresolved (*Shaw*, 2008).

This realization has prompted even the reconsideration of the relevance of the standard model for solar evolution and therefore the faintness of the early sun. *Sackmann and Boothroyd* (2003) proposed a sun about 7% more massive than present as a solution for the paradox. The sun loses mass due to coronal mass ejections, solar

wind and mainly through thermonuclear reactions. If present loss rates are assumed constant, the mass loss is small and amounts to only 0.05% of the total mass throughout the history of the solar system (*Minton and Malhotra*, 2007). Therefore a much larger mass loss would be required at some point in the solar evolution in order to explain a more massive early sun. For younger stars, it appears that the mass loss rate due to solar wind can be higher by up to 2 orders of magnitude than present (*Wood*, 2006), however this loss rate is still short of what would be required to solve the paradox. Solar analogs appear to show no evidence for the magnitude (less than 0.3% compared to about 2.5 % required) and time scale (less than 1 Ga compared to 1 to 2 Ga required) of mass loss required to explain an early bright sun (*Minton and Malhotra*, 2007).

The meridional heat transport can also change under different forcing conditions, potentially providing a stabilizing influence on climate, specially for the onset of snowball solutions (e.g. *Lindzen and Farrell*, 1980). The moderating influence of meridional heat transport has been discussed in the context of the faint young sun paradox by *Endal and Schatten* (1982) who proposed a much more effective ocean heat transport in an early earth with small continents. However, a more effective heat transport would also produce a larger value for the critical insolation for the onset of a snowball earth. *Gerard et al.* (1990), based on the maximum entropy principle (*Paltridge*, 1978), deduced that the heat transport becomes less efficient for lower solar luminosities and therefore they obtain solutions that are stable to an ice-albedo feedback for the whole evolution of the solar constant.

Besides purely dynamical or radiative mechanisms to account for the moderate temperatures under lower solar luminosity, the rise of life and subsequent changes in atmospheric composition may have played a role in the climate stabilization required to explain the paradox. For instance, the rise of early bacteria could have increased methane fluxes into an early anoxic atmosphere (e.g. *Pavlov et al.*, 2000) providing methane concentrations of about 100 times present concentrations (*Pavlov et al.*, 2003). The enhancement of the weathering rate due to the rise of life has also been proposed as a negative feedback on climate (*Volk*, 1987; *Schwartzman and Volk*, 1989, 2004) and moreover as a potential self-regulating mechanism for the biosphere (*Lovelock and Whitfield*, 1982).

Water clouds on the other hand, have been only rarely invoked as a possible solution to the paradox, although changes in their composition, height and areal extent can potentially provide large changes in both A and T_g. For instance, the zero-th dimensional model predicts temperatures above freezing for zero planetary

albedo. However, it is hard to imagine a water covered planet with no clouds. Given our ignorance about cloud feedbacks the usual approach when dealing with the faint young sun paradox is to regard clouds as constant. The rationale and limitations for the assumption of constant cloud properties are summarized by *Kasting and Catling* (2003): *If the goal is to determine what is required to create a climate similar to that of today, it is reasonable to assume no change in cloud properties. For model planets that are either much hotter or much colder than present Earth, however, the neglect of cloud feedback may lead to serious error.* Complementary to the previous quote, one should state that if cloud feedbacks, either positive or negative, are strong, there is no real justification for assuming no change in cloud properties, even in the case of climates having temperatures *close* to present. The matter of how much colder (or hotter) a climate should be so that the effect of cloud feedbacks becomes important has been the subject of some previous studies on the role of clouds in the early earth climate (*Henderson-Sellers and Cogley*, 1982; *Rossow et al.*, 1982). In those studies a decrease in cloud liquid water in colder climates (see chapter 2) is associated with a decrease in planetary albedo large enough to produce mean global surface temperatures above freezing for $S \gtrsim 0.8S_0$.

Here, we focus on testing the feasibility of a solution based on changes in the cirrus cloud coverage in the tropics. We are primarily interested whether a plausible change in the coverage of thin cirrus clouds can solve the faint young sun paradox, regardless of the origin of such a change. We focus on tropical cirrus clouds because contrary to extratropical clouds, in which cloud coverage is mostly related to the relative area of ascent and descent in baroclinic disturbances, the mechanism of formation of cirrus in the tropics appears to be particularly susceptible to a surface temperature dependence. An example of a mechanism that could relate sea surface temperature to thin cirrus cloud coverage is the iris hypothesis discussed in the previous chapters.

5.1.2 Tropical thin cirrus as a possible solution

Thin cirrus clouds are a ubiquitous feature of the current tropical atmosphere. Recent global data using satellite lidar and radar instruments place the frequency of thin cirrus clouds ($\tau <$ 3-4) at $\sim$ 25% over the tropics (30°S- 30°N) (*Sassen et al.*, 2008). Trajectory studies show that at least two mechanisms explain the formation of cirrus clouds in the tropics; a direct detrainment from convective clouds and also a triggering by gravity waves further away from the original convective region (*Mace et al.*, 2006). Although cirrus clouds are believed to have a net positive radiative

effect, there remains uncertainty on this point (*Liou*, 2005). Nevertheless, recent satellite estimations of the cloud radiative effect of cirrus clouds (*Choi and Ho*, 2006) seem to confirm the long held idea that thin cirrus clouds (that is clouds with visible optical depths $\tau \lesssim 10$) have a much larger infrared heating effect than a shortwave cooling, and therefore a strong positive cloud radiative effect.

1-D radiative convective simulations, including at least some representation of cirrus clouds, have already shown the potential of thin cirrus clouds to produce significant surface warming. In the seminal paper by *Manabe and Wetherald* (1967), the addition of a layer of full black cirrus cloud was enough to increase the equilibrium surface temperature from 280 K to 320 K. Similarly, *Liou and Gebhart* (1982) show radiative-convective equilibrium simulations in which the inclusion of a thin cirrus cloud can increase surface temperatures to $\sim$ 320 K for total coverage, with the surface temperature being relatively independent of the height of the cloud base. In the next sections, we present results from a simple radiative-convective model in which the tropical thin cirrus cloud coverage (f) is specified.

5.2 Model Assumptions

The 1-D model is a simple radiative-convective equilibrium model based on the original formulation by *Manabe and Strickler* (1964) and *Manabe and Wetherald* (1967). The model has 140 levels in pressure from the 1000 hPa to 0.04 hPa, following the sigma-level pressure coordinates defined in *Manabe and Wetherald* (1967). The model is run for 600 days from an initial moist-adiabatic atmosphere with surface temperature of 300 K, with time step of 1 day (equilibrium between incoming shortwave and outgoing longwave radiation is reached within less than 1 W/m^2). We use a similar relative humidity profile as in *Manabe and Wetherald* (1967) with a surface relative humidity of 0.8 and a constant stratospheric water vapor mixing ratio of $3{\cdot}10^{-6}$. At each time step we use solar and infrared radiative parameterizations (developed for general circulation models (*Chou and Suarez*, 2002; *Chou et al.*, 2003)) to estimate the radiative heating rates in each vertical layer. A convective adjustment is performed at each time step, so unstable layers are adjusted to a reversible moist-adiabat (which, at least for the tropics, seems to be a very good approximation for the temperature vertical distribution (*Emanuel*, 2007)). In all the runs, unless otherwise noted, the concentration of the radiatively active gases (except for water vapor) is kept fixed and approximately equal to the present atmospheric levels (PAL). That is, CO_2 = 350 ppmv and CH_4=1.75 ppmv.

5.2.1 Incorporating thin cirrus clouds in a 1-D tropical atmosphere

We assess the effect of the coverage of tropical cirrus clouds on surface temperature with some very simple assumptions. The effect of clouds other than thin cirrus (hereafter $\tau < 9$) is not explicitly incorporated, but rather enters as a constant planetary albedo fixed to about 0.2 (this is only part of the planetary albedo, since the radiative parameterization calculates explicitly the scattering by the clear atmosphere and thin cirrus clouds). In this way an incoming solar radiation and a coverage of 0.16 for thin cirrus, will provide a surface temperature close to the observed in the present (298 K for the mean tropical temperature). The incoming solar radiation that provides the current tropical average temperature ($\sim 285 W/m^2$ after correcting by the solar zenith angle and constant planetary albedo), will serve as a basis for changing the solar constant in the model, mimicking the solar history. The solar zenith angle is kept constant and equal to 60°. The treatment of clouds in the radiative parameterization is explained in detail in *Chou and Suarez* (2002); *Chou et al.* (2003). The cloud optical thickness in the visible spectral region (τ_c) is a function of both the effective radius of the cloud particles r_e and the ice water path (IWP) of the cloud, and it is parameterized as

$$\tau_c = IWP \frac{1.64}{r_e}, \tag{5.3}$$

where IWP has units of gm^{-2} and r_e has units of μm. The parameterization of the cloud radiative effect in the visible is independent of the solar spectral bands. The value of r_e is calculated according to the empirical regression by *McFarquhar* (2001) as a function of both the local temperature and the value of the cloud water content. The parameterization of the infrared optical depth of the cloud, takes into account the absorption and scattering of radiation by the cloud (*Chou et al.*, 1999). The extinction coefficient, the single scattering albedo and the asymmetry factor are all dependent on r_e and on the particular spectral band (*Chou et al.*, 2003). By specifying the thickness of the cloud (here equal to one model vertical layer) and by specifying the cloud water content, both IWP and r_e can be calculated.

In the control case, we specify the value of cloud liquid water content to $7 \cdot 10^{-4} g/g$, so that a cloud with a thickness of 9 hPa results in an $IWP \sim 44\ g/m^2$. The cloud is first located at a fixed level of 200 hPa (we will discuss the effect of relaxing this assumption to make it consistent with the changes in the vertical temperature structure over the range of solar forcings). We use a single cloud as a proxy for the radiative effect of all types of thin cirrus clouds in the tropics. The selection of

this particular cloud is not arbitrary, rather it is such that it roughly matches the radiative forcing from observations in current climate as estimated by *Choi and Ho* (2006). For the control run, the selected cloud provides a longwave cloud radiative effect of +115 W/m^2 and a shortwave cloud radiative effect of -50 W/m^2. These values coincide roughly with the observed values derived by *Choi and Ho* (2006) for both the longwave and the shortwave radiative effect as well as the net positive cloud radiative effect of these clouds, which is about +46 W/m^2 for all clouds with $\tau < 4$.

5.3 Results

5.3.1 Single column radiative-convective simulation

In the first run we explore the behavior of the the tropical surface temperature in radiative convective equilibrium for different values of the thin cirrus cloud coverage. Figure 5-2.a shows the results for this tropics-only column. For the current solar insolation S_0 and current cloud coverage $f \sim 0.16$ the surface temperature is $\sim$ 298 K. An increase in the coverage of this thin cirrus cloud from $f = 0.16$ to $f = 1$ would produce an increase in the surface temperature in the tropics to about 325 K. From the same figure, we notice that the mean tropical temperature is above freezing for constant atmospheric conditions (lower gray line), even at solar insolations of about $S \sim 0.81 S_0$. We note that the usual statement of the faint young sun paradox is made in terms of mean surface temperature. Therefore a solution is considered as such when the mean surface temperature is above freezing (hereafter, this is what we will consider a solution). A weaker version of the paradox can be envisioned in which temperatures are above freezing for a significantly large area of the planet. One can also envision a stronger version of the paradox in which one takes the absence of evidence of glaciation as an indication of a completely ice-free earth.

The three black dashed lines in each of the panels of Fig. 5-2 represent three different relative rates of change for the thin cirrus cloud coverage (so a -10%/K rate of change represents a change from 0.16 to 0.176 from 298 K to 297 K. We will denote this rate of change as $\gamma = \frac{1}{f}\frac{\partial f}{\partial T_t}$, where T_t is the mean tropical rate. The rate of change γ represents implicitly the magnitude of the climate feedback associated with increase in thin cirrus clouds. The dashed lines in each of the panels of Fig. 5-2 are for magnitudes of γ = -5%/K, -10%/K and -20%/K. For this tropics-only case, to sustain surface temperatures above freezing for $S = 0.7 S_0$, one would need a cirrus coverage of about 0.8. This surface coverage is accomplished with a mere -6%/K

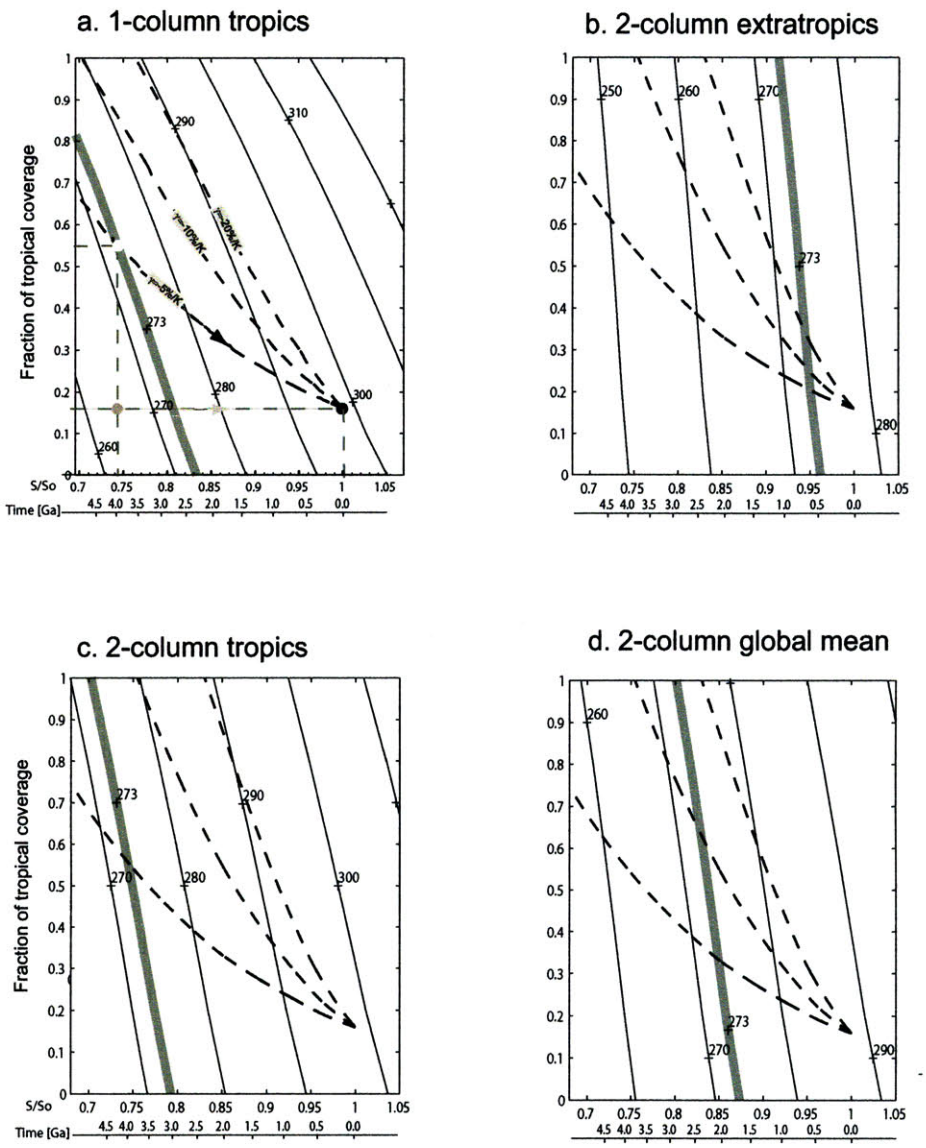

Figure 5-2: Equilibrium surface temperature corresponding to a) 1-column, tropics-only simulation. b) Extratropical column in the 2-column simulation, c) tropical column in the 2-column simulation and d) global mean in the 2-column simulation. The temperature is indicated by the color scale and also by the solid black lines. The solid white line indicates the freezing temperature of pure liquid water. In panel a) a black dot indicates current climate conditions. The white dot indicates the climate surface temperature corresponding to a luminosity of $\sim 0.74 S_0$ and a cloud coverage of 0.55. This climate occurs for a rate of change of -5%/K in the coverage of thin cirrus clouds in the tropics. The two other dashed lines represent rates of change in the cloud coverage of -10%/K and -20%/K as labeled. The gray dot is the equilibrium temperature of a climate with the same luminosity as the white dot but with no cloud feedback. The time scale in the abscissa is calculated according to equation 5.2

change in the cloud coverage.

5.3.2 2-column radiative-convective simulation

Since in the previous simulation we only deal with a tropical column, we can not test the paradox in its more usual framing, that is, with respect to global mean temperature. Also, since the incoming solar radiation in the single column has been tuned so as to produce the observed current tropical temperature, the heat transported out of the tropical column (implicit in the tuning) decreases in the same proportion as the solar insolation.

We add an extratropical column to the model and we will assume a diffusive heat transport between the two columns, with a constant transport coefficient $K = 3 \cdot 10^6 m^2/s$ over the depth of the model, so that at each time step, the temperature in each layer is calculated as the sum of three tendencies; the radiative heating, the convective adjustment and the meridional transport between the columns.

The results for the 2-column simulations are shown in Fig. 5-2.b, c and d. Fig. 5-2.c can be directly compared to Fig. 5-2.a. We see that assumption of a diffusive transport makes the 2-column tropics warmer than the single-column tropics for low cirrus coverages ($f \lesssim 0.45$), and colder for relatively high coverages. Since no change other than the cirrus coverage in the tropical column is made, all change in temperature with cloud coverage in the extratropical column shown in Fig. 5-2.b is due to the transport from the tropical column. Fig. 5-2.d shows the global mean surface temperature (calculated as simply the average between the surface temperature in the two columns). We see that for constant atmospheric composition (that is following a line of constant $f = 0.16$ in Fig. 5-2.d) the global mean surface temperature in our 2-column model remains below freezing up until $S = 0.86 S_0$ giving somewhat warmer temperatures than with previous 1-D radiative-convective simulations ($\sim$ 265 K at $S = 0.8 S_0$ compared to $\sim$ 262 K for the same insolation as in *Haqq-Misra et al.* (2008)). We are confident that these differences are not due to the peculiarities of the radiative parameterization or to the convective adjustment since our own 1-D tropical simulations with no cloud cover can be used to recover a temperature of about 263 K for $S = 0.8 S_0$ similar to the ones reported for current atmospheric composition at $S = 0.8 S_0$ (*Kasting and Catling*, 2003; *Haqq-Misra et al.*, 2008).

The dashed curves in Fig. 5-2.d indicate that for some value of γ between -10%/K and -20%/K, there is a solution of the paradox up to $S = 0.8 S_0$ or for a the range between 2.9 and 1.9 Ga. This solution would imply a total cirrus coverage for the

tropics, and a tropical mean temperature of about 285 K. A smaller rate of change of about -7%/K however, can sustain global mean temperatures of only $\sim$ 261 K for $S = 0.72S_0$, although tropical mean surface temperatures in this case would be just above freezing, suggesting that even this moderate rate of change in cloud coverage could explain ice-free conditions for large regions of earth.

5.3.3 Thin cirrus and increased greenhouse gases

CO_2 alone can provide enough greenhouse effect to overcome the paradox. However, geological evidence seems to point to less CO_2 present in the atmosphere than would be required. For instance, *Rye et al.* (1995) argue on the basis of the absence of siderite in paleosols that CO_2 concentrations higher than about 10 times the present atmospheric level (10 PAL) at 273 K are unlikely at about 2.8 Ga ($S \sim 0.81S_0$). This limit is temperature-dependent and goes up to about 50 PAL at temperatures above 300 K. *Kasting* (1993) quotes levels of CO_2 that are several times higher than the paleosol limit ($\sim$ 50 PAL for reaching $T_s \sim$ 273 K for $S = 0.8S_0$). The discrepancy between required and estimated CO_2 concentrations is also found in other geological and theoretical evidence. Fig. 5-3 adapted from *Rollinson* (2007), shows some of the constraints on CO_2 proposed on the basis of geological evidence. Values of CO_2 much higher than those deduced from the absence of siderite can be inferred from the existence of Nahcolite in samples of sediments at 3.4 Ga (*Lowe and Tice*, 2004). Also, a lower limit for CO_2 of about 10 PAL can be deduced from weathering rinds at about 3.2 Ga (*Hessler et al.*, 2004).

It would appear that if geological constraints on CO_2 are somewhat accurate, the paradox is unresolved if only CO_2 and water vapor were the main greenhouse gases. CH_4, with a much longer lifetime in an anoxic atmosphere than in the present atmosphere, could provide an additional greenhouse effect. However, recent calculations by *Haqq-Misra et al.* (2008) show that the required concentrations of CH_4 are larger than previously believed. Also the CH_4 greenhouse effect is limited by the formation of a reflective organic haze when CH_4/CO_2 is higher than $\sim$ 1.

In this subsection, we will show calculations with a thin cirrus cloud feedback as the one previously described, operating at the same time as an atmosphere with larger CO_2 concentrations. We perform the same runs as in the control case for 3 different CO_2 concentrations for $S = 0.8S_0$. The longwave parameterization by *Chou et al.* (2002) is deemed appropriate even for concentrations of about 100 times present atmospheric levels of CO_2.

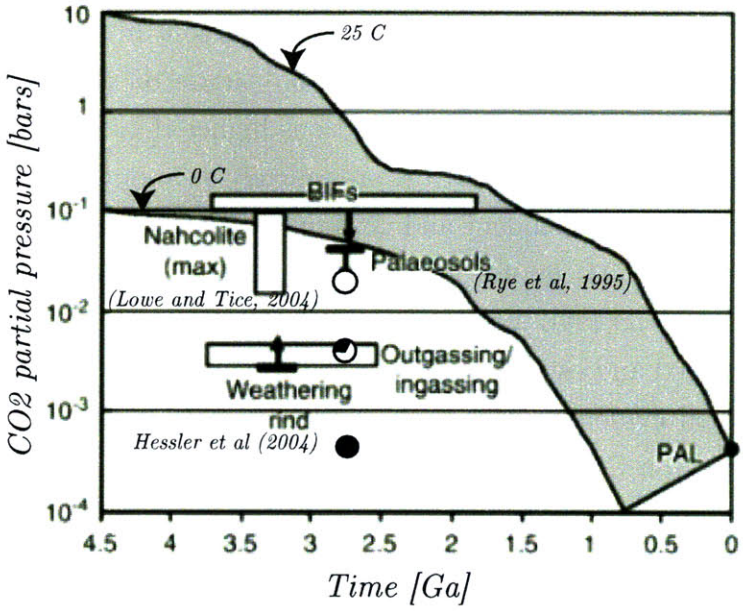

Figure 5-3: CO_2 levels needed to solve the paradox according to a single column radiative convective model (*Kasting*, 1993). The shaded region corresponds to temperatures between 25 C and the freezing level. Also indicated are some of the geological constraints deduced for the CO_2 concentration (rectangles). The filled circles indicate the fractional coverage of thin cirrus required to solve the paradox for S=0.8. Black is full coverage, white is no coverage. Adapted from *Rollinson* (2007)

Fig. 5-4, shows the surface temperature for 3 different CO_2 concentrations at $S = 0.8S_0$. We see that for the current climate value of $f = 0.16$ (vertical dashed gray line) and for the present value of CO_2 (1 PAL), the surface temperature is about 266 K. For a constant cloud coverage the amount of CO_2 required for mean global temperatures to rise above 273 is about 20 PAL CO_2. We recover here the well known result that the paradox can not be solved solely on the basis of a higher concentration of CO_2, without getting a result inconsistent with the paleosol data. If we focus on values of CO_2 allowed by the paleosol constraints, a solution to the paradox can be found with relatively small values for the cloud feedback magnitude. For instance, for 1 PAL CO_2, the tropical coverage required to solve the paradox is about 1. For the case in which $CO_2 \sim 10$ PAL, the paradox can be solved with a tropical coverage of only 0.35 and the magnitude of the cloud rate of change required for providing these cloud coverage is $\gamma \sim -5\%/K$ (see the partially filled circle in Fig. 5-3). This solution is consistent with the paleosol constraint and of course stronger values of the cloud feedback could solve the paradox for lower levels of CO_2. We stress that both consistency with the paleosol data and global mean temperatures above freezing can be achieved (at least for this particular value of solar insolation) invoking only a small magnitude of the cloud rate of change. We also note that while cirrus coverage is less than full, the effect of further increasing cirrus coverage in the mean temperature is mostly linear with cloud coverage as opposed to the effect of the increase in CO_2 (or other greenhouse gases) in the mean temperature that are only logarithmic.

5.3.4 Sensitivity to cloud water content

Our results so far, have been obtained with a single cloud with optical depth 1.3. We explore the sensitivity to changes in the cloud water content of the cloud. Table 5.1 summarizes the cloud properties of the different clouds. The cloud radiative effects were calculated with the runs corresponding to $f = 0.2$. The clouds with either much larger or much smaller cloud water content than the control case produce smaller net radiative effects. Even though there is a net positive cloud radiative effect for the $cwc = 28 \cdot 10^{-4}$ run, the cloud radiative effect becomes negative for higher cloud fractions and temperatures decrease with cloud coverage (Fig. 5.1.b). For the thinner cloud case, the net radiative effect is smaller but positive and very similar to the control case (Fig. 5.1.a). This "optimal" net radiative for the control case coincides with the ordering provided by *Choi and Ho* (2006) with respect to shortwave optical depth; smaller positive radiative effect for thinner clouds and smaller and even

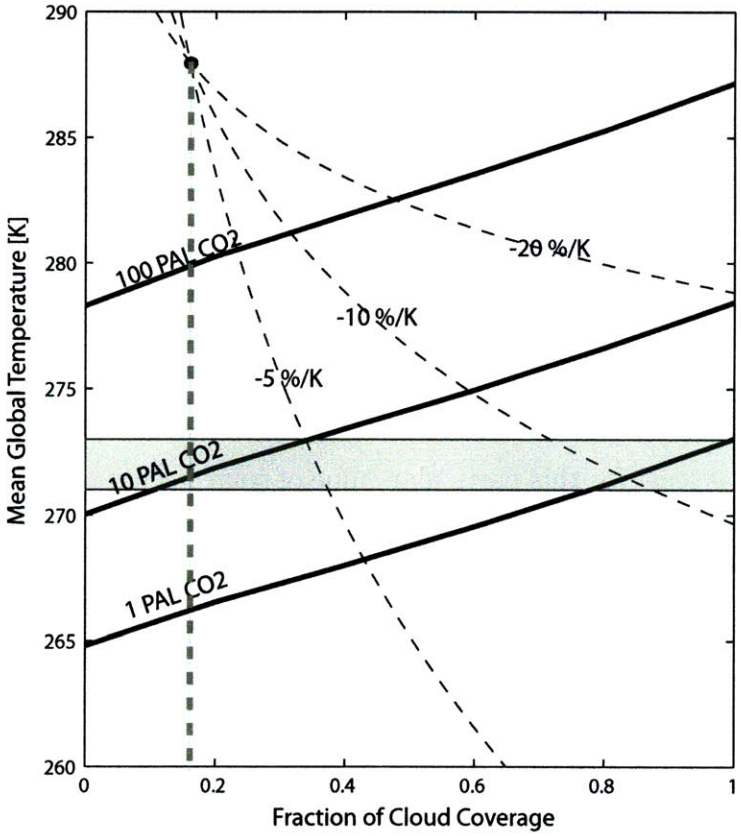

Figure 5-4: Mean surface temperature corresponding to the 2-column radiative convective model for $S = 0.8S_0$. The black solid lines are three different concentrations of CO_2 (PAL stands for Present Atmospheric Level). The dashed lines represent different rates of change in the thin cirrus cloud coverage from the present value of 0.16. The gray horizontal strip is meant to represent a range of temperatures for freezing water between 271 and 273 K .

cwc $[10^{-4}g/g]$	IWP $[g/m^2]$	τ	r_e $[\mu m]$	LW $[W/m^2]$	SW $[W/m^2]$	NET $[W/m^2]$
7	46	1.3	59	120	-70	50
3.5	23	0.73	52	70	-35	35
28	185	4	75	140	-130	10

Table 5.1: Value of the cloud microphysical and radiative properties for the sensitivity runs. The LW, SW, and NET columns represent the cloud radiative forcing in the longwave, shortwave and net, respectively. For all runs the thickness of the cloud is fixed at $\sim$ 200 m, an the cloud is located at 200 hPa

negative radiative effects for thicker clouds.

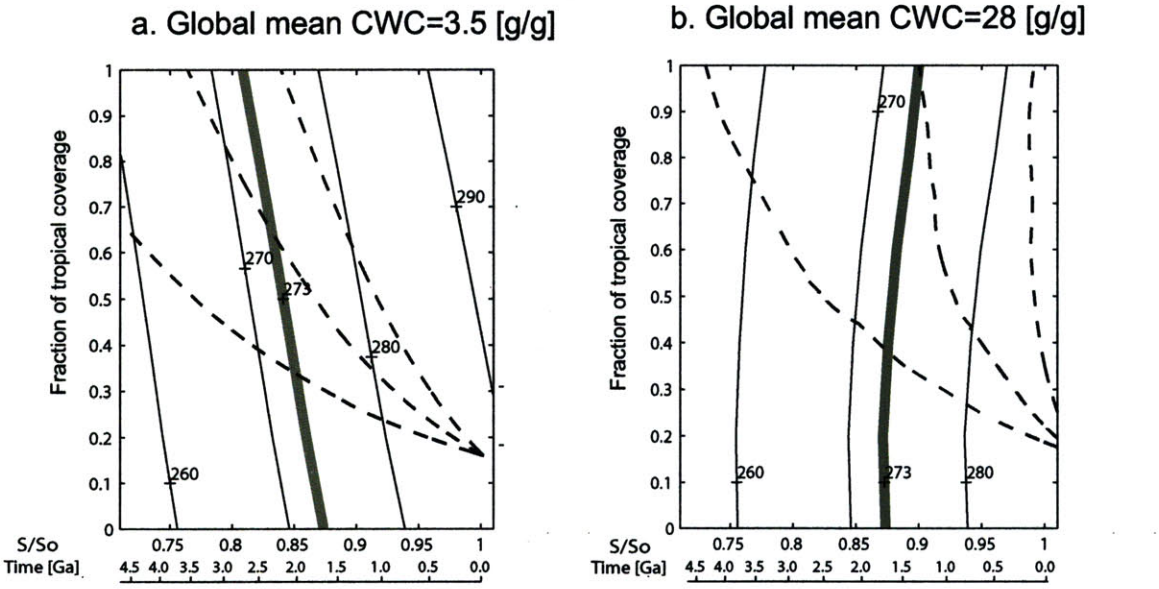

Figure 5-5: Same as Fig. 5-2.d but for clouds with different cloud water content. a) 3.5 [g/g] b) 28 [g/g]

5.3.5 Sensitivity to the fixed height assumption

We have also tested the possibility that the results are sensitive to the assumption of a fixed height or fixed pressure level cloud. An alternative to specifying the cloud at a constant pressure level is the fixed anvil temperature proposed by *Hartmann and Larson* (2002). They propose that the level at which radiative cooling decreases substantially is controlled by the distribution of water vapor, which is the main infrared substance near the tropopause. At the same time, the total amount of water vapor is a strong function of temperature as a consequence of the Clausius-Clapeyron

relation. Therefore, radiative cooling rates in the troposphere are a strong function temperature (as long as water vapor is the main driver of the radiative cooling). In particular, the divergence of the radiative cooling would then occur at about the same temperature no matter the surface temperature of the climate considered. Since convective heating balances radiative cooling in the tropical free troposphere, the level at which convection detrains would be strongly constrained to be near a fixed temperature. In Fig. 5-6 we show the results for the global mean surface temperature for the 2-column model in the case in which the cloud is located at the 220 K level (this is done iteratively at each time step in the tropical column). The results show that the magnitude of the cloud effect is only modestly reduced. For instance for $S = 0.81S_0$, the tropical coverage required for global mean temperatures to be above 273 K in the control case is $f \gtrsim 0.87$. For the fixed anvil temperature case $f \sim 1$.

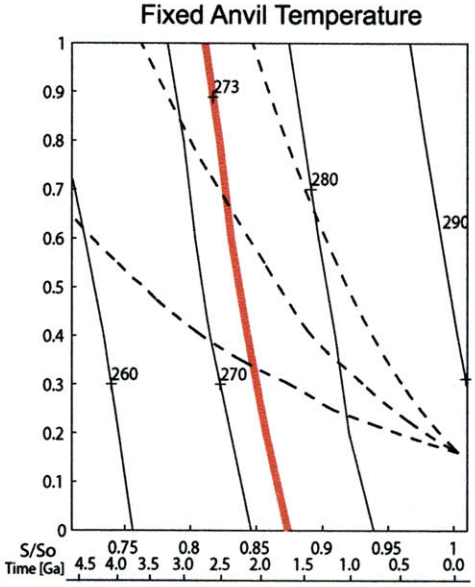

Figure 5-6: Same as Fig. 5-2.d but for a fixed temperature anvil cloud at the 220 K level

5.3.6 Sensitivity to water vapor feedback

So far we have followed the customary assumption of a constant relative humidity profile. In the context of our 1-D single column tropical model, the assumption of strict relative humidity invariance gives a water vapor feedback factor, $\beta \sim 0.4$ [1]. Recent studies suggest that the strong positive water vapor feedback implied by

[1] β is defined following, for instance, *Held and Soden* (2006). If water vapor is the only feedback acting on the climate response to a given forcing, $\Delta T = \Delta T_0/(1-\beta)$, where ΔT is the response

the invariance of relative humidity may be within reasonable agreement with satellite observations (*Dessler et al.*, 2008), even though the vertical profile of relative humidity is not strictly conserved (see also (*Sun and Held*, 1996)). *Renno et al.* (1994), for instance, showed in the context of a radiative-convective equilibrium model with an explicit hydrological cycle, that changes in the microphysical parameters that control the conversion of water to precipitation and vapor could produce very different equilibrium climates, with different vertical distributions of relative humidity. Since we do not have an explicit parameterization for water vapor in our model, we specify changes in relative humidity with surface temperature to explore the sensitivity of the results to the water vapor feedback strength.

We vary the relative humidity in the model from the original relative humidity profile according to

$$RH(500hPa) = \alpha \cdot (T_s - 288) + RH_0(500hPa) \tag{5.4}$$

where RH_0 is the original relative humidity (based on *Manabe and Wetherald* (1967) profile). Between 200 hPa and 800 hPa, the humidity profile is interpolated from the original profile to the new value at 500hPa using a cubic spline. Since we have specified the change in the feedback in terms of a change in relative humidity, the magnitude of the feedback will have a dependence on temperature. We use the model output to calculate the magnitude of the water vapor feedback for each case. Figure 5-7 shows the temperature dependence of the feedback factor for three different values of $\alpha = -0.015, 0, +0.015$. The feedback factor decreases with temperature for all cases. For the imposed changes in relative humidity, the spread of the water vapor feedback tends to decrease with temperature. This is already an indication that uncertainties in the water vapor feedback factor for current climate will be less consequential in determining the temperature for lower global mean surface temperatures.

Figure 5-8 shows the mean surface temperature for 2-column model as a function of the cloud fraction for $S = 0.8S_0$. Global mean temperatures $\sim$ 273 K, are found at about $f \sim 1$. Changing α from -0.015/K to 0.015/K has little effect on the total cirrus cloud cover needed for temperatures above freezing. Fig. 5-8 also hints to the fact that changes in water vapor feedback are more efficient for relatively low cloud coverage, since changes in water vapor in the free troposphere are buffered by the presence of the cloud above (notice the shaded regions in Fig. 5-8 showing the reduced range of variation in f required for a given temperature for low coverage).

including the feedback whereas ΔT_0 is the nonfeedback response or Planck response

The two effects, namely the decrease in strength of the feedback with temperature and the decrease in strength of the feedback for large cirrus coverage, suggest that the range of the solution has a low sensitivity to the strength of the water vapor feedback in the context of the present model.

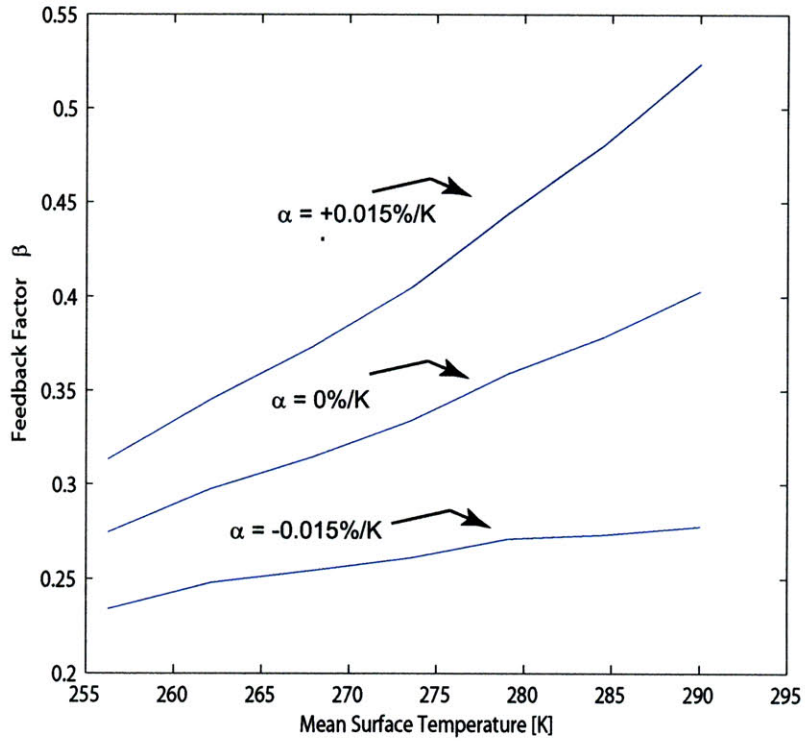

Figure 5-7: Water vapor feedback factor β as a function of temperature for three different values of the strength of the relative humidity change in Eq. 5.4 (α =-0.015, 0 and 0.015).

5.3.7 Sensitivity to the meridional heat flux

We have so far assumed a linear diffusivity law for the heat transport between the tropical and extratropical column. An alternative to the simple linear diffusivity would be to assume a constant temperature difference between the two columns so as to crudely represent a baroclinic adjustment over the different possible climates considered (e.g. *Stone*, 1978). This is accomplished in the model by allowing the diffusivity coefficient to change while keeping a constant target temperature difference between the two columns (in this case 20 K). In Fig. 5-9 we see the result of this modification. The situation in the global mean is not very different from the constant diffusivity depicted in Fig. 5-2.d, so that the main result does not change appreciably;

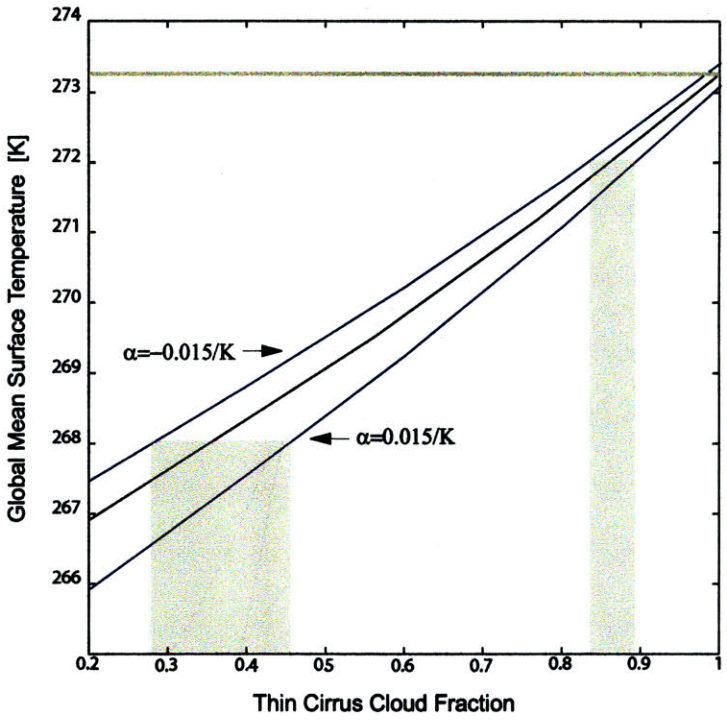

Figure 5-8: Sensitivity of the results for $S = 0.8S_0$ to the water vapor feedback strength. The two shaded regions show the value of the cloud coverage required to obtain a given global mean temperature (in this case 268 and 272 K)

the mean global temperature can be above freezing for luminosities $\sim$ 0.81 and full tropical cirrus coverage. However, since in the case of the fixed temperature difference the tropics are colder than in the control case (for instance, the mean tropical temperature is 282 K for S=0.81S_0 and $f = 1$ in the fixed meridional temperature case and 285 K in the linear diffusivity case for the same conditions) the values of γ required to accomplish the needed full tropical cirrus coverage are therefore smaller in the fixed meridional temperature case ($\gamma \sim$ -12%/K compared to $\gamma \sim$ -15%/K in the control case). By providing warmer extratropical temperatures, this alternative treatment for the meridional heat flux would also delay the onset of solutions unstable to an eventual ice-albedo feedback. Besides the control case and the constant temperature case, we have a third assumption about the meridional heat transport. In the case of a single column tropics depicted in Fig. 5-2 the meridional heat transport is implicit (since the incoming solar radiation is tuned to obtain current tropical temperatures) and reduced by the same fraction as the reduction in incoming solar radiation. In the single column tropical cases the heat transport becomes less effective as the climate cools (similar to the decrease in transport efficiency predicted from maximum

entropy considerations (*Gerard et al.*, 1990)). This isolation of the tropics from the extra tropics also allows for a more effective functioning of the tropical cirrus clouds in resisting the changes in the solar constant and would provide a more robust 'partial' solution to the paradox, with relatively warm oceans in the tropical regions of the planet.

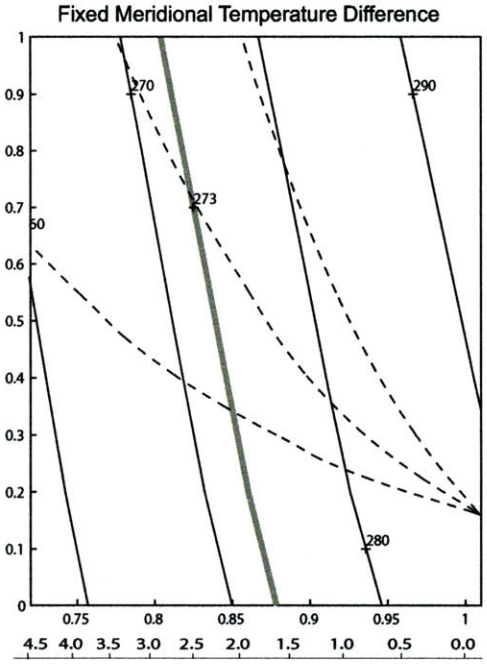

Figure 5-9: Same as Fig. 5-2.d but for a fixed difference in surface temperature between the tropical and the extratropical column.

5.4 Discussion

We have presented simplified radiative-convective equilibrium calculations to investigate the role of thin cirrus clouds in providing a solution for the faint young sun paradox. In the context of our model, solutions do in fact exist. Tropical thin cirrus clouds can either solve the paradox in the sense of providing *global* mean temperatures above freezing (after $\sim$ 2.9 Ga) or in a weaker sense, less than full tropical cirrus coverage can provide *tropical* mean temperatures above freezing for all earth's existence (in the context of this model). The solutions are characterized by a colder tropical temperature and therefore by thin cirrus clouds acting as a net negative feedback to the solar forcing.

Given that thin cirrus clouds can indeed solve the paradox, we focus the discussion

on the question of the plausibility of these solutions. There is the suggestion that a negative feedback such as the one required might in fact be operating in current climate (*Lindzen et al.*, 2001). We have discussed the functioning of the Iris hypothesis in chapter 3. Apparent confirmation for the iris effect came from the analysis of the OLR trends over the last two decades, showing a strong increase in the OLR compared to a relatively smaller decrease in the shortwave reflectivity in the tropics (*Wielicki et al.*, 2002; *Chen et al.*, 2002). Using a combination of datasets, *Hatzidimitriou et al.* (2004) traced the OLR increase mainly to a decrease in the upper level cloud coverage and a drying of the upper troposphere. As pointed out by *Chou and Lindzen* (2005) this large increase in OLR was also consistent with a much larger value in the relative change in cloud fraction with temperature than the original -22 $\%/K$ found by *Lindzen et al.* (2001). The OLR trends were recently revised down to only about a quarter of the original value (*Wong et al.*, 2006), although the OLR trend continues to be larger than the Planck response expected from an increase in the tropical mean temperature over the same period. Here, we simply point out that present climate trends in tropical mean OLR can not rule out the existence of a negative feedback such as the one required to solve the paradox.

We have assumed so far that the magnitude of the cloud changes with respect to temperature is absolute, that is, it already contains any possible dependence on changes in convective activity that will arise as the incoming radiation at the surface decreases. Theoretical arguments and model simulations both indicate that changes in precipitation with global mean temperature are relatively small ($\sim$ 2-4%/K (*Held and Soden*, 2006; *O'Gorman and Schneider*, 2008; *Stephens and Ellis*, 2008)). Even with such small changes, a correction to account for the reduction of precipitation or convective activity will indeed be required. One can diagnose from the surface budget, the total convective heating in the model, which, in the tropics has to be equal to the precipitation. The changes in precipitation in the model depend on the magnitude of the feedback itself, given that a stronger feedback would reduce the net incoming solar radiation at the surface more rapidly than in the case of a weaker feedback. This is illustrated in figure 5-10 which shows the increase in precipitation with temperature for three different values of the absolute cloud change γ. One can write $\gamma' = \gamma - \frac{1}{P}\frac{\partial P}{\partial T_t}$, so that the relative changes in cloud fraction γ', have to be higher than the absolute value of the change γ required to compensate for the decrease of precipitation in a colder climate. Fitting exponential functions to the model-diagnosed precipitation one finds that the quantity $\frac{1}{P}\frac{\partial P}{\partial T_t}$ goes from about 3%/K to 7%/K. Recently, *Stephens and Ellis* (2008) provided an explanation for the

relative smallness in the changes in precipitation with respect to changes in water vapor that are thought to scale as Clausius-Clapeyron in current general circulation models. Precipitation rates are bound to satisfy a global balance that involves mainly the net radiative cooling in the free troposphere and the latent heat released that is equivalent to the precipitation. On the other hand, a water vapor feedback such as the one found in current models, implies a Clausius-Clapeyron scaling of the water content. As discussed previously, the radiative cooling does not scale linearly with water content, but rather as a power law, with an exponent of about 0.5. *Stephens and Ellis* (2008) argue about the potential for clouds to disturb this balance and change the precipitation dependence, however they dismiss the possibility of a cloud effect on the basis of the smallness of the net cloud radiative effect compared to the magnitude of the net clear sky radiation. However, the net cloud effect does not constrain the value of the feedback needed to estimate the change in precipitation. In other words, the same argument used to derive a small change in precipitation could be used to argue that since water vapor variations have a relatively small effect in the clear sky radiation, changes through clouds could potentially dominate the response in precipitation. In fact, our simple model shows how cloud feedbacks could substantially modify the precipitation rate of change at same time that the water vapor content in the atmosphere follows a Clausius-Clapeyron scaling.

Regarding observed value of γ', different datasets and analyses point to values between -2%/K to -22%/K for current climate (see chapter 3 for a discussion of the methodological issues in quantifying the rate of change from data). These empirically derived rates of change γ', usually refer to some observable that is a proxy for the thin cirrus clouds rather than the thin cirrus clouds themselves. Nevertheless, the magnitude of these changes is consistent with what is required to solve the paradox (for instance from Figs.5-2.c and d, the tropical temperature for $S = 0.8S_0$ and $f = 1$ is about 285 K which gives a rate of change of $\gamma \sim$ -15%/K, $\gamma' \sim$ -20%/K)

One can ask what happens in the situation in which the tropical atmosphere is already completely covered by cirrus clouds and temperatures continue to decrease. One could expect that if the cloud feedback still operates beyond full coverage, an increase in the cloud water content or in the thickness of the cirrus clouds would ensue. The cloud feedback can only operate until the cloud is thick enough ($\tau \sim 10$) that surface cooling instead of heating is obtained (as in Fig. 5-5.b). At the same time, if the cloud cover is thick enough to reflect most of the incoming solar radiation, convection (and therefore the source of the cloud) will shut off. Microphysical effects such as an enhanced precipitation from the cirrus cloud might prevent this from

happening. However, without a mechanistic model one can not go beyond speculation on this point. We only note here that the mechanism such as the one described will have a limit for low temperatures. The availability of water for sustaining a total cirrus coverage does not pose a problem. Even with a weaker hydrological cycle as expected in a colder climate (rainfall rate estimated in $\sim$ 2 mm/day for a surface temperature of $\sim 270K$ (*O'Gorman and Schneider*, 2008)) and with a 44 g/m^2 cloud (with an accompanying water vapor layer of 400 g/m^2) and assuming that a typical ice particle dissipates over a day, the detrainment flux required to sustain such a cloud is only about $\sim 2\%$ of the precipitation rate.

Although the literature about the paradox usually focuses on greenhouse gas solutions (*Kasting and Catling*, 2003; *Shaw*, 2008), solutions based on cloud feedbacks have been put forth in the past. Based on the model developed by *Wang et al.* (1981) in which cloud cover is considered proportional to the convective heating (or total precipitation), *Rossow et al.* (1982) (see also *McGuffie and Henderson-Sellers*, 2005,

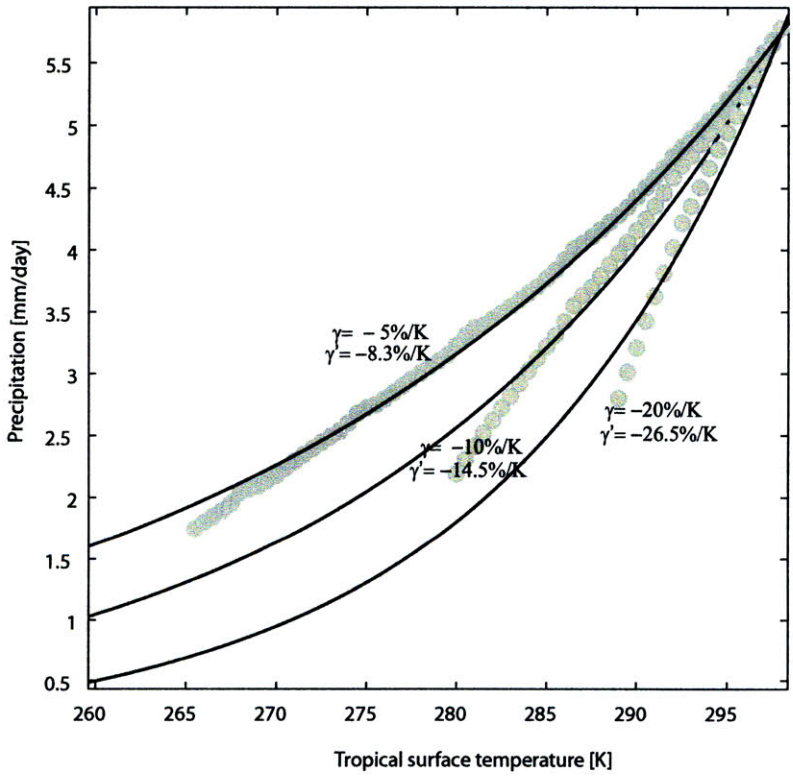

Figure 5-10: Changes in precipitation diagnosed from the surface balance in the tropical column of the model. The gray dots show the precipitation diagnosed from the model for three values of the magnitude of the feedback $\gamma = 5$, 10 and 20 %/K. The black lines are exponential fits to the precipitation curves from which a value of γ' was deduced.

section 4.6.1) proposed a solution to the paradox based on the negative feedback resulting from a decrease in planetary albedo and a decrease in the cloud water content (and therefore in the visible optical depth) of clouds in a colder climate. Our solution on the other hand leaves the albedo almost unchanged as it mostly depends on the longwave radiative effect of upper level thin cirrus clouds. The solution by *Rossow et al.* (1982) and our solution are not mutually exclusive. Several cloud feedbacks other than the one resulting from the change in thin cirrus are possible in reality and have been muted in the present model (for instance area coverage and composition of stratocumulus clouds in the subtropics). Despite progress since the time of the writing of the study by *Rossow et al.* (1982), clouds continue to be "the major source of uncertainty" in climate models (e.g. *Schwartz*, 2008). As in previous studies dealing with clouds and the faint young sun problem (*Cogley and Henderson-Sellers*, 1984, contains references to previous work on this issue) (see also the mechanism proposed by *Shaviv*, 2003), we conclude that a negative cloud feedback can indeed solve the paradox if the Archean climate was somewhat colder than present. (How much colder will also depend on the strength of the feedback). We have followed the customary assumptions of neglecting the ice-albedo feedback, fixing the relative humidity and muting the effect of clouds to a large extent, we have also assumed a very simplified treatment for the heat transport between tropics and extratropics. None of these assumptions is entirely satisfactory. Given the simplified nature of this radiative-convective model, our study is only exploratory.

Solving the paradox down to a luminosity of $S = 0.8S_0$, requires a climate with an equilibrium sensitivity parameter to solar forcing $\lambda = \Delta T_s/\Delta S$ of about 0.29 $K/(Wm^{-2})$. This sensitivity value is certainly smaller than any of the sensitivities to CO_2-forcing in current GCMs (*Solomon et al.*, 2007), but it is within the lower range of estimates made from observations (e.g. *Schwartz*, 2008). One finds values of $\lambda \sim 0.4\ K/(Wm^{-2})$ for the 1-D radiative-convective models without clouds (using for instance the results by *Kasting*, 1987); we also found a nearly identical value for λ in our 2-column radiative convective model with no cloud feedback. As shown in section 5.3.3, small changes in the rate of change of cloud coverage can reduce the amount of greenhouse gases needed to reach consistency with the geological evidence. These clouds changes are associated with small changes in the model climate sensitivity (a -5%/K rate of change in the thin cirrus coverage is equivalent to a sensitivity $\lambda \sim 0.37K/(Wm^{-2})$) in the present model).

5.5 Concluding Remarks

Using simple radiative-convective simulations we have tested the idea that a coverage of tropical cirrus clouds much larger than present could resolve the faint young sun paradox. We have found that relatively modest cloud changes can indeed provide sufficient cirrus coverage for the mean global temperature to be above freezing for $S \gtrsim 0.8S_0$ and for the mean tropical temperature to be above freezing for $S \gtrsim 0.7S_0$ without additional greenhouse gases. The model cloud is specified to have similar cloud radiative effect as reported in current climate observations. We tested the sensitivity of the results to cloud water content, to the assumption of a constant pressure level of detrainment and to a range for the strength of the water vapor feedback. We also looked at two different treatments for the meridional heat transport. We find small sensitivities to all these factors in the present model. Although we describe a very specific cloud negative feedback, our results can be understood in a more general perspective with respect to the faint young sun paradox; a moderate negative climate feedback can indeed resolve the paradox without resorting to large changes in the greenhouse gas content of the Archean atmosphere. By necessity our solutions imply colder climates than present. Therefore, everything being equal, the content of CO_2 would be expected to be higher, related to smaller weathering rates. With the help of this additional greenhouse gases our solution does not demand a very low climate sensitivity.

Chapter 6

Conclusions and Outlook

In this thesis we have studied observationally the relation between local sea surface temperature and the area of upper level clouds in the tropics. In particular we have confirmed a relatively strong decrease in the area of upper level cloud per unit convection with SST. The decrease in area per unit convection appears as a robust result over different datasets and periods of time.

As we have stated in the previous chapters, the change in area is one of several aspects of a possible cloud feedback acting through deep convection in the tropics. The feedback also requires that the direction of causality is such that temperature mostly influences the cloud. It has been argued that coupled general circulation models also show a decrease in the upper level cloud area with sea surface temperature, simply because of a shading effect of clouds on sea surface temperature (*Sherwood et al.*, 2009). Although this effect might play a role, several of the observational results presented, either due to the methodology used or due to the scales considered, do not appear to be subject to such shading effect. It will be worth exploring in a coupled model what are the limitations of our observational technique to the possibility that the ocean is not merely passive boundary condition to clouds.

The main difficulty in testing directly the mechanism for a negative feedback on climate such as the iris effect is that the part of the cloud that is observed (either as brightness area in chapter 3 or as stratiform precipitation area in chapter 4) is not necessarily the part of the cloud that has the net positive cloud radiative effect. For instance, *Choi et al.* (2005) show that the detection of the area of upper level clouds in the tropics using a brightness temperature threshold of 260 K, as we have used in chapter 3, underestimates the area of high clouds by a factor of two compared to the area of high cloud using the 1.38 μ m in the Moderate-resolution imaging spectroradiometer (MODIS). Only the clouds with visible optical depths smaller than 10, are

in fact clouds having a net positive radiative effect (*Choi and Ho*, 2006; *Kubar et al.*, 2007). These clouds have brightness temperatures *higher* than 260 K. Even if the detection of the cloud were accurate, there would still remain an attribution problem. *Massie et al.* (2002) determined that half of cirrus clouds are produced within 5 days of the original convective detrainment, the rest of the clouds is formed by in-situ processes. *Pfister et al.* (2001) also calculated back trajectories were most of the cirrus directly related to convection had their origin between 0.5 days to 3 days from the time of the most recent convection. This shows the possibility that a cirrus cloud can be potentially advected several thousand kilometers from the region in which originated (*Luo and Rossow*, 2004; *Mace et al.*, 2006), or originate as a consequence of water vapor detrained originally detrained from convection but further triggered as a cloud by other processes, for instance, gravity waves. In most of our analysis we assume that $\sim$ 1 day and $\sim$ 1°are typical scales in which most of the anvil cloud is formed and dissipated, and therefore a direct relation with SST, and also with the originating convection can be discerned. This difficulty, at least for an analysis using geostationary data, was controlled by *Horváth and Soden* (2008) using Lagrangian trajectories. In their analysis, they also found a decrease in the area of cirrus per unit of area of convective clouds quantitatively similar to the one found in our analysis, providing confidence in that the negative relation between upper level cloud and SST is not simply due to griding artifacts. A similar analysis extended for longer trajectories and including the identification of thin cirrus clouds directly from data would provide a more direct test for the iris hypothesis. Also, vertical profiles of cloud liquid and ice water can be obtained from the recently available datasets from the A-Train (*Stephens et al.*, 2002). A combination of Lagrangian trajectories calculated from the high sampling geostationary information and the detailed information from Cloudsat would help one to characterize the processes involved in the detrainment of deep convection and in the formation of the optically thin cirrus clouds.

Together with this mechanistic approach, one can also explore the possibility of directly observing the effect of a cloud feedback of the sort proposed by the iris hypothesis, by looking at variations of the top of the atmosphere radiative fluxes at the interanual or intraseasonal scales. In fact, *Lindzen and Choi* (2009) conducted such analysis, finding a major discrepancy between atmospheric model responses and observations of changes in the longwave radiative flux compared to changes in the average tropical temperature in intraseasonal scales. A total negative feedback can be deduced from the outgoing longwave response of the tropics. If one accepts observational analysis that indicate a strong positive water vapor feedback (e.g. *Dessler*

et al., 2008), then the combined effect of water vapor feedback and lapse rate feedback must be more than compensated by a strong unknown process acting on modifying the longwave flux. This process can not be distinguished from the bulk of the longwave response in this analysis, but it most likely resides in the combined cloud and water vapor behavior of the tropics.

A major problem when studying climates that are very different from ours is the difficulty in constraining physical models for processes that we are not able to observe. Even current cloud parameterizations differ widely in the representation of clouds for the observed tropical conditions. Current climate variations in temperature allow us to observe convective systems over a very narrow range of temperatures, between about 27 and 31 C. Temperature dependencies that might be too small to be observed in current tropical climate, can potentially provide large feedbacks for climates very different than present. In studying the faint young sun paradox, we have mostly followed the traditional approach in problems related to the early earth (e.g *Kasting and Ackerman*, 1986), which is to use a simplified radiative-convective model with limited representation of latitude variations, clouds and meridional heat transport. The faint young sun paradox itself, needs a bit of elaboration. It is usually framed in terms of the global mean surface temperature being above freezing, but for instance, one can imagine a weak version of the paradox: even under a much fainter sun, at least some (large) portion of the surface was covered by liquid water. This would ensure for instance, an stable environment for the development of life, which we believe occurred during the period in which the paradox is unsolved. According to our results this weaker version of the paradox is not very hard to solve, in the sense that even a relatively small cloud feedback can ensure that tropical regions are able to sustain temperatures above freezing. Depending on the assumption made about the meridional heat transport, we can even obtain mean tropical temperatures well above freezing, between 280 K to 290 K. On the other hand, a stronger version of the paradox, one in which one sees the absence of evidence of glaciation as an indication that the complete surface of the planet has to be above freezing, is a much harder one to solve. We have neglected the ice-albedo feedback in our calculations, which will generally make matters even more difficult for the resolution of the paradox, specially in a climate with a vigorous meridional heat transport. The role of meridional heat transport seems to be particularly neglected in the literature, mostly due to the simplified nature of the models used to explore the hypothesis. It would be worth exploring how the thin cirrus solution proposed interacts with other processes within the framework of a more realistic general circulation model. In particular with respect

to the ice-albedo feedback, the meridional heat transport and possible variations in the size of the tropical regions due to changes in the width of the Hadley Cell. Another interesting aspect of the study is the fact the magnitude of the cloud feedback is related to the response in terms of precipitation in our simplified model. Some of the literature that discusses changes in precipitation with climate focuses on two aspects of the issue, namely, that the precipitation increase is much weaker than the Clausius-Clapeyron scaling, and that the precipitation change seems to be a robust result in current global circulation models *Held and Soden* (2006); *Stephens and Ellis* (2008). Our simple model illustrate the point that cloud feedbacks can potentially provide large changes in precipitation, and therefore, while uncertainties in the magnitude of the cloud feedback prevail no claim of robustness for changes in precipitation can be made confidently.

Appendix A

Degraded sampling using geostationary data

Given the nearly hourly resolution of the geostationary satellite we can test the effect of a reduction in the sampling frequency on the statistics, in particular, in the relation between the cloud weighted SST and the normalized anvil area. Here we describe some additional supporting data analysis carried out with 1 year of geostationary data over the Western Tropical Pacific Region (130-180E, 10S-10N). The data are geostationary infrarred brightness from the GMS-5 geostationary satellite as stored by the ARM program. We follow a similar methodology as in *Su et al.* (2008) only that in this approach, we use only geostationary data, and therefore the mean precipitation is replaced by the mean deep convective activity (that is the mean fraction of area coverage below 220 K).

We perform the analysis using geostationary radiances to identify anvil and core regions of the cloud systems using brightness temperature thresholds. We calculate the daily value of the cloud weighted SST ($\overline{T}_t$) as,

$$\overline{T}_t = \frac{\sum_n f_{n,t} \cos\theta_n T_{n,t}}{\sum_n f_n \cos\theta_n}, \tag{A.1}$$

where n is an index that runs over the 1°× 1°grids, f_n is the relative coverage by anvil cloud with respect to the total area of the grid and $T_{n,t}$ is the SST value for each grid n at the time t retrieved from the TMI satellite. The mean anvil and convective core fractions are calculated as

$$\overline{f}_n = \frac{\sum_n f_{n,t} \cos\theta_n}{\sum_n \cos\theta_n} \tag{A.2}$$

$$\overline{c}_n = \frac{\sum_n c_{n,t} \cos\theta_n}{\sum_n \cos\theta_n}, \tag{A.3}$$

respectively. The normalized area is then

$$\tilde{f} = \frac{\overline{f}_n}{\overline{c}_n}. \tag{A.4}$$

The values of $f_{n,t}$ and $c_{n,t}$ are constructed using the full geostationary temporal resolution and also selecting a given number of images per day. Furthermore, we selected the images starting at two different times to test for sensitivy to the diurnal cycle. The results are shown in table A.1.

images/day	1	2	8	12	24
$\Delta\tilde{f}/\Delta\overline{T}$ (1:30 UTC)	-30	-37	-39	-41	-41
$\Delta\tilde{f}/\Delta\overline{T}$ (7:30 UTC)	-51	-42	-40	-41	-41
$\Delta\tilde{f}_{24}/\Delta\overline{T}$	-41	-38	-42	-40	-41

Table A.1: Slopes of the regression between $\tilde{f}$ and $\overline{T}$ for different sampling using geostationary data. The regressions are exponential least-square fits.

When 24 images/day (nearly full temporal sampling) are used, we find a very large slope of about -41 %/K. This is a relatively large value for the slope, however similar values were reported by *Lindzen et al.* (2001) for subdomains of the data in the original analysis. However, since the focus of this analysis is not the absolute magnitude of the slope but rather whether there is a dependence of the slope with sampling, we simply compared the values obtained by degrading the sampling with the full resolution value. When both f_n and c_n are degraded by choosing less than 24 images per day, the results are significantly different than when the full resolution is used. This is particularly evident when only 1 image per day is used. The slope converges rapidly to the full sampling value and even 8 images per day seems enough to obtain an answer close to the full sampling. The difference in slope when different starting hours are used (that is if there are 2 images per day they are equally spaced in time and therefore the statistics are calculated with the image closer to 1:30 UTC and 13:30 UTC in the first row, and 7:30 UTC and 19:30 UTC in the second row in table A.1) indicates the influence of the diurnal cycle when both anvil and core

fractions are degraded. To be fair, the normalization is performed in the analysis by *Su et al.* (2008) using precipitation data having relatively high sampling. This is mimicked in the third row in table A.1 by degrading only the anvil part in the calculation of the normalized fraction and keeping the full temporal resolution in the calculation of $\bar{c}_n$. In this case the estimates are closer to the full resolution even when only 1 image per day are used in the anvil calculation. Even though the diurnal cycle of convection is relatively weak over the oceans, the bias of the slopes for coarse sampling seems to be related to the diurnal cycle in convective activity. It might underestimate or overestimate the value of the slope depending on whether one is mostly underestimating or mostly overestimating the deep convective activity.

Appendix B

Sensitivity to stratiform-convective horizontal separation algorithm

For completeness, we include a detailed account of the stratiform-convective separation algorithm based on the work of *Steiner et al.* (1995) and *Yuter and Houze* (1997). The rules applied in order to classify each pixel are highly dependent on the horizontal resolution of the radar and they need to be calibrated by selecting arbitrary thresholds. The calibration is done by inspecting the vertical radar reflectivity in which coherent high reflectivity levels and bright bands can be identified and the thresholds be set accordingly. The method only uses the horizontal information for the classification of the echoes. The the lowest level reflectivity measured by the radar (base reflectivity) is examined and the following rules are applied to identify convective regions:

1. Pixels in which the radar intensity exceeds a threshold Z_{th} are immediately classified as convective. This default threshold value is initially set to 40 dBZ.

2. Pixels for which the background reflectivity Z_{bg} (measured as the arithmetic average reflectivity of an area of 11 km radius surrounding each precipitating pixel) exceeds a background reflectivity threshold given by the formula,

$$\Delta Z_{th} = a \cos\left(\frac{\pi}{2b} Z_{bg}\right), \tag{B.1}$$

   are also classified as convective

3. Finally, after the two previous rules have been applied the algorithm selects a region around each convective pixel in which pixels will be classified as convective.

The radius of this region is designed to be a function of the mean background reflectivity $\overline{Z_{bg}}$, under the premise that a brighter background region will indicate a more active and larger convective region.

The technique has many degrees of freedom and therefore requires calibration against some independent dataset, usually the vertical profile of reflectivity from which a bright band can be identified (*Steiner et al.*, 1995). Here we explore the sensitivity of the Kwajalein results to the design parameters of the algorithm.

We have performed a sensitivity study using the base reflectivity data for the complete period of 1999-2003. Once the algorithm is applied and a classification between stratiform and convective echoes is achived, the surface rainfall is recalculated applying the calibration and corrections described by *Houze et al.* (2004). Table B summarizes the results of the sensitivity tests using the different parameters the stratiform convective for the particular period. The rows labelled from 1a to 4 refer to the results of the sensitivity to the parameters. The row 1a attempts to simulate the classification found in the original dataset with minor differences.

Correlations between $\mathcal{A}_s$ and SST are relatively insensitive to the parameters of the classification, whereas a more significant variation (from 3 % to 23 %) is observed in the change of ϵ_c with respect to the classifications parameters. Both correlations are relatively insensitive to changes in the reflectivity threshold Z_{th} (compare cases 1a to 3a and 3b), presumably because pixels that are left out of the convective classification by a stronger threshold (as in case 3a) will still be considered convective by one of the other two criteria. On the other hand, a larger sensitivity is obtained, especially for the slope of the regreesion with ϵ_c, by changing the parameter a (cases 2a and 2b) which is related to the area surrounding a particularly intense reflectivity region that is considered convective. We conclude that to the extent that the algorithm parameters are modified within reasonable values from those used for calibrating the algorithm, the correlations are not significantly modified. It is also clear that critical for an accurate quantification of the variation of ϵ_c with SST is accuracy on the detection of the size of the convective region.

	a	b	Z_{th}	Method	ϵ_c		$\mathcal{A}_s$	
	[dBZ]	[dBZ]	[dBZ]	(M/N)[1]	%/K	r	%/K	r
1a	10	55	40	M	8.0	0.38	-27	0.40
1b	10	45	40	M	6.5	0.38	-25	-0.49
1c	10	65	40	M	9.3	0.39	-25	-0.51
2a	5	55	40	M	3.1	0.35	-25	-0.50
2b	15	55	40	M	23	0.49	-26	-0.52
3a	10	55	45	M	8.2	0.37	-25	0.51
3b	10	55	35	M	9.8	0.47	-27	-0.51
4	10	55	40	N	7.25	0.29	-24	-0.52

Table B.1: Sensitivity of the correlations between ϵ_c and $\mathcal{A}_s$ with SST to the different parameters of the stratiform-convective separation algorithm using the University of Washington Kwajalein base data set. The calculations were repeated in each case for the complete 1999-2003 period.

Appendix C

Statistical significance of the Kwajalein Results

We have tested the statistical significance of these results by using some of the observed characteristics of the time series of SST and ϵ_c and constructing a simple statistical model to apply a Monte Carlo method. The appropriate statistical model satisfies the null hypothesis H_0 : ϵ_c and SST are independent. Therefore the approach to test the significance of the results will be to simulate through this statistical model calibrated through the observations, several pairs of values ($\epsilon_c^{t,n}$,$SST^{t,n}$), where $t = 1..t_f$ are the times over which the series of measurements are taken (in this case each t represents an 8-day period), n is an index that indicates a single realization.

First we define an idealized time series for the SST based on the observed time series for SST in Kwajalein as,

$$SST^{t,n} = \overline{SST} + \cos(2\pi t/t_y) + \mathcal{N}^{t,n}(0, \sigma_{SST}), \tag{C.1}$$

where $\overline{SST} \sim 28$ C and $\sigma_{SST} \sim 0.3$ C are the observed mean and standard deviation of the high pass filtered time series of SST. The time t_y is the number of periods in a year so the cosine is meant to represent an annual cycle in SST with an amplitude of 1 C. $\mathcal{N}^{t,n}$ is a realization from the normal distribution meant to represent the high frequency variability of SST.

From these realizations of SST we can propose a model for the behavior of ϵ_c consistent with the null hypothesis. That is,

$$\epsilon_c^{t,n} = \overline{\epsilon_c} + \mathcal{N}^{t,n}(0, \sigma_{\epsilon_c}) \tag{C.2}$$

We have pointed out that the variance of ϵ_c seems to decrease with SST (due

in part to a decrease in the component of the variance related to sampling) so that the statistical significance determined from Montecarlo simulations can be affected by whether we consider σ_{ϵ_c} as a constant or as a function of SST. So strictly speaking two slightly different null hypotheses will be discussed: one in which there is strict independence and the other one in which the dependence is constrained to appear only in the SST-dependence of the variance. Figure C-1 shows the original time-series for SST and ϵ_c and a single realization of the model using the sampling dependence of the variance.

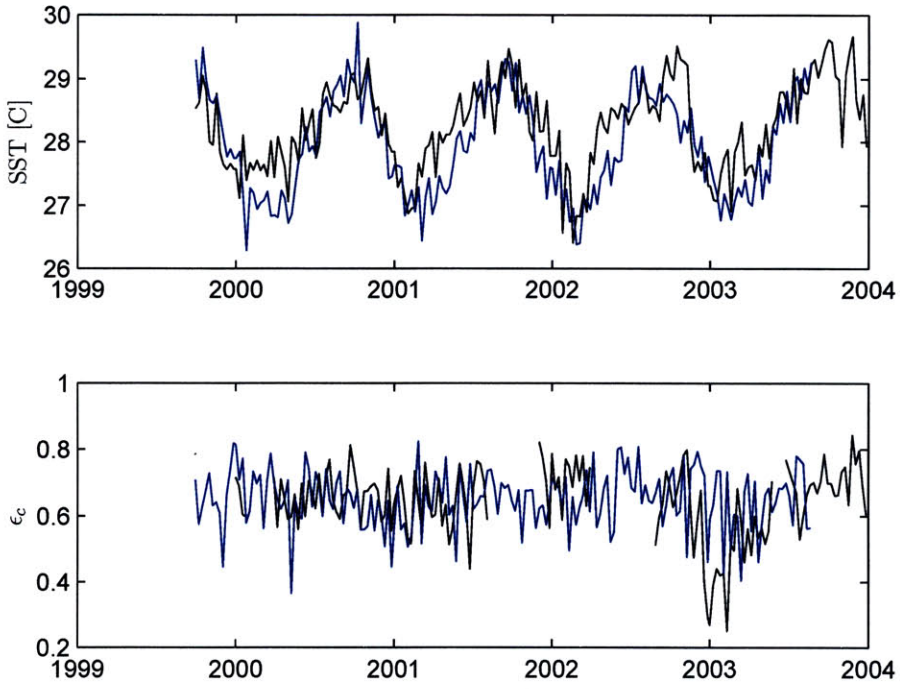

Figure C-1: The upper panel shows the actual SST time series (black) and one of the Montecarlo simulations according to equation C.1. The lower panel is the actual ϵ_c corresponding to the plotted months, and the simulated ϵ_c from equation C.2 (blue).

For the cases in which there is an SST-dependent variance a simple linear dependence is written,

$$\sigma_{\epsilon_c}(SST) = (SST_0 - SST)\beta + \sigma_{\epsilon_c}(SST_0), \tag{C.3}$$

with empirically derived values for $\beta = 0.025$ and $\sigma(SST_0 = 26C) = 0.14$.

Results for the Montecarlo simulations of the statistical— process described in equation C.2 using a constant value for σ_{ϵ_c} equal to the empirically observed value of

0.1 and a value of $\overline{\epsilon_c} = 0.667$ are shown in Figure C-2. The results are for 10000 realizations. The empirical distribution for both the slopes and the correlation coefficients are centered around zero. Comparing the values for the slope and the correlation coefficient obtained for the 8-day period averages, the null hypothesis is rejected under this assumption at a relatively high significance level (slopes higher than 4.4 % and correlation coefficients higher than 0.22 are significant at the 0.1 % level).

However, as previously mentioned, a test in which the variance of the statistic ϵ_c is regarded as constant might be liberal in rejecting the null hypothesis. In fact, introducing an $SST-$dependence in the value of σ_{ϵ_c} according to equations C.2 and C.3, we observe that the distribution of slopes and correlation coefficients becomes skewed toward positive values. Therefore, a relatively larger value in the slopes and correlation coefficient is required (slopes higher than 5.2 % and correlation coefficients higher than 0.28 are significant at the 0.1 % level). When comparing the value of the statistics related to these significance numbers to the values of the slope and correlation coefficient obtained in the corresponding observations (i.e. $r = 0.42$ and slope 11.8 % we conclude that even in this case the null hypothesis is rejected with a high confidence level. Similar analyses performed for $\mathcal{A}_s$ show that the decrease with SST is also statistically significant.hapter

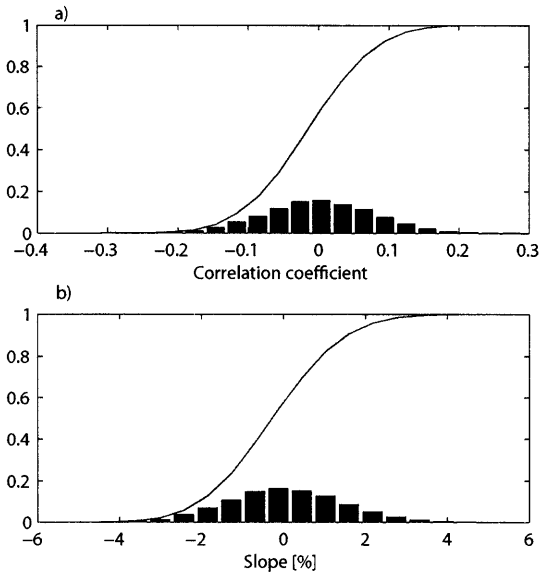

Figure C-2: Empirical distribution and cumulative frequency of the montecarlo simulations of the processes for a constant variance

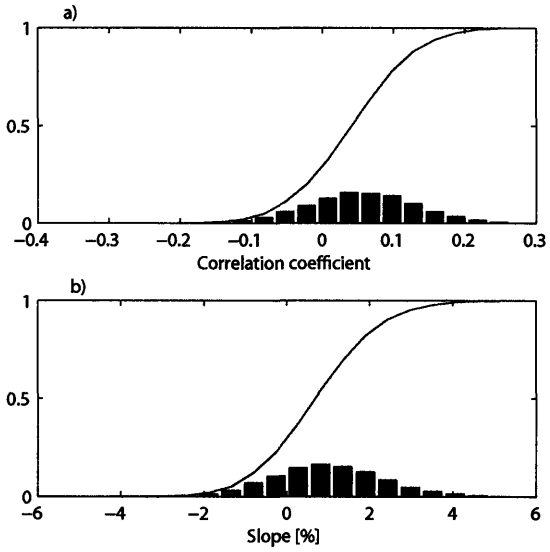

Figure C-3: Same as Fig. C-2 but for an SST-dependent variance according to C.3

Bibliography

Anderson, N., C. Grainger, and J. Stith, Characteristics of Strong Updrafts in Precipitation Systems over the Central Tropical Pacific Ocean and in the Amazon, *Journal of Applied Meteorology*, *44*(5), 731–738, 2005.

Awaka, J., T. Iguchi, H. Kumagai, and K. Okamoto, Rain type classification algorithm for TRMM precipitation radar, *Geoscience and Remote Sensing*, *4*, 1633–1635, 1997.

Bell, T., and P. Kundu, Dependence of Satellite Sampling Error on Monthly Averaged Rain Rates: Comparison of Simple Models and Recent Studies, *J. Climate*, *13*(2), 449–462, 2000.

Berg, W., C. Kummerow, and C. Morales, Differences between East and West Pacific Rainfall Systems, *J. Climate*, *15*(24), 3659–3672, 2002.

Betts, A., Climate-Convection Feedbacks: Some Further Issues, *Climatic Change*, *39*(1), 35–38, 1998.

Betts, A., and Harshvardan, Thermodynamic constraint on the cloud liquid water feedback in climate models, *Journal of Geophysical Research*, *92*(D7), 8483–8485, 1987.

Betts, A., and W. Ridgway, Climatic Equilibrium of the Atmospheric Convective Boundary Layer over a Tropical Ocean, *Journal of the Atmospheric Sciences*, *46*(17), 2621–2641, 1989.

Bony, S., J. Dufresne, H. Le Treut, J. Morcrette, and C. Senior, On dynamic and thermodynamic components of cloud changes, *Climate Dyn.*, *22*(2), 71–86, 2004.

Bony, S., R. Colman, V. M. Kattsov, R. P. Allan, C. S. Bretherton, J. L. Dufresne, A. Hall, S. Hallegatte, M. M. Holland, W. Ingram, D. A. Randall, B. J. Soden, G. Tselioudis, and M. J. Webb, How well do we understand and evaluate climate change feedback processes?, *J. Climate*, *19*(15), 3445–3482, 076FT Times Cited:0 Cited References Count:231, 2006.

Bowen, E., The Formation of Rain by Coalescence, *Australian Journal of Physics*, *3*, 193, 1950.

Catling, D., and J. Kasting, *Planets and Life: The emerging science of astrobiology*, chap. Planetary atmospheres and life, pp. 91–116, Cambridge University Press, 2007.

Chen, J., B. Carlson, and A. Del Genio, Evidence for strengthening of the tropical general circulation in the 1990s, *Science*, *295*(5556), 838–841, 2002.

Choi, Y., C. Ho, and C. Sui, Different optical properties of high cloud in GMS and MODIS observations, *Geophys. Res. Lett.*, *32*(23), 2005.

Choi, Y.-S., and C.-H. Ho, Radiative Effect of Cirrus with Different Optical Properties over the Tropics in MODIS and CERES Observations, *Geophys. Res. Lett.*, *33*(L21811), doi:10.1029/2006GL027403, 2006.

Chou, M., and R. Lindzen, Comments on "Tropical convection and the energy balance at the top of the atmosphere", *J. Climate*, *15*(17), 2566–2570, 2002.

Chou, M., and R. Lindzen, Comments on ?Examination of the Decadal Tropical Mean ERBS Nonscanner Radiation Data for the Iris Hypothesis?, *Journal of Climate*, *18*(12), 2123–2127, 2005.

Chou, M., and M. Suarez, A Solar Radiation parameterization for atmospheric studies, *Tech. Rep. NASA/TM-1999-10460*, NASA Tech. Memo, 2002.

Chou, M., K. Lee, S. Tsay, and Q. Fu, Parameterization for Cloud Longwave Scattering for Use in Atmospheric Models, *Journal of Climate*, *12*(1), 159–169, 1999.

Chou, M., K. Lee, and P. Yang, Parameterization of shortwave cloud optical properties for a mixture of ice particle habits for use in atmospheric models, *J. Geophys. Res*, *107*(D21), 4600, 2002.

Chou, M., M. Suarez, X. Liang, and Y. MMH, A Thermal Infrared Radiation Parameterization for Atmospheric studies, *Tech. Rep. NASA/TM-2001-104606*, NASA Tech. Memo, 2003.

Churchill, D. D., and R. A. Houze, Development and structure of winter monsoon cloud clusters on 10 december 1978, *J. Atmos. Sci.*, *41*(6), 933–960, 1984.

Clement, A., and B. Soden, The sensitivity of the tropical-mean radiation budget, *J. Climate*, *18*, 3189–3203, 2005.

Cogley, J., and A. Henderson-Sellers, The origin and earliest state of the earth's hydrosphere., *Rev. Geophys*, 1984.

Cotton, W., G. Alexander, R. Hertenstein, R. Walko, R. McAnelly, and M. Nicholls, Cloud venting?A review and some new global annual estimates, *Earth Science Reviews*, *39*(3-4), 169–206, 1995.

Del Genio, A., and W. Kovari, Climatic Properties of Tropical Precipitating Convection under Varying Environmental Conditions, *J. Climate*, *15*(18), 2597–2615, 2002.

Del Genio, A. D., W. Kovari, M.-S. Yao, and J. Jonas, Cumulus microphysics and climate sensitivity, *J. Climate*, *18*(13), 2376–2387, 2005.

Dessler, A. E., Z. Zhang, and P. Yang, Water-vapor climate feedback inferred from climate fluctuations, 2003-2008, *Geophysical Research Letters*, *35*(20), doi: http://dx.doi.org/10.1029/2008GL035333, 2008.

Doviak, R. J., and D. S. Zrnic, *Doppler Rada and Weather Observations*, Dover Publications, Inc, 1993.

Emanuel, K., J. David Neelin, and C. Bretherton, On large-scale circulations in convecting atmospheres, *Quarterly Journal of the Royal Meteorological Society*, *120*(519), 1994.

Emanuel, K. A., *Atmospheric Convection*, 580 pp., Oxford University Press, 1994.

Emanuel, K. A., *The Global Circulation of the Atmosphere*, chap. Quasi-Equilibrium Dyamics of the Tropical Atmosphere, pp. 186–218, Princeton University Press, 2007.

Emanuel, K. A., and R. T. Pierrehumbert, Microphysical and dynamical control of tropospheric water vapor, in *Clouds, Chemistry and Climate*, vol. 135, edited by V. Ramanathan, pp. 17–28, Springer-Verlag, Berlin, Heidelberg, 1996.

Endal, A., and K. Schatten, The faint young sun-climate paradox- Continental influences, *Journal of Geophysical Research*, *87*, 7295–7302, 1982.

Ferrier, B., J. Simpson, and W. Tao, Factors responsible for precipitation efficiencies in midlatitude and tropical squall simulations, *Mon. Wea. Rev.*, *124*(10), 2100–2125, 1996.

Fu, Q., M. Baker, and D. Hartmann, Tropical cirrus and water vapor: an effective Earth infrared iris feedback, *Atmos. Chem. Phys*, *2*, 31–37, 2002.

Gamache, J. F., and R. A. Houze, Water budget of a mesoscale convective system in the tropics, *J. Atmos. Sci.*, *40*, 1835–1850, 1983.

Gerard, J., D. Delcourt, and L. Francois, The maximum entropy production principle in climate models: application to the faint young sun paradox, *Quarterly Journal of the Royal Meteorological Society*, *116*(495), 1990.

Gough, D., Solar interior structure and luminosity variations, *Solar Physics*, *74*(1), 21–34, 1981.

Haqq-Misra, J. D., S. D. Domagal-Goldman, K. P. J., and K. J. F., A revised, hazy methane greenhouse for the archean earth, *Astrobiology*, 2008.

Hartmann, D., and K. Larson, An important constraint on tropical cloud- Climate feedback, *Geophysical Research Letters*, *29*(20), 12–1, 2002.

Hartmann, D., and M. Michelsen, Large-Scale Effects on the Regulation of Tropical Sea Surface Temperature, *Journal of Climate*, *6*(11), 2049–2062, 1993.

Hartmann, D., and M. Michelsen, No evidence for iris, *Bulletin of the American Meteorological Society*, *83*(2), 249–254, 2002.

Hartmann, D., L. Moy, and Q. Fu, Tropical convection and the energy balance at the top of the atmosphere, *Journal of Climate*, *14*(24), 4495–4511, 2001.

Hatzidimitriou, D., I. Vardavas, K. Pavlakis, N. Hatzianastassiou, C. Matsoukas, and E. Drakakis, On the decadal increase in the tropical mean outgoing longwave radiation for the period 1984–2000, *Atmos. Chem. Phys*, *4*, 1419–1425, 2004.

Held, I., and B. Soden, Water vapor feedback and global warming, *Annual Review of Energy and the Environment*, *25*, 441–475, 2000.

Held, I., and B. Soden, Robust Responses of the Hydrological Cycle to Global Warming, *J. Clim*, *19*, 5686–5699, 2006.

Henderson-Sellers, A., and J. Cogley, The Earth's early hydrosphere, 1982.

Hessler, A., D. Lowe, R. Jones, and D. Bird, A lower limit for atmospheric carbon dioxide levels 3.2 billion years ago, *Nature*, *428*(6984), 736–738, 2004.

Heymsfield, G., B. Geerts, and L. Tian, TRMM Precipitation Radar Reflectivity Profiles as Compared with High-Resolution Airborne and Ground-Based Radar Measurements, *J. Appl. Meteor.*, *39*(12), 2080–2102, 2000.

Horváth, Á., and B. Soden, Lagrangian Diagnostics of Tropical Deep Convection and Its Effect upon Upper-Tropospheric Humidity, *Journal of Climate*, *21*(5), 1013–1028, 2008.

Houze, R., Mesoscale convective systems, *Rev. Geophys*, *42*(10.1029), doi:10.1029/2004RG000150, 2004.

Houze, R. A., *Cloud Dynamics*, vol. 53, Academic Press, San Diego, 1993.

Houze, R. A., Stratiform precipitation in regions of convection: A meteorological paradox?, *Bull. Amer. Meteorol. Soc.*, *78*(10), 2179–2196, 1997.

Houze, R. A., S. Brodzik, C. Schumacher, S. E. Yuter, and C. R. Williams, Uncertainties in Oceanic Radar Rain Maps at Kwajalein and Implications for Satellite validation, *J. Appl. Meteor.*, *43*(8), 1114–1132, 2004.

Iguchi, T., T. Kozu, R. Meneghini, and J. Awaka, Rain-Profiling Algorithm for the TRMM Precipitation Radar, *J. Appl. Meteor.*, *39*(12), 2038–2052, 2000.

Imaoka, K., and R. Spencer, Diurnal Variation of Precipitation over the Tropical Oceans Observed by TRMM/TMI Combined with SSM/I, *Journal of Climate*, *13*(23), 4149–4158, 2000.

Johnson, R., T. Rickenbach, S. Rutledge, P. Ciesielski, and W. Schubert, Trimodal Characteristics of Tropical Convection, *J. Climate*, *12*(8), 2397–2418, 1999.

Kasting, J., Theoretical constraints on oxygen and carbon dioxide concentrations in the Precambrian atmosphere, *Precambrian research*, *34*(3-4), 205–229, 1987.

Kasting, J., Earth's early atmosphere, *Science*, *259*(5097), 920–926, 1993.

Kasting, J., and T. Ackerman, Climatic consequences of very high carbon dioxide levels in the earth's early atmosphere, *Science*, *234*(4782), 1383–1385, 1986.

Kasting, J., and D. Catling, Evolution of a Habitable Planet, *Annual Review of Astronomy and Astrophysics*, *41*, 429–463, 2003.

Kasting, J., O. Toon, and J. Pollack, How climate evolved on the terrestrial planets, *Scientific American*, *258*(2), 90–97, 1988.

Kuang, Z., and D. Hartmann, Testing the Fixed Anvil Temperature Hypothesis in a Cloud-Resolving Model, *Journal of Climate*, *20*(10), 2051–2057, 2007.

Kubar, T., D. Hartmann, and R. Wood, Radiative and Convective Driving of Tropical High Clouds, *J. Climate*, *20*, 5510–5526, 2007.

Kuhn, W., and S. Atreya, Ammonia photolysis and the greenhouse effect in the primordial atmosphere of the earth, *Icarus*, *37*(1), 207–213, 1979.

Kummerow, C., W. Barnes, T. Kozu, J. Shiue, and J. Simpson, The tropical rainfall measuring mission trmm sensor package, *J. Atmos. Oceanic Technol.*, *15*, 809–817, 1998.

Lau, K., and H. Wu, Warm rain processes over tropical oceans and climate implications, *Geophys. Res. Lett.*, *30*(24), doi:10.1029/2003GL018567, 2003.

Lau, K., H. Wu, Y. Sud, and G. Walker, Effects of Cloud Microphysics on Tropical Atmospheric Hydrologic Processes and Intraseasonal Variability, *Journal of Climate*, *18*(22), 4731–4751, 2005.

Lin, B., T. Wong, B. Wielicki, and Y. Hu, Examination of the decadal tropical mean ERBS nonscanner radiation data for the iris hypothesis, *Journal of Climate*, *17*(6), 1239–1246, 2004.

Lin, B., B. A. Wielicki, P. Minnis, L. Chambers, K. M. Xu, Y. X. Hu, and A. Fan, The effect of environmental conditions on tropical deep convective systems observed from the TRMM satellite, *J. Climate*, *19*(22), 5745–5761, 2006.

Lindzen, R., and B. Farrell, The role of polar regions in global climate, and a new parameterization of global heat transport, *Monthly Weather Review*, *108*(12), 2064–2079, 1980.

Lindzen, R., and S. Nigam, On the Role of Sea Surface Temperature Gradients in Forcing Low-Level Winds and Convergence in the Tropics, *Journal of the Atmospheric Sciences*, *44*(17), 2418–2436, 1987.

Lindzen, R., M. Chou, and A. Hou, Comment on" No Evidence for Iris", *Bulletin of the American Meteorological Society*, *83*(9), 1345–1349, 2002.

Lindzen, R. S., Some remarks on cumulus parameterization, *Pageoph*, *126*, 123–134, 1988.

Lindzen, R. S., The interaction of waves and convection in the tropics, *J. Atmos. Sci.*, *60*(24), 3009–3020, 2003.

Lindzen, R. S., and Y.-S. Choi, On the determination of climate feedbacks from erbe data, *Geophys. Res. Lett.*, *36*, L16,705, doi:10.1029/2009GL039628, 2009.

Lindzen, R. S., M.-D. Chou, and A. Y. Hou, Does the earth have an adaptive infrared iris?, *Bull. Amer. Meteorol. Soc.*, *82*(3), 417–432, 2001.

Liou, K., *Yearbook of Science and Technology*, chap. Cirrus clouds and climate, McGraw-Hill 2005, 2005.

Liou, K., and K. Gebhart, Numerical experiments on the thermal equilibrium temperature in cirrus cloudy atmospheres, *Meteorological Society of Japan, Journal*, *60*, 570–582, 1982.

Lovelock, J., and M. Whitfield, Life span of the biosphere, *Nature*, *296*, 561–563, 1982.

Lowe, D., and M. Tice, Geologic evidence for Archean atmospheric and climatic evolution: Fluctuating levels of CO_2, CH_4, and O_2 with an overriding tectonic control, *Geology*, *32*(6), 493–496, 2004.

Luo, Z., and W. Rossow, Characterizing Tropical Cirrus Life Cycle, Evolution, and Interaction with Upper-Tropospheric Water Vapor Using Lagrangian Trajectory Analysis of Satellite Observations, *Journal of Climate*, *17*(23), 4541–4563, 2004.

Mace, G., M. Deng, B. Soden, and E. Zipser, Association of Tropical Cirrus in the 10–15-km Layer with Deep Convective Sources: An Observational Study Combining Millimeter Radar Data and Satellite-Derived Trajectories, *Journal of the Atmospheric Sciences*, *63*(2), 480–503, 2006.

Manabe, S., and R. Strickler, Thermal Equilibrium of the Atmosphere with a Convective Adjustment, *Journal of the Atmospheric Sciences*, *21*(4), 361–385, 1964.

Manabe, S., and R. Wetherald, Thermal Equilibrium of the Atmosphere with a Given Distribution of Relative Humidity, *Journal of the Atmospheric Sciences*, *24*(3), 241–259, 1967.

Massie, S., A. Gettelman, W. Randel, and D. Baumgardner, Distribution of tropical cirrus in relation to convection, *J. Geophys. Res*, *107*(D21), 4591–4606, 2002.

McFarquhar, G., Comments on 'Parametrization of effective sizes of cirrus-cloud particles and its verification against observations' by Zhian Sun and Lawrie Rikus (October B, 1999, 125, 3037-3055), *Quarterly Journal Royal Meteorological Society*, *127*, 261–266, 2001.

McGuffie, K., and A. Henderson-Sellers, *A Climate Modelling Primer*, Wiley, 2005.

Minton, D., and R. Malhotra, Assessing the Massive Young Sun Hypothesis to Solve the Warm Young Earth Puzzle, *The Astrophysical Journal*, *660*(2), 1700–1706, 2007.

O'Gorman, P., and T. Schneider, The hydrological cycle over a wide range of climates simulated with an idealized GCM, *J. Climate*, *21*, 2008.

Owen, T., R. Cess, and V. Ramanathan, Enhanced CO_2 Greenhouse to Compensate for Reduced Solar Luminosity on Early Earth, *Nature*, *277*(5698), 640–642, 1979.

Paltridge, G., The steady-state format of global climate, *Quarterly Journal of the Royal Meteorological Society*, *104*(442), 1978.

Parodi, A., and K. Emanuel, A theory for bouyancy and velocity scales in deep moist convection, *Journal of Atmospheric Sciences*, in press, 2009.

Pavlov, A., J. Kasting, L. Brown, K. Rages, and R. Freedman, Greenhouse warming by CH4 in the atmosphere of early Earth, *Journal of Geophysical Research*, *105*(11), 981–11, 2000.

Pavlov, A., M. Hurtgen, J. Kasting, and M. Arthur, Methane-rich Proterozoic atmosphere?, *Geology*, *31*(1), 87–90, 2003.

Pfister, L., H. Selkirk, E. Jensen, M. Schoeberl, O. Toon, E. Browell, W. Grant, B. Gary, M. Mahoney, and T. Bui, Aircraft observations of thin cirrus clouds near the tropical tropopause, *Journal of Geophysical Research*, *106*(D9), 9765–9786, 2001.

Pierrehumbert, R., Thermostats, radiator fins, and the local runaway greenhouse, *J. Atmos. Sci.*, *52*(10), 1784–1806, 1995.

Pierrehumbert, R. T., *Principles of Planetary Climate*, 2009.

Pinti, D., The Origin and Evolution of the Oceans, *Lectures In Astrobiology*, *330*(380), 4–1, 2005.

Ramanathan, V., and W. Collins, Thermodynamic regulation of ocean warming by cirrus clouds deduced from observations of the 1987 El Niño, *Nature*, *351*, 27–32, 1991.

Rapp, A., C. Kummerow, W. Berg, and B. Griffith, An Evaluation of the Proposed Mechanism of the Adaptive Infrared Iris Hypothesis Using TRMM VIRS and PR Measurements., *J. Climate*, *18*(20), 4185–4194, 2005.

Renno, N., K. Emanuel, and P. Stone, Radiative-convective model with an explicit hydrologic cycle. 1. Formulation and sensitivity to model parameters, *J. Geophys. Res.*, *99*, 14,429–14,442, doi:10.1029/94JD00020, 1994.

Rogers, R. R., and M. K. Yau, *A Short Course in Cloud PhysicsCho*, Pergamon, New York, 1989.

Rollinson, H., *Early Earth Systems: A Geochemical Approach*, Blackwell Publishing, 2007.

Rossow, W., A. Henderson-Sellers, and S. Weinreich, Cloud Feedback: A Stabilizing Effect for the Early Earth?, *Science*, *217*(4566), 1245–1247, 1982.

Rutledge, S. A., and R. A. Houze, A diagnostic modeling study of the trailing stratiform region of a midlatitude squall line, *J. Atmos. Sci.*, *44*(18), 2640–2656, 1987.

Rye, R., P. Kuo, and H. Holland, Atmospheric carbon dioxide concentrations before 2. 2 billion years ago, *Nature*, *378*(6557), 603–605, 1995.

Sackmann, I., and A. Boothroyd, Our Sun. V. A Bright Young Sun Consistent with Helioseismology and Warm Temperatures on Ancient Earth and Mars, *The Astrophysical Journal*, *583*(2), 1024–1039, 2003.

Sagan, C., and G. Mullen, Earth and Mars: Evolution of Atmospheres and Surface Temperatures, *Science*, *177*(4043), 52–56, 1972.

Sarachik, E., Tropical sea surface temperature- An interactive one-dimensional atmosphere-ocean model, *Dynamics of Atmospheres and Oceans*, *2*(5), 455–469, 1978.

Sassen, K., Z. Wang, and D. Liu, Global distribution of cirrus clouds from CloudSat/Cloud-Aerosol Lidar and Infrared Pathfinder Satellite Observations (CALIPSO) measurements, *Journal of Geophysical Research*, *113*(D23), 2008.

Schneider, E., Axially symmetric steady-state models of the basic state for instability and climate studies. Part II: Nonlinear calculations, *J. Atmos. Sci*, *34*, 280–296, 1977.

Schneider, T., and P. O'Gorman, Precipitation and its extremes in changed climates, in *Proceedings of the 15th 'Aha Huliko'a Hawaiian Winter Workshop*, edited by C. G. P. Muller and D. Henderson, pp. 61–66, 2007.

Schumacher, C., and R. Houze, Stratiform Rain in the Tropics as Seen by the TRMM Precipitation Radar, *J. Climate*, *16*(11), 1739–1756, 2003.

Schumacher, C., and R. Houze, Stratiform precipitation production over sub-Saharan Africa and the tropical East Atlantic as observed by TRMM, *Quart. J. Roy. Meteor. Soc.*, *132*(620), 2235–2255, 2006.

Schumacher, C., and R. A. Houze, Comparison of radar data from the trmm satellite and kwajalein oceanic validation site, *J. Appl. Meteor.*, *39*, 2151–2164, 2000.

Schwartz, S., Uncertainty in climate sensitivity: Causes, consequences, challenges, *Energy & Environmental Science*, *1*(4), 430–453, 2008.

Schwartzman, D., and T. Volk, Biotic enhancement of weathering and the habitability of Earth, 1989.

Schwartzman, D., and T. Volk, Does Life Drive Disequilibrium in the Biosphere?, *Scientists Debate Gaia: The Next Century*, p. 129, 2004.

Shaviv, N., Toward a solution to the early faint Sun paradox: A lower cosmic ray flux from a stronger solar wind, *J. Geophys. Res*, *108*, 1437, 2003.

Shaw, G. H., Earth's atmosphere - Hadean to early Proterozoic, *Chemie Der Erde-Geochemistry*, *68*(3), 235–264, doi:10.1016/j.chemer.2008.05.001, 2008.

Sherwood, S. C., R. Roca, T. M. Weckwerth, and N. G. Andronova, Tropospheric water vapor, convection and climate: a critical review, *Reviews of Geophysics*, submitted, 2009.

Soden, B., and I. Held, An Assessment of Climate Feedbacks in Coupled Ocean–Atmosphere Models, *Journal of Climate*, *19*(14), 3354–3360, 2006.

Solomon, S., D. Qin, M. Manning, M. Marquis, K. Averyt, M. Tignor, H. Miller, and Z. Chen, *Climate changee 2007: the physical science basis*, Cambrige (United Kingdom). Intergovernmental Panel on Climate Change, 2007.

Somerville, R., and L. Remer, Cloud optical thickness feedbacks in the CO 2 climate problem, *J. Geophys. Res.*, *89*(D6), 9668–9672, 1984.

Steiner, M., R. A. Houze, and S. E. Yuter, Climatological characterization of three-dimensional storm structure from operational radar and rain gauge data, *J. Appl. Meteorol.*, *34*(9), 1978–2007, 1995.

Stephens, G., and T. Ellis, Controls of Global-Mean Precipitation Increases in Global Warming GCM Experiments, *Journal of Climate*, *21*(23), 6141–6155, 2008.

Stephens, G., D. Vane, R. Boain, G. Mace, K. Sassen, Z. Wang, A. Illingworth, E. O'Connor, W. Rossow, S. Durden, et al., The CloudSat mission and the A-Train, *Bulletin of the American Meteorological Society*, *83*(12), 1771–1790, 2002.

Stone, P., Baroclinic adjustment, *Journal of the Atmospheric Sciences*, *35*(4), 561–571, 1978.

Su, H., J. H. Jiang, Y. Gu, J. D. Neelin, J. W. Waters, B. H. Kahn, N. J. Livesey, M. L. Santee, and W. G. Read, Variations of tropical upper tropospheric clouds with sea surface temperature and implications for radiative effects, *J. Geophys. Res.*, *113*, 2008.

Sun, D., and I. Held, A Comparison of Modeled and Observed Relationships between Interannual Variations of Water Vapor and Temperature, *Journal of Climate*, *9*(4), 665–675, 1996.

Sun, D., and R. Lindzen, Water vapor feedback and the ice age snowline record, *Annales Geophysicae*, *11*(2-3), 204–215, 1993a.

Sun, D., and R. S. Lindzen, Distribution of tropical tropospheric water vapor, *J. Atmos. Sci.*, *50*(12), 1643–1660, 1993b.

TRMM Precipitation Radar Team, *Tropical Rainfall Measuring Mission (TRMM) Precipitation Radar Algorithm, Instruction Manual for Version 6*, Japan Aerospace Exploration Agency National Aeronautics and Space Administration, 2005.

Vecchi, G., and B. Soden, Global warming and the weakening of the tropical circulation, *Journal of Climate*, *20*(17), 4316–4340, 2007.

Volk, T., Feedbacks between weathering and atmospheric CO 2 over the last 100 million years, *American Journal of Science*, *287*(8), 763, 1987.

Walker, J., P. Hays, and J. Kasting, A negative feedback mechanism for the long-term stabilization of the earth's surface temperature, *Journal of Geophysical Research*, *86*(C10), 9776–9782, 1981.

Wallace, J. M., and P. V. Hobbs, *Atmospheric Science, An Introductory Survey*, *International Geophysics Series*, vol. 92, 2nd ed., Academic Press, 2006.

Wang, W., W. Rossow, M. Yao, and M. Wolfson, Climate Sensitivity of a One-Dimensional Radiative-Convective Model with Cloud Feedback, *Journal of the Atmospheric Sciences*, *38*(6), 1167–1178, 1981.

Wielicki, B., T. Wong, R. Allan, A. Slingo, J. Kiehl, B. Soden, C. Gordon, A. Miller, S. Yang, D. Randall, et al., Evidence for Large Decadal Variability in the Tropical Mean Radiative Energy Budget, *Science*, *295*(5556), 841, 2002.

Wilde, S., J. Valley, W. Peck, and C. Graham, Evidence from detrital zircons for the existence of continental crust and oceans on the Earth 4.4 Gyr ago, *Nature*, *409*(6817), 175–178, 2001.